Summer 8-26-2013

Calcium Remodeling through Different Signaling Pathways in Heart Failure: Arrhythmogenesis Studies of Pyk2, Dystrophin, and β-adrenergic Receptor Signaling

Di Lang
Washington University in St. Louis

WASHINGTON UNIVERSITY IN ST. LOUIS

School of Engineering and Applied Sciences

Department of Biomedical Engineering

Dissertation Examination Committee:
Igor R. Efimov, Chair
Nada Abumrad
Jianmin Cui
Tatiana Efimova
Vitaly Klyachko
Jeanne Nerbonne

Calcium Remodeling through Different Signaling Pathways in Heart Failure: Arrhythmogenesis

Studies of Pyk2, Dystrophin, and β-adrenergic Receptor Signaling

By

Di Lang

A dissertation presented to the
Graduate School of Arts and Sciences
of Washington University in
partial fulfillment of the
requirements for the degree
of Doctor of Philosophy

August 2013

Saint Louis, Missouri

Contents

List of Figures

List of Table

Acknowledgements

This dissertation would not have been possible without the help of many people in endless ways. First and foremost, I would like to express my sincere gratitude and deepest appreciation to my thesis advisor, Dr. Igor R. Efimov, for his indispensable guidance and ceaseless support. More importantly than providing me with all the resources to succeed, Dr. Efimov has helped me to grow as a scientist and as a person.

I would like to thank my committee members, Dr. Jeanne Nerbonne, Dr. Jianmin Cui, Dr. Vitaly Klyachko, Dr. Nada Abumrad, and Dr. Tatiana Efimova, for their sharing their knowledge with me. All of them have made significant contributions not only to my thesis, but also to my intellectual growth.

I would like to thank all the people whom I have been fortunate enough to work with during my doctoral study. I thank all the current and former members of the Efimov Laboratory: Dr. Vadim Fedorov, Dr. Alexey Glukhov, Dr. Qing Lou, Dr. Wenwen Li, Dr. Deborah Janks, Dr. Christina Ambrosi, Dr. Aili Cai, Dr. Hyejin Hwang, Dr. Jacob Laughner, Katherine Holzem, Matt Sulkin, Sarah Gutbrod, Chris Gloschat, Chaoyi Kang, John Yun Qiao, Colleen Rhoades, Mengqian Xiao. I would also like to thank Megan Flake for tirelessly managing the lab.

I am also grateful to the friendship I made during the time in graduate school. They have been a tremendous source of support and fun over the last five years. I especially would like to thank Xi Lu who came to Washington University in St. Louis at the same time I did. His invaluable help and encouragement have helped to support me through many of my hardships.

Lastly, I would like to thank my parents, Huanming Lang and Guifen Zhao, for their unconditional love and encouragement, without whom I would have never realized my own potential. I am blessed to have seen the silent strength and unyielding love that you have shown me in my life and they will continue to be my guide as I make my journey through life.

Di Lang

Washington University in St. Louis

August 2013

ABSTRACT OF DISSERTATION

Calcium Remodeling through Different Signaling Pathways in Heart Failure: Arrhythmogenesis Studies of Pyk2, Dystrophin, and β-adrenergic Receptor Signaling

By

Di Lang

Doctor of Philosophy in Biomedical Engineering

Washington University in St. Louis, 2013

Professor Igor R. Efimov, Chairperson.

Heart failure is a common clinical syndrome that ensues when the heart is no longer able to generate sufficient cardiac output to meet the demands of the body. It is one of the leading causes of death worldwide but with limited and non-ideal therapies at the moment. One reason behind this may be the complexity of significant alterations in multiple signaling pathways and concomitant structural and functional remodeling, especially Ca handling. Ca is critical in both the electrical and mechanical properties of cardiac myoctyes, and much is known about ionic currents and the normal excitation-contraction coupling process. In heart failure, distinct impaired signaling pathways induce significant alterations in how cardiac Ca handling is regulated. These alterations either directly cause certain arrhythmias or facilitate arrhythmias by association with electrical remodeling. The goal of this dissertation was to investigate the mechanisms of calcium remodeling through different signaling pathways in heart failure, and mechanisms on how the intricate and dynamic interactions between Ca handling and signaling pathways impairment facilitate arrhythmias in heart failure. To achieve this goal, a dual optical mapping system was designed to investigate electrical activity and Ca transient simultaneously. High spatio-temporal resolution mapping allows for quantifying conduction, repolarization and Ca cycling, especially on the interactions between action potential

and Ca handling. In this dissertation, I investigated Ca remodeling in three different signaling pathways: stress activated signaling, cytoskeletal signaling and β adrenergic receptor signaling pathway.

Proline-rich tyrosine kinase 2 (Pyk2) is a non-receptor protein kinase regulated by intracellular Ca. It mediates a typical stress activated signaling pathways along with c-Src, P38 MAPK and regulates a broad range of key biological responses. By optically mapping the genetically engineered mouse model: Pyk2 knockout, I detected a protective role of Pyk2 with respect to ventricular tachyarrhythmia during parasympathetic stimulation by regulation of gene expression related to calcium handling.

The *mdx* mouse model was introduced in the investigation of cytoskeletal signaling pathway. *mdx* mice is a common model for Duchenne muscular dystrophy, which is a clinical syndrome resulted from recessive of dystrophin and eventually develops into heart failure. The project suggested the association of mechanical stimulation and deficiency of dystrophin account for the cardiac mechanical defects and resulting Ca mishandling, but not either of the two above-mentioned entities alone. Ca mishandling leads to Ca cycling dispersion, which facilitates generation of arrhythmias.

β Adrenergic receptor signaling pathway was investigated on explanted donor and failing human hearts. Distinct β adrenergic receptor subtypes were found to regulate remodeling differently. The association between remodeling of action potential and Ca transient provides crucial arrhythmic drivers and substrate in heart failure.

Chapter 1
Introduction

1.1 Heart failure

Heart failure (HF) is a common, progressive and lethal clinical syndrome that ensues when the heart is no longer able to generate sufficient cardiac output to meet the demands of the body. During HF, the heart undergoes a complex series of changes in both myocyte and non-myocyte compartments in an attempt to compensate for the reduction in cardiac function.[1] These changes are associated with a number of cardiac and hemodynamic abnormalities that impair the electrophysiology of myocardium, excitation-contraction (EC) coupling and contraction. Specifically chronic hyperadrenergic state, altered calcium (Ca) signaling, prolongation of action potential duration and conduction slowing are the hallmarks of HF.[1-5] These abnormalities are initiated by functional and proliferative responses that are regulated by different signaling pathways.[6-8]

In the United States, HF has been diagnosed in more than 5 million people and in almost 10% of individuals over the age of 65. [9] Based on a long-term follow-up study reported in the American Heart Association (AHA), 80% of men and 70% of women under the age of 65 who have HF will die within 8 years. The one-year mortality rate of HF is also extremely high, with one out of five dying after this period. This high mortality rate is largely attributable to an electrical abnormality known as ventricular arrhythmia. Ventricular arrhythmia has been noted frequently in the patients

with HF and reported to be the major cause of cardiac sudden death. It is responsible for up to 50% of the mortality in HF.[9]

1.2 Arrhythmia

Arrhythmias result when the normal sequence of electrical activation and recovery in the heart is disrupted.[10] Multiple mechanisms may be responsible for arrhythmias in HF. They may arise from abnormalities in impulse formation and/or impulse conduction. Abnormal impulse formation is mainly due to abnormal or enhanced automaticity and triggered activity; while abnormal conduction mainly refers to reentry mechanism. All three mechanisms are related to remodeling of Ca homeostasis.

1.2.1 Abnormal automaticity and enhanced automaticity

Automaticity refers to the spontaneous electrical discharges in the form of action potentials that can originate in a specific group of cells within the heart even in the absence of any external input. Abnormal or enhanced automaticity may result in arrhythmias from diverse pacemaker cells. Sinus bradycardia and tachycardia are common atrial arrhythmias that are associated with alterations in the rate of impulse initiated by the sinus node, the main pacemaker of the heart. Secondary pacemaker activities from the atrio-ventricular node (AV node) or His-Purkinje system may also be enhanced or dysregulated and lead to arrhythmias. In HF, remodeled expression of and/or remodeled regulation of ion channels such as outward delayed rectifying K^+ channel, T type and L type Ca^{2+} channels could lead to abnormal depolarization or accelerated depolarization overdriving

sinus rhythm. Such abnormality could originate even from a region of ventricular cells and forms abnormal/enhanced automaticity. Although automaticity is not responsible for the most rapid arrhythmias, it can precipitate or trigger reentrant arrhythmias.

1.2.2 Triggered activity

Triggered activity refers to the depolarization arising from membrane potential oscillations that occur during or following an action potential. Triggered action potentials may be the source of another triggered response, thus leading to self-sustaining triggered activities and arrhythmias. There are two types of triggered activity: early afterdepolarization (EAD) and delayed afterdepolarization (DAD). For both types of triggered activities, remodeling of Ca homeostasis plays a crucial role by inducing net inward current.

EAD refers to the oscillatory potentials that occur during the plateau phase or late repolarization phase during action potential. A net inward current of L-type Ca window current is responsible for the generation of EADs. This current occurs when the channel undergoes a transformational change from inactivated to closed and then to opened states. Thus, Ca channels that inactivate during the action potential upstroke may reopen as the action potential repolarizes toward the voltage range of L-type Ca window current. In HF, action potential prolongation resulting from a decrease in outward current and/or an increase of inward current is frequently observed. This remodeling facilitates the evocation of window currents and the formation of EADs.

DAD induced triggered activity occurs after full repolarization. Initiation of DAD is mainly associated with cytoplasmic Ca overload that can result from a variety of physiological and pathological conditions, such as β-adrenergic stimulation, hypertrophy and ischemia. In HF, Ca

overflow from an overloaded sarcoplasmic reticulum (SR) may be the main cause for increased intracellular Ca concentration ($[Ca^{2+}]_i$), thus inducing Ca overload.[11] High intracellular Ca initiates a transient inward current (I_{Ti}) that depolarizes membrane potential, and when it reaches the threshold for activation, DADs are elicited. This inward current is mainly composed of the net current from a membrane exchanger: Na/Ca exchanger (NCX) while pumping out one Ca^{2+} with three Na^+ into the cytoplasm. A Ca-dependent nonspecific ion channel also slightly contributes to this current.[12]

1.2.3 Reentry

Reentry arrhythmia is the circulation of the cardiac impulse around an obstacle, leading to repetitive excitation of the heart at a frequency that depends on the conduction velocity and the perimeter of the obstacle. Historically, reentry has been classified as either anatomical or functional. Anatomical reentry is defined when there is a clear relationship between the reentry pathway and the underlying tissue. Functional reentry occurs where there is no obvious connection to the tissue structure. Both reentries occur when an activation wavefront is blocked by a ring-like region of tissue and is forced to propagate around it. This unexcitable region of tissue could be an anatomical structure such as a scar or fibrosis. The path around the unexcitable obstacle should be long enough so that the revolution time could exceed the refractory period time of the tissue, and the impulse could reenter the originally excited area and form the reentry circle. Thus, the occurrence of reentry requires that the path-length is greater than the wavelength.[13, 14] Wavelength is defined in Equation 1.1.

$$\text{Wavelength} = \text{Conduction velocity} \times \text{Refractory period} \quad (1.1)$$

Another requirement for reentry is unidirectional block. It assures that the wave does not propagate around both sides of the unexcitable obstacle in the same time course, which could reduce the path-length and extinguish both waves through collision. Moreover, trigger excitation sometimes is needed to evoke reentry. Programmed electrical stimulation can be used to induce trigger excitations in the reentry studies. The idea of programmed electrical stimulation (PES) was first proposed by Durrer group [15] and Coumel group [16] independently, which was later extended for the study of ventricular arrhythmia. In HF, focal activations play the role of triggers to initiate reentry arrhythmias.

1.3 Arrhythmic substrates

The development of arrhythmia typically requires complicated arrhythmic factors. It has been postulated that arrhythmia occurs under a particular combination of arrhythmic substrate, triggers and modulators.[17] Two main requirements are needed to initiate reentrant arrhythmias: the formation of a unidirectional block pathway and wavelengths short enough to assure the propagation along this pathway. Arrhythmic substrates appear during pathological conditions in which significant structural, mechanical and electrophysiological remodeling occurs. Typical arrhythmic substrates include conduction remodeling, repolarization, electrical or mechanical dynamic instability, amplification of heterogeneity and dysfunctional Ca cycling. Detailed mechanism of each substrate will be discussed below.

1.3.1 Conduction

The spread of electrical activation through the normal heart is a discontinuous process.[18] This discontinuous conduction is affected by several factors including the underlying architecture of the myocardium, the rate and magnitude of rise of the inward currents and the excitation threshold. Abnormal conduction can be involved in several arrhythmogenic mechanisms.

Slow conduction is a key promoter for the initiation of reentrant arrhythmias. In healthy hearts, conduction velocity is too rapid to accommodate a reentrant circuit within the atrium or ventricle. Reduction of conduction velocity results in the shortening of wavelength and could evoke arrhythmias when a unidirectional block forms. Three different mechanisms cause conduction slowing in HF. Connexin 43 (Cx43) is a hemichannel protein that is mainly located at intercalated disc. Cx43 can form channel-like structure called gap junctions that provide the primary means of electrical continuity between myocytes.[19] Reduction and lateralization of Cx43 in HF result in decreased internal resistance[20], thus leading to slowing conduction. Conduction also slows down when amplitude of plasma membrane depolarization current deceases or excitation threshold increases.

Conduction heterogeneity also increases the chances of arrhythmogenesis. In the heart, the fiber orientation rotates continuously through the thickness of the ventricular wall and is non-uniform in planes parallel to the epicardial surface.[21] Conduction of excitations along fiber orientation is faster than that in the perpendicular direction due to gap junctions at the intercalated disks.[22] This is known as axial anisotropy. Increased anisotropy would facilitate the initiation of arrhythmia as it could contribute to the formation of the unidirectional block loop.

Furthermore, upstroke velocity of conduction also affects arrhythmia initiation. Upstroke velocity is a determinant of excitability. Rate and magnitude of inward currents decide the upstroke velocity and activation distance of a propagating impulse. In cardiomycoytes, this inward current

mainly consists of a Na current. Different upstroke velocity determines whether unidirectional block is formed. Normal tissue can activate resting muscle up to a certain distance. In failing hearts, when the excitable wave propagates along a piece of gradient impaired tissue, the activation distance shortens as the excitability progressively decreases and eventually dies out at the most severely depressed region even if the length of this region is less than the normal activation distance. The wave from retrograde direction might propagate through the most severely depressed region when this region is shorter than normal activation distance, thus forming the unidirectional block.

1.3.2 Repolarization

Action potential represents the net electrical activity of a group of membrane ion channels. Repolarization in human heart is largely attributed to the rapid and slow K^+ currents, L type Ca current, Na/Ca exchanger current, I_{KATP} and I_{k1} current. Remodeling of repolarization contributes to in different arrhythmogenesis mechanisms.

As discussed previously, two main conditions are needed for the initiation of reentrant arrhythmias: unidirectional block and short wavelength to assure the reentry to ensue around it. The remodeling of repolarization actually contributes to both conditions.

Clinically, either prolongation or reduction of APD due to repolarization remodeling has a significant relevance for arrhythmias. APD prolongation is a hallmark of HF that is attributed mainly to remodeling of K currents. Reduction of APD could occur in tissue experiencing ischemia or pathological condition resulting in strong parasympathetic stimulation. Clinically, remodeling of repolarization could be measured by ECG and is quantified by the parameter known as QT interval. Both long QT syndrome[23] and short QT syndrome[24] are recognized to be associated with

increased risk of ventricular arrhythmias and sudden cardiac death. Prolongation of APD along with other factors that facilitate the initiation of triggered activities is the major arrhythmogenesis mechanism for long QT syndrome (torsade de pointes arrhythmias for example). Reduction of APD is associated with the reduction of refractory period, which in turns shortens the wavelength.

1.3.3 Dynamic instability: alternans

Cardiac alternans is another important arrhythmogenic substrate that has been recognized to predict and is associated with arrhythmias development over the course of decades.[25] Cardiac alternans refers to mechanical (contractile) electrical (repolarization) oscillations that occur every other beat.

Association of dynamic repolarization alternans with arrhythmogenesis started with the observation of beat-to-beat changes of T-wave morphology from ECG recordings. This T-wave alternans is thought to reflect cyclic changes of APD that is known as APD alternans or repolarization alternans. APD alternans occurs due to instability in the kinetics of membranes channels that govern cardiac action potential. Since the recovery time of each channel varies, APD of proceeding beat is dependent on the time period between the recoveries of the channels from the previous beat to the onset of the next one. This period of time is known as diastolic interval (DI). As the heart rate increases, APD shortens to preserve the coronary flow and DI. The relationship between APD and DI can be plotted as a restitution curve. Repolarization alternans generated by the dynamic perturbation of APD or DI is amplified by interactions between them. This process can be depicted by a cobweb diagram plotting APD against the preceding DI (Figure 1.1).[26] Basically, when the heart is paced at a fixed cycle length, APD and DI are directly related to the basic cycle

length (CL) as shown in Equation 1.2 that shows that APD of the current beat depends on the DI from the previous beat.

$$CL = APD_n + DI_{n-1} \quad (1.2)$$

The relationship in Equation 1.2 can be illustrated by a straight line with slope of -1 as shown in Figure 1.1. The slope of the restitution curve represents the electrical stability of the myocardium.[27, 28] Restitution curve with a steep slope (>1) is inherently unstable as small changes in DI are translated into large and alternating shifts in APD. As seen in Figure 1.1, a small perturbation of DI of beat 0 started at * leads to the next beat (beat 1: in purple) with a relatively short APD (point a), and results in a prolonged DI of beat 1. This DI then creates a longer APD of beat 2 (in yellow) shown at point c, which in turn causes an even shorter DI at point d. This perturbation is amplified in this pattern until typical alternans formed as the figure depicts. The resulting alternans have been proven to be closely associated with arrhythmias.[29] Alternans resulting from steep restitution can significantly amplify repolarization gradients that can then facilitate formation of unidirectional block, thus eliciting reentrant excitation even in absence of structural heterogeneities. Under baseline condition, the spatial gradient is the same over all regions; however, as heart rate increases, the depolarization of neighboring region starts to alternate with an opposite phase and forms a unidirectional block. During this process, the orientation of repolarization undergoes nearly a complete reversal in direction from beat to beat making the heart vulnerable to the initiation of reentrant arrhythmias. Moreover, repolarization alternans could also increase dynamic wave instability, enhance wave break and promote degeneration of VT to VF.[28-32]

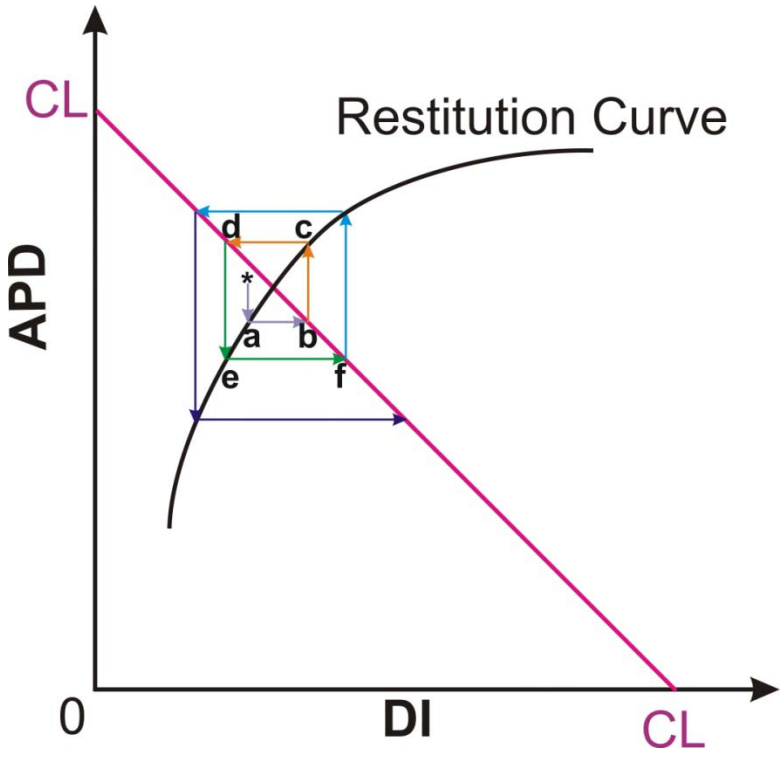

Figure 1.1 Cobweb diagrams of repolarization alternans.

1.3.4 Heterogeneity or dispersion

As previously discussed, one of the arrhythmogenesis mechanisms associated with the alternans is the amplification of repolarization heterogeneity. As an important arrhythmic substrate, heterogeneity not only results from repolarization dispersion but also from non-homogeneous conduction.[14] Transmural (between subendocardium and subepicardium) and spatial (focus more on the surface of ventricular free wall) heterogeneities have been investigated in cardiac arrhythmogenesis.

Transmural heterogeneity

Multiple sources of heterogeneity exist in ventricular myocardium that may have functional, structural or dynamic basis. One source is due to the intrinsic electrophysiological difference between myocytes. A typical example is the transmural heterogeneity through the ventricular free wall. The ventricular free wall consists of three functionally and electrophysiologically distinguishable groups of myocytes: endocardial, midmyocardial and epicardial myocytes. These distinct cells compose the three layers of ventricular wall (subendocardium: endo; midmyocardium: mid and subepicardium: epi) that differ principally with respect to repolarization characteristics, leading to different APD. As electrical impulse propagates from the endo to epi layer under normal conditions, repolarization heterogeneity assures the optimized timing for the contraction of the heart. However, amplification of transmural heterogeneity is closely associated with reentrant arrhythmias as it could facilitate the formation of unidirectional block.

Spatial heterogeneity

Heterogeneity could exist not only through the transmural pattern but may also be exhibited between left and right ventricles[33, 34] or across different regions of the ventricular free wall. Such spatial heterogeneity can be attributed to structural change under different pathological conditions such as acute myocardial ischemia, chronic myocardial infarction and fibrosis. Spatial heterogeneity, e.g. between cardiac base and apex, is reported to largely occur during cardiac dysfunction due to regionally distinct stimulation or regulation [35][35] such as during mechanical stress.

1.4 Ca handling

Ca handling is crucial in cardiac function under normal physiological and pathological conditions such as HF. A major role of cardiac Ca handling is to regulate heart contractions that are activated by electrical signals known as electrical-contraction (EC) coupling. Intracellular Ca dynamics is regulated by a variety of Ca regulatory mechanisms including key Ca handling proteins such as L type Ca channel, Ryanodine receptor (RyR), sarco(endo)plasmic reticulum Ca2+-ATPase (SERCA) and Na-Ca exchanger (NCX). Moreover, it also responds to and participates in different stimulations through distinct signaling pathways. In HF, abnormal Ca dynamics can result from a variety of causes and be affected by different signaling pathways. Defective Ca handling not only affects ventricular mechanics but also affects electrophysiology. Intracellular Ca and action potential are intricately linked by a variety of Ca medicated channels and transporters. Thus, Ca handling is also an important arrhythmogenic substrate and its investigation will bridge its related signaling pathways to arrhythmogenesis effects.

1.4.1 Ca and EC coupling

Ca is a highly versatile intracellular signal that can regulate many different cellular functions, such as cell proliferation and EC coupling [3, 36]. Basic EC coupling in ventricular cardiac myocytes begins with the action potential. The initial depolarization of the plasma membrane activates voltage-gated L-type Ca current, which triggers calcium release from SR mediated by local Ca induced Ca release (CICR) through Ca channel - ryanodine receptor-2 (RyR2)[37] and Ins(1,4,5)P3Rs[4]. Both channels are sensitive to Ca[4]. This process elevates cytosolic Ca level, which causes Ca binding to the myofilaments protein troponin C and make contraction. The

contractile force in myocardium is determined by the amplitude of the Ca transient.[38, 39] Many calcium-signaling effectors (such as calmodulin, troponin C), calcium-sensitive enzymes (such as Ca/calmodulin-dependent protein Kinases (CaMK)) and transcription factors are also activated, driving events such as gene transcription to regulate cellular functions. During relaxation, Ca^{2+} must be transported out of the cytosol, thereby allowing Ca^{2+} dissociation from troponin and deactivation of the myofilaments. The decline of intracellular calcium concentration may be mediated in following ways: 1) sarco(endo)plasmic reticulum Ca^{2+}-ATPase (SERCA2a), 2) sarcolemmal Na-Ca exchanger 1 (NCX1), 3) sarcolemmal Ca-ATPase, and 4) mitochondrial Ca^{2+} uniporter. Under normal conditions, SERCA takes up about 70% of the Ca involved in the Ca transient back into SR, whereas nearly 30% is extruded via NCX from the cardiomyocyte [40],. The activity of SERCA2a is regulated by the binding of phospholamban (PLB)[41]. In its non-phosphorylated form, PLB inhibits SERCA2a activity. The amount of Ca that enters the cell with each steady-state beat must equal the amount that is extruded. Thus the integrated Ca entry via I_{ca} is about the same as that extruded via NCX, and the amount released by the SR is the same as that taken back up.[2] Given that both Ca entry via I_{ca} and Ca extrusion via NCX cause inward current, Ca movements are strongly coupled to electrophysiological effects.

1.4.2 Ca remodeling in HF

Impaired Ca homeostasis has been characterized to play a crucial role in the onset and progression of cardiac hypertrophy and HF.[3] In HF, there is typically a down-regulation of SERCA2a and up-regulation of NCX function.[42, 43] Both of these effects tend to shift Ca out of the cell and reduce SR's Ca content. Bers DM et al. also found that a large increase in NCX function can compensate for a moderate decrease in SERCA2a function in HF [43]. Most HF studies have

found relatively unaltered L type Ca channel density in ventricular myocytes. However, some have suggested that there may be a reduction in the number of Ca channels while at the same time there is a higher activity per channel; this effect could also affect the membrane potential [44]. Calcium transients are small in HF and there may be a greater integrated Ca influx due to less Ca-dependent inactivation of L type Ca channels. This property may then affect the intracellular Ca concentration and SR Ca concentration, which furthermore affects overall Ca signaling.

While the majority of calcium-regulatory proteins studied in HF were focused on LTCC, RyRs, NCX, SERCA, PLN and CaMK, a great number of other calcium-sensitive or calcium-dependent effecter proteins and signaling pathways may also affect electrophysiological properties and are implicated in calcium signaling and regulation of calcium homeostasis. Investigations of these proteins and the role of Ca in these signaling pathways will help to complete the understanding of calcium handling and pathways in HF and provide potential therapeutic targets.

1.4.3 Ca and arrhythmia

Ca has been reported to associate with a variety of mechanisms of arrhythmias. It has been discussed in the previous section that Ca plays a key role in the arrhythmias resulting from abnormal automaticity and triggered activity. Furthermore, it associates and promotes electrical arrhythmic substrates and contributes to arrhythmia.

Ca and impulse propagation

Both theoretical and experimental models have suggested that under specific circumstances the L type Ca current and intracellular Ca concentration could affect cardiac conduction.[45-47] Accumulation of intracellular Ca could initiate the inactivation of L type Ca channel L type Ca currents of the myocyte at the region of a current-to-load mismatch is crucial for the impulse conduction. Moreover, intracellular Ca concentration can regulate gap junction conductance, thus affecting excitation propagation.

Ca alternans and repolarization dynamic instability

Like repolarization, intracellular Ca cycling is also a dynamic active process. It has been reported that repolarization alternans is driven by the Ca oscillations.[48-50] Underlying mechanism may be due to several key membrane currents that govern action potential activity also participate Ca cycling in cardiomyocytes, such as L-type Ca current, NCX current and non-selective Ca-dependent current. Intracellular Ca transient alternans have been related to the amount of Ca released from the SR, which is determined by several factors including the trigger (L type Ca current), the SR load, the metabolic and phosphorylation state as well as the sensitivity of RyR. The amount of Ca released during any beat depends on the Ca influx during the preceding action potential. When SR Ca storage ability is diminished, APD determines concomitant Ca release. The acute changes of $[Ca^{2+}]_i$ result from the alteration of Ca release turns out to affect the membrane currents and thus provide a feedback mechanism that controls APD of the concurrent beat.

1.5 Murine model for arrhythmia studies

Murine hearts have been suggested to offer a versatile and robust model for cardiac studies especially for the human ventricular arrhythmias. Mice share a great degree of genetic homology with human. Murine model are small, inexpensive and easily maintained and reproducible. The low cost of technology and feasibility for genetic engineering in this species make it a convenient tool for cardiac studies. Transgenic and knockout murine models have dramatically widened investigation on the role of target proteins in specific signaling pathways that have helped to facilitate the understanding of mechanisms of arrhythmia initiation and maintenance.[51-53]

Electrical similarities and differences between humans and mice

The significant difference between human and murine lies in the properties of ionic currents responsible for action potential repolarization as shown in Figure 1.2. Repolarization in human heart is largely attributed to the rapid and slow K currents, mainly I_{kr} and I_{ks}. In mice, it is the fast and slow transient outward K currents named $I_{to,f}$ and $I_{to,s}$ which take the dominant role for the ventricular repolarization. Such difference results in the absence of the plateau phase and a shorter action potential duration (APD).

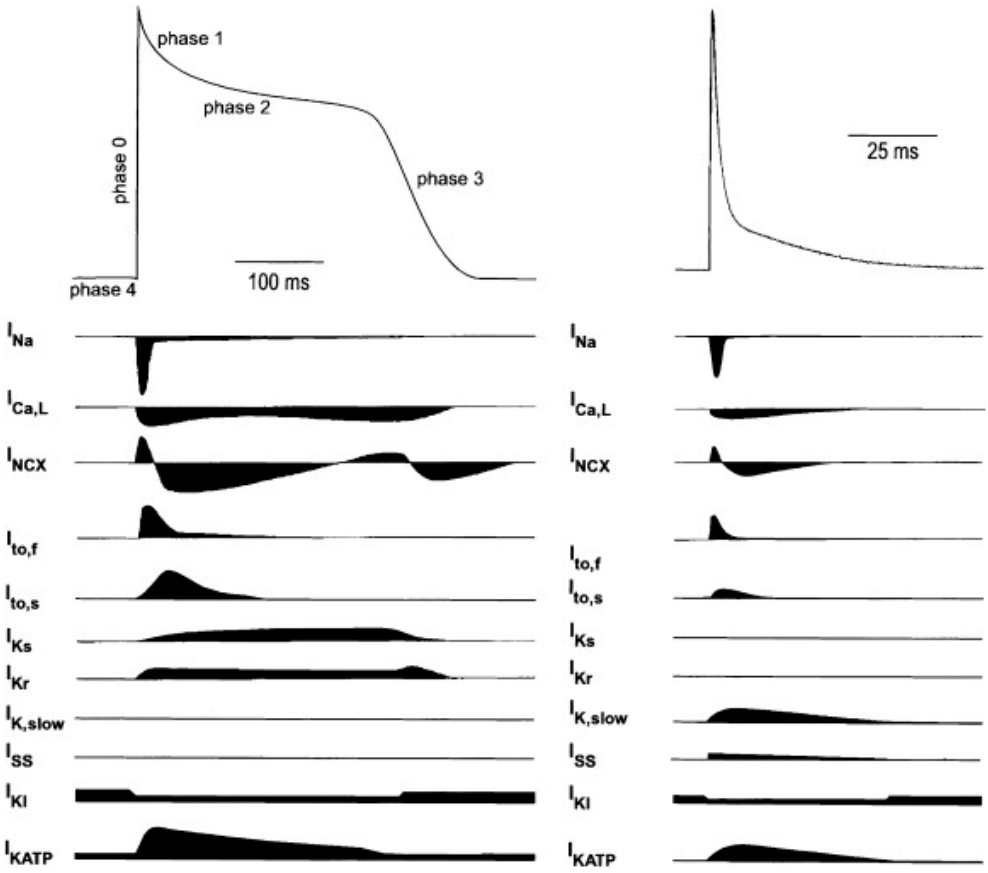

Figure 1.2 Ionic currents underlying human and murine ventricular action potentials. From Nerbonne et al.[54]

Despite the electrical difference and notable difference in the size and basal heart rate, human and murine hearts share a number of key features that make mice an eligible model for arrhythmia studies. In both species, ventricular action potential share a rapid depolarization phase attributable to Na current carried by the voltage-activated Na channel.[55] I_{KAPT} and I_{K1} play important role in repolarization and during diastole in both humans and murine.[56] Despite a significantly shortened APD, the refractory period in mice still follows a common pattern with the human case: the refractoriness precedes complete repolarization and this qualifies the murine model

for the study repolarization as arrhythmic substrate. Furthermore, determinates of conduction regulation in both spices are identical.[57] Due to great genetic homology, it is important to notice both humans and mice share similar functional and proliferative regulating signaling pathways and makes it convenient to study the arrhythmogenic role of specific proteins or signaling pathways.

1.6 Motivation and scope of dissertation

Ca is critical in both the electrical and mechanical properties of cardiac myoctyes, and much is known about ionic currents and the normal excitation-contraction coupling process. However, in HF, there are significant alterations in how cardiac Ca is regulated through different stimulatory and signaling pathways. These alterations are critical for dictating contractile dysfunction and facilitating the arrhythmias that are characteristic of heart failure directly or associated with other electrophysiological arrhythmic substrates. A numbers of studies focused on key regulatory proteins such as L-type Ca channel, RyR, SERCA, PLB and NCX. Yet, the signaling pathways that regulate Ca handling upstream are not clearly elucidated. These pathways could be severely impaired or modified in HF, thus solving the nature of these intricate and dynamic interactions promises to be an important area of research for a better recognition and understanding of the nature of Ca and arrhythmias. These investigation would then further bridge dysfunction of different signaling pathways result from either acute stimulations or genetic modifications with arrhythmic effects in HF.

In this dissertation, I aim to investigate the remodeling of Ca handling in different signaling pathways that underlie different damages form HF, and bridge these remodeling to arrhythmia effects. Here I studied the role of proline rich tyrosine kinase 2 (PYK2), which is a key protein in

stress-activated signaling pathway; dystrophin for mechanical stimulation signaling pathway and β adrenergic receptor signaling pathway in HF.

I first developed a dual optical mapping system combined with monophasic action potential recording technique to build up a platform that promises to not only study the dynamics of Ca on the whole heart or tissue level but also the association of Ca with electrical arrhythmic substrates and eventually to explain the nature and mechanism of impaired signaling pathways to facilitate arrhythmias in HF. For these purposes, I introduced genetically manipulated murine models and also applied experiments with human heart tissue.

Chapter 2 contains a description of the dual optical mapping system. Chapter 3 focuses on role of Ca activated PYK2 in arrhythmogenesis. Chapter 4 will discuss regional remodeling of Ca handling under mechanical stretch in an mdx mouse heart model. Chapter 5 describes how different β adrenergic subtype receptors behave and facilitate arrhythmogenesis in HF. Finally summary and future direction are presented in Chapter 6.

Chapter 2

Designing a Dual Optical Mapping Platform for Transmembrane Potential and Ca Transient detection

2.1 Abstract

Fluorescence imaging has revolutionized the investigation of cardiac electrophysiology. Currently, single fluorescent parameter imaging is most commonly used. Given the growing emphasis on the simultaneous imaging of more than one cardiac variable and the importance of Ca in cardiac electrophysiology, I have designed a dual optical mapping system that allows for the simultaneous measurement of both transmembrane potential (V_m) and intracellular Ca transient (CaT) from the same region of a heart. This system can be rapidly set up, permits dichroic imaging separation, dual-rate imaging, and offers high temporal-spatial resolution. In addition, the system is applicable to any two-camera measurement. Experiment on intact mouse hearts suggested accuracy and reliability on V_m and CaT morphology, time scale and the time relations between these two dynamic parameters.

Contents of this chapter were published in Journal of Visualized Experiments[58] and reprinted with the permission of the publisher.

2.2 Introduction

Synchronous contraction of the heart depends on regular propagation of electrical impulse by the flow of local electrical currents between excited and resting cells.[59] Remodeling of normal propagation patterns and electrical parameters of the myocardium is closely associated with arrhythmias. Investigations of the mechanism underlying arrhythmias have relied on the visualization of activation spread. Although much has been learned regarding the ionic basis of cardiac action potential using intracellular microelectrodes, single cell impalements cannot be used to record action potentials from a large number of recording sites simultaneously. Visualization of activation, conduction velocity, action potential duration, and other parameters at a myriad of sites cannot be achieved using cellular studies or surface electrogram techniques with low spatial resolution, but is solved by optical mapping.[60-62] EC coupling is characterized by action potentials and intracellular calcium dynamics; therefore it is critically important to map both V_m and CaT simultaneously from the same location. [25, 35, 60, 63] However, current techniques based on surface unipolar and bipolar electrograms cannot be practically applied for the studies of non-electrical parameters such as Ca. Optical mapping, on the other hand , makes it feasible to simultaneously record V_m and CaT dynamics with high temporal and spatial resolution by using proper intracellular Ca and voltage probes.

Mouse heart is a popular model used for cardiovascular studies due to the low cost technology available for genetically modifying this species as discussed in Chapter 1. Cardiovascular physiological phenotyping of the mouse heart could be easily done using fluorescence imaging that employs various probes for V_m, CaT, and other parameters. Simultaneous optical mapping from Langendorff perfused mouse hearts has the potential to elucidate mechanisms underlying heart

failure, arrhythmias, metabolic disease, and other heart diseases. In this chapter, I designed a voltage-Ca dual optical mapping system in combination with monophasic action potential (MAP) recordings on mouse heart to build an efficient platform for studying the interaction and association of cardiac electrical signals and Ca dynamics as well as their roles in arrhythmogenesis. I will present the instrumentation setup and experimental conditions. Consistent optical recordings obtained with this system illustrate that simultaneous optical mapping of Langendorff perfused mouse hearts is both feasible and reliable.

2.3 Material and Methods

2.3.1 V_m and CaT Fluorescent Dyes

Optical mapping uses different fluorescence probes to stain cardiac tissue. Visualization of different parameters relies in the registering changes in optical dye properties. By using photo-detectors with appropriate optical setup, fluorescent signals could be captured and carefully interpreted. Different probing mechanisms of fluorescent dyes require different design on optics and signal acquisition.

Voltage sensitive dye

Voltage sensitive dye is a group of dyes that could bind to the cell membrane. Figure 2.1 showed an example of a typical voltage sensitive dye: di-4-ANEPPS. After embedding in the membrane, optical properties of voltage sensitive dyes such as light absorption or emission fluorescence vary when membrane potential changes. This correspondence change is linear and occurs on the microsecond level, which ensures the accuracy of voltage sensitive dyes representing cardiac electrical activities. Briefly, as the membrane depolarizes, the emission spectrum shifts

towards the direction of a shorter wavelength, so that a decrease in fluorescence (ΔF) from background fluorescence (F) would be observed. By collecting the sum of fluorescence of wavelength longer than a specific value, such decrease could be maximally detected and represent the membrane potential change (Figure 2.2). To maximize the change of fluorescence captured, it is best to choose this filter wavelength at a steep portion of the spectrum. In this way the electrical signals from alteration of membrane potential could be expressed as ΔF/F.

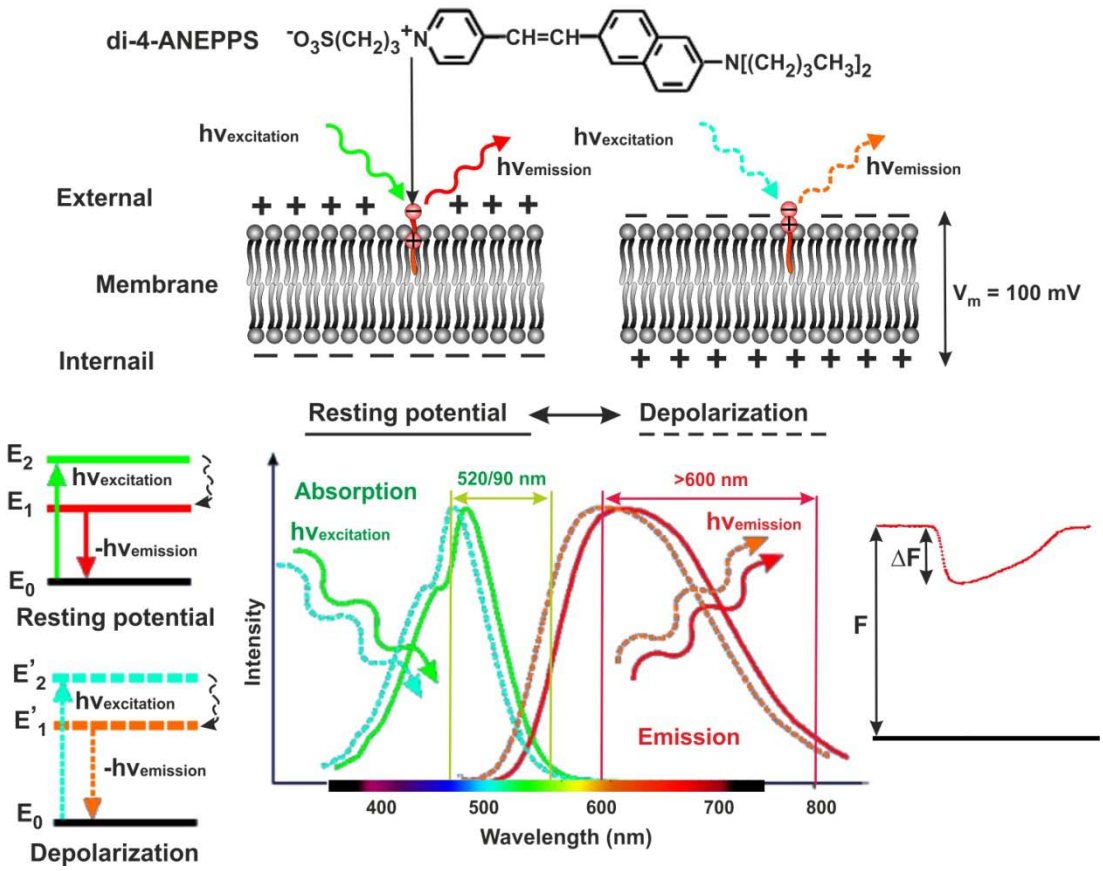

Figure 2.1 Voltage sensitive dye. Spectrum property and voltage sensing mechanism of di-4-ANEPPS. When the dye is embedded in the outer side of the membrane, it could be excited at a specific wavelength. During depolarization, the emission spectrum shifts towards direction of short wavelength, thus generating a decrease of total fluorescence (ΔF).

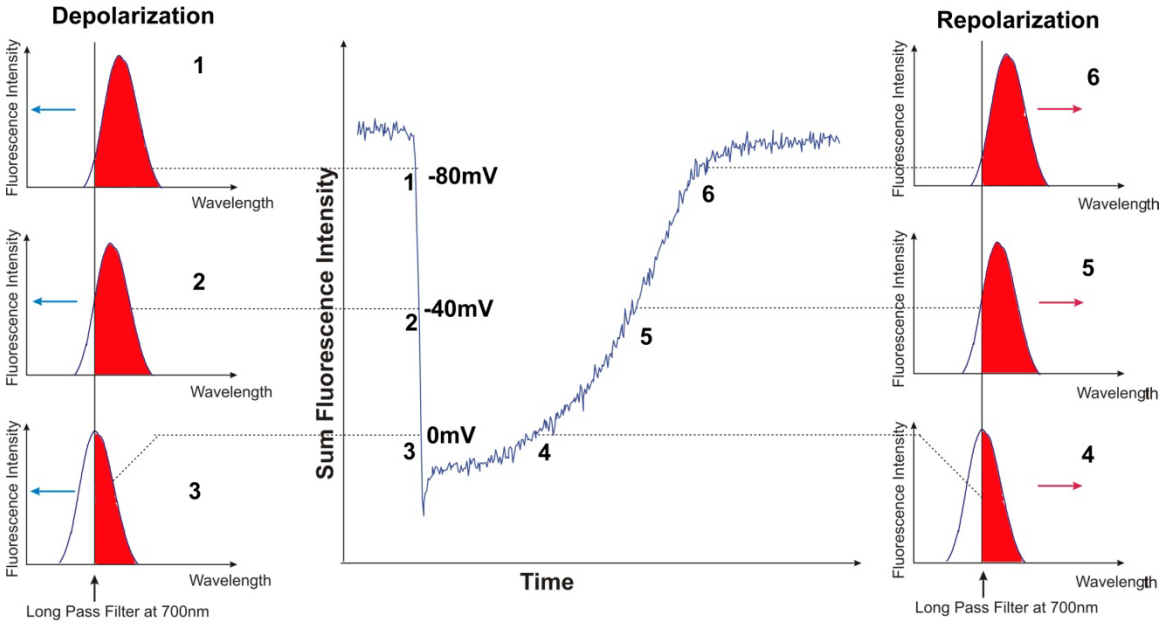

Figure 2.2 Probing mechanism of voltage sensitive dye. Emission spectrum shifts towards short wavelength as V_m depolarized. When V_m changes from -80 to -40 mV, the sum intensity of fluorescence decreases as well, as depicted on the right side. Fluorescence intensity dynamics represents the membrane potential change. Real time sum intensity is plot out and action potential can be visualized.

Spectral properties of RH-237 and Rhod-2AM

Many aspects need to be considered in the choice of dye for a given experiment (e.g. how sensitive is the dye to potential changes). For the dual optical mapping system, it is extremely important to differentiate voltage signals and Ca signals effectively, meaning that the emission of both dyes should avoid spectral overlap.

N-(4-Sulfobutyl)-4-(6-(4-(Dibutylamino)phenyl)hexatrienyl)Pyridinium, Inner Salt (RH-237) is a widely used voltage sensitive dye whose molecular structure is shown in Figure 2.3. Its excitation peak wavelength (Ex) is around 528 nm and emission peak wavelength is around 782 nm (It is reported to be 782 nm when diluted in methanol solution. In cell membranes, spectra of styryl dyes

are typically blue-shifted by as much as 80 nm for emission).[64] The long emission spectral peak of RH237 makes it a good candidate for multiple probe imaging.

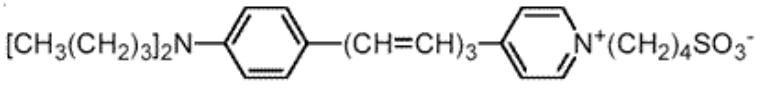

Figure 2.3 Molecular structure of RH-237.

Xanthylium, 9-[4-[bis[2-[(acetyloxy)methoxy]-2-oxoethyl]amino]-3-[2-[2-[bis[2-[(acetyloxy)methoxy]-2-oxoethyl]amino]phenoxy]ethoxy]phenyl]-3,6-bis(dimethylamino)-, bromide, also known as Rhod-2 AM was selected as probe Ca for couple of reasons. The molecular structure is shown in Figure 2.3. Its excitation/emission is 556nm/576nm. The emission fluorescence spectrum is easy to separate from RH-237.[65] The spectral overlap does not affect the accuracy of the signals. Furthermore, its excitation wavelength is close to RH-237, which makes the light source for excitation of both probes more effective.

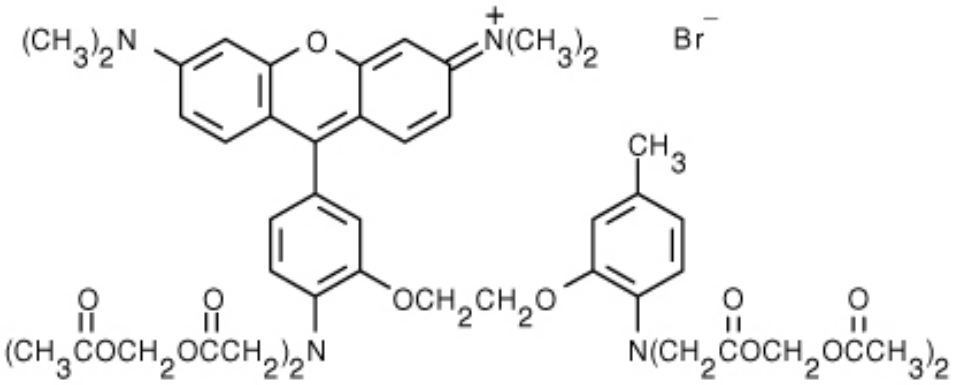

Figure 2.4 Molecular structure of Rhod-2 AM.

Optical modalities are determined according to the different properties of dyes. Based on the spectral emission, a dichroic mirror of 635nm cut off was used to separate fluorescence signals. For RH237, a 700 nm long pass filter is applied, so that the maximum ΔF can be collected at every 100 mV alternation of membrane potential. Rhod-2 AM has a different mechanism for probing intracellular $[Ca^{2+}]_i$ The emission fluorescence intensity fluctuates only when $[Ca^{2+}]_i$ changes. Without spectral shifting, the peak wavelength of emission is relatively stable, thus a band pass filter of 590±15nm is used to collect the Ca fluorescent signals.

The feasibility of using these two dyes in dual optical mapping can be evaluated by the degree of spectral overlap errors. The error from spectral overlap of the two dyes could be calculated as the amplitude of the signal error (fake signal collected due to the other probe) normalized to the amplitude of its real signal as shown in Formula 2.1 and 2.2. The errors in spectral overlap for both dyes are reported as being less than 5%[65] and proved to not affect outcome in our experiments.

$$\%error[Ca^{2+}]_i = \frac{error[Ca^{2+}]_i}{[Ca^{2+}]_i} 100\% \quad (2.1)$$

$$\%errorV_m = \frac{errorV_m}{V_m} 100\% \quad (2.2)$$

2.3.2 Dual Optical Mapping Setup

Light source

The light source was selected according to the preparation type, side of the imaging area, wavelength and desired signal to noise ratio. Four types of light sources are currently being used in optical mapping: tungsten-halogen (TH) lamps, short arc lamps, lasers and light emitting diode (LED). TH lamps and LED have a moderate light intensity and a flat spectrum in the visible range, which provides flexibility in choosing the excitation wavelength. TH lamps generate low noise level while LEDs are usually low cost. Arc lamps have a flat spectrum in the visible range but provide strong intensity. Lasers, on the other hand, only emit light at discreet wavelengths.

Considering the effects of dye bleaching, photodynamic tissue damage that might be caused by a strong intensity light source as well as the wide band wavelength of excitation needed in the experiment, halogen lamp and LED are chosen as the light sources for the dual optical mapping system.

Focusing Optics

To collect and focus the emitted fluorescent signals on the photo detector, lenses are used with the properly design optics. Based on the desired optical magnification, single and tandem lens configurations are used. In a single lens configuration, as shown in Figure 2.5A, when the distance between the lens and photo detector is fixed (f+xi), magnification (M=xi/f) depends on the working distance of the system, in other words, when using the single lens configuration, for a specific field of view, the working distance is fixed. When this working distance is not convenient for conducting the experiment or when the desired magnification could not be achieved from using a single lens, tandem lens configuration is used as shown in Figure 2.5 B. In the tandem lens configuration, magnification can be calculated by the ratio of focal length of two lenses (f1/f2) and is not dependent on the lens separation. However, extension of distance between two lenses would

increase the loss of marginal light rays and lead to vignetting. Tandem lens configuration also provides better light collection efficiency. According to Libbus group, the signal-to-noise ratio of recordings made with the tandem lens configuration was significantly greater than that made with the single lens configuration. Signal-to-noise ratio depends on magnification and numerical aperture (NA) of the lens. For a single lens configuration, there is a linear relationship between the magnification and signal-to-noise, while for tandem lens configuration, different magnifications are obtained with different lens combination therefore resulting in a nonlinear relationship between them.

An important parameter for choosing objective lens is the NA, which in photographic lenses that in an optical mapping setup is given by the F-number, which is equal to 1/(2NA). NA is proportional to the number of photons collected by a lens. Therefore in the mapping system, the lens with smallest F-number or highest NA should be chosen. Microscope lenses with NA ranges from 0.25 to 1.3 provide the best light collection efficiency.

Single lens configuration was used in the dual optical mapping system for the mouse heart preparation (Figure 2.8) and tandem lens configuration was used for human heart preparation (Figure 2.9). The lenses used in the setups are Nikon NIKKOR 55 mm 1:1.4 235052 with NA =0.36 and Nikon NIKKOR 50 mm 1:1.2 384854 with NA=0.42. The choice of lens is also dependent on the size of the photo detector.

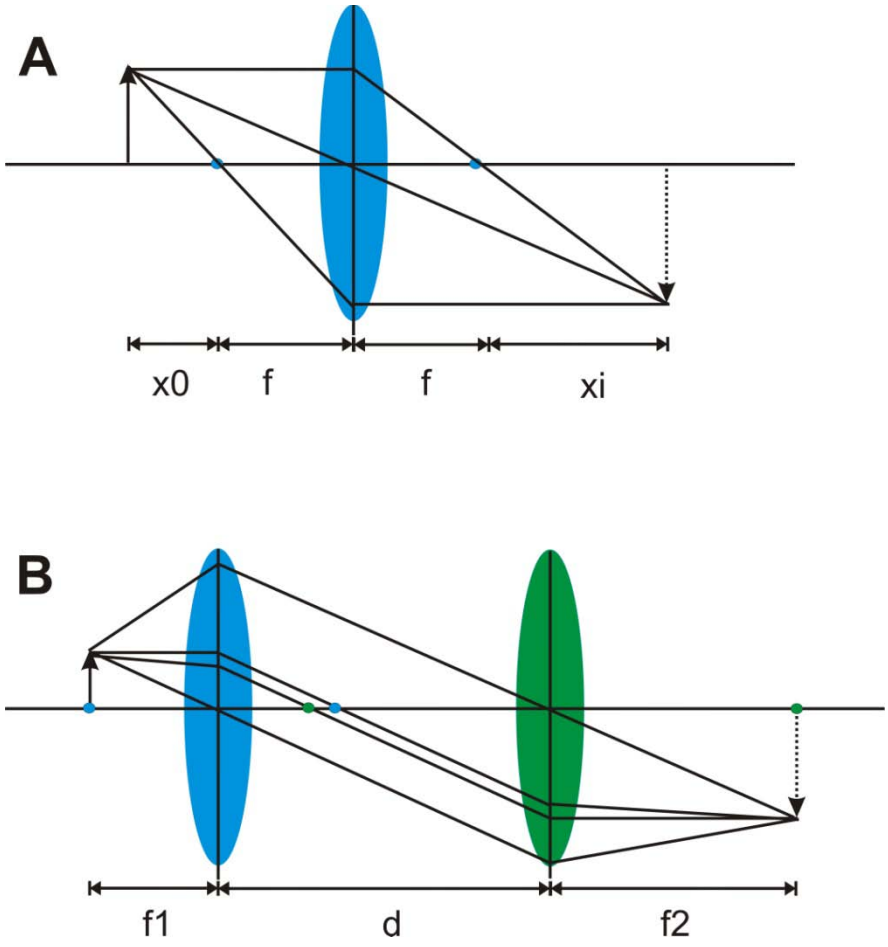

Figure 2.5 Single and tandem lens configuration. A. Single lens configuration, magnification (M) of such configuration depends on focal length (f) and the distance the object is away from the lens. When this distance is fixed, the focal distance is also fixed. B. Tandem lens configuration. M in this configuration is defined by the ratio of length of two lenses (f1/f2) and is not dependent on the lens separation. However extension of d would increase the loss of marginal light rays and lead to vignetting.

Photodetector

Photodiode arrays (PDA), CCD cameras and CMOS cameras are frequently used in optical mapping systems. All camera types consist of two-dimensional arrays of silicon elements that transduce the energy of light photons into electrical charges.

PDA usually offers the highest temporal resolution while CCD camera has the higher spatial resolution. CMOS cameras can be considered in between both sides. It can acquire data fast enough for cardiac electrophysiological investigations while also providing high spatial resolution to visualize and reconstruct the propagation of excitation impulses. I used a MiCAM ULTIMA CMOS camera from SciMedia in our dual optical mapping system. The actual sensor size of this camera is 10 by 10 mm^2 with a spatial resolution of 100 by 100 pixels. It can acquire data up to 3,300 frames per second. For the two-camera setup, the acquisition alternates for each camera, so that the actual temporal resolution for the dual optical mapping system is up to 1,650 frames per second. Data is saved as the structure shown in Figure 2.6. The import of data and separation of voltage and Ca^{2+} signals are based on such a data structure.

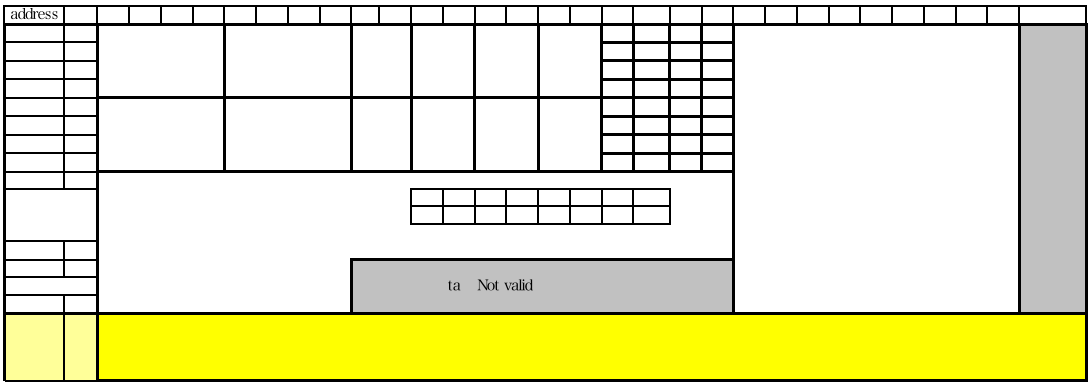

Figure 2.6 Data structure of the acquisition system.

Dual optical mapping system

To precisely align its different components, the whole mapping setup is built on an optical breadboard. Optical rails and other mounting equipment are used. The schematic diagram of the setup is shown in Figure 2.7. Briefly, after staining with both voltage and Ca^{2+} probes, preparation is

excited by the light source with the specified wavelength. The emission fluorescence signals propagate through the tandem lens optics and are separated by the dichroic mirror before they are collected by photodetectors. The acquisition process is aligned with the light source shutter. Both excitation light source and acquisition system are controlled by computer. The detailed description of the setup is as follows.

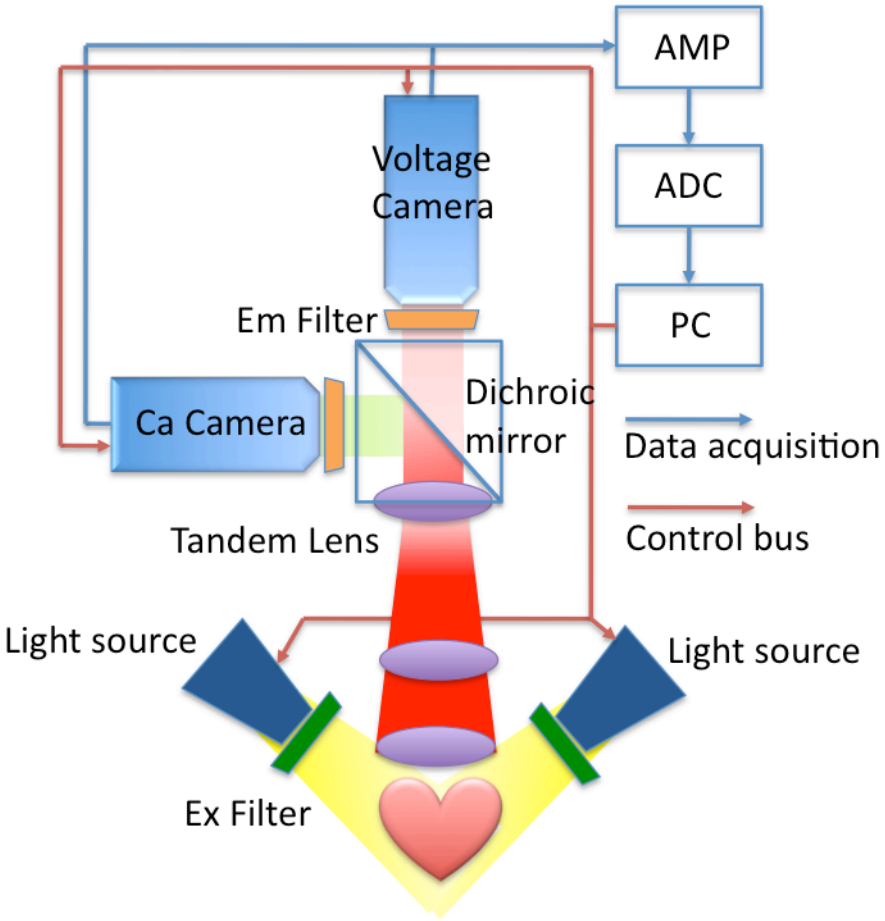

Figure 2.7 Schematic diagram of dual optical mapping setup.

The dual optical mapping apparatus consists of two MiCAM Ultima-L CMOS cameras (SciMedia, Costa Mesa, CA) that have high spatial (100x100 pixels, 230±20 μm per pixel) and

temporal (up to 3,000 frames/sec) resolution. A band-pass filter (590±15 nm, Thorlabs, Newton, NJ) is fixed in front of the designated calcium imaging camera; while, a long-pass filter (>700 nm, Thorlabs, Newton, NJ) is positioned in front of the designated voltage imaging camera. The cameras are arranged perpendicularly to one another by a holder, which contains a dichroic mirror (635 nm cutoff, Omega Optical, Brattleboro, VT). Immediately below the dual camera holder is a lens (Nikon NIKKOR 85 mm 1:1.4 235052), which focuses the emission light coming from the heart onto the dichroic mirror (Figure 2.8). For larger field of view experiments such as with human and rabbit hearts, different magnifications are needed, thus a tandem lens configuration is designed as shown in Figure 2.9 with an adjustable working distance.

The excitation light is generated by a halogen lamp (Newport Oriel Instruments, Stratford, CT; SciMedia, Costa Mesa, CA) and is passed through a heat filter, shutter, and excitation band-pass filter (520±45nm). A flexible light guide directs the band-pass filtered light onto the preparation, and a computer-controlled shutter ensures that the preparation is exposed to light only during image acquisition in order to avoid photo bleaching of the dyes.

Custom made $Ag/AgCl_2$ electrodes for pacing and sensing are installed in the chamber prior to the experiment and placing of the heart. Amplifiers and filters are adjusted to the appropriate levels. Real-time monophasic action potential recording is also combined with the setup to capture acute changes in the experiment that may not be completely recorded by the mapping system.

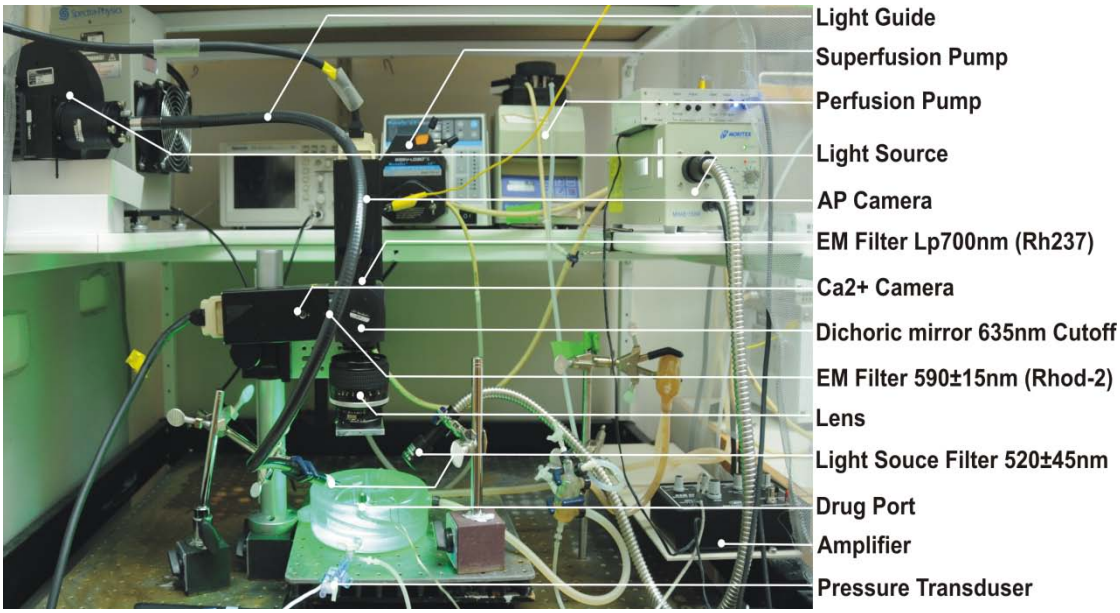

Figure 2.8 Dual optical mapping setup for intact mouse heart preparation.[58]

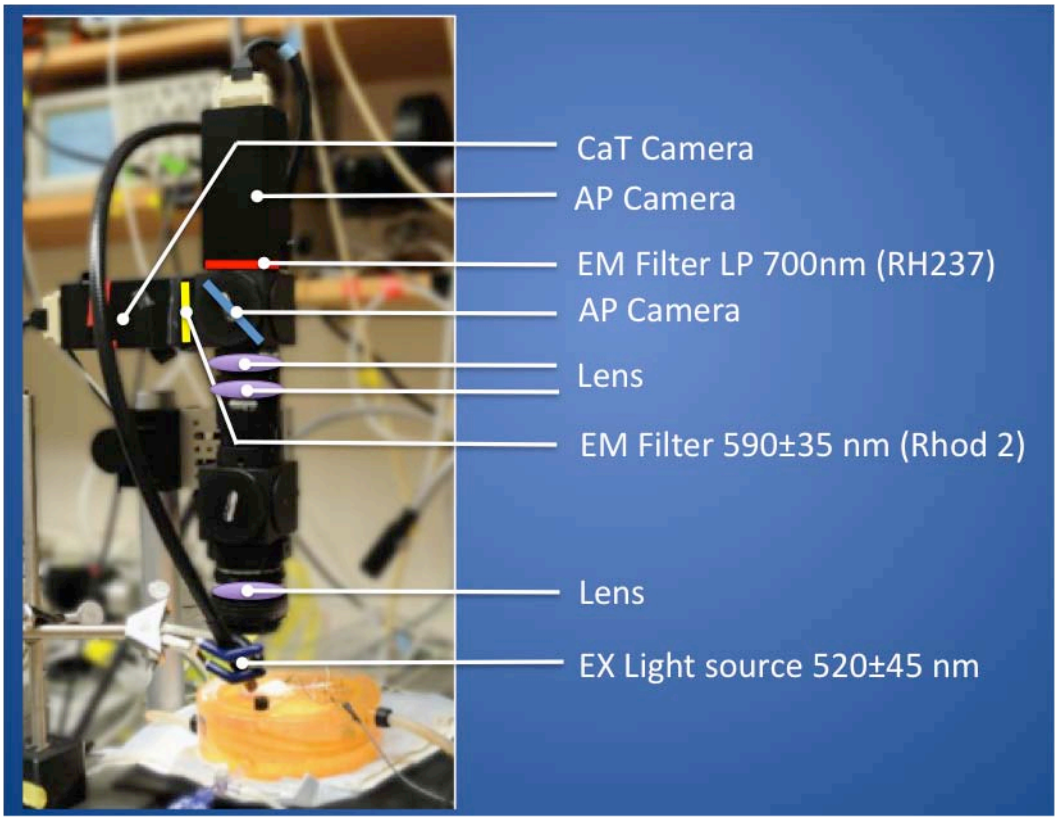

Figure 2.9 Dual optical mapping setup for human ventricular wedge preparation.

2.3.3 Experimental Protocol

A detailed dual optical mapping procedure on Langendorff-perfused isolated intact mouse heart is described in the following section. A brief flow chart is shown in Figure 2.10.

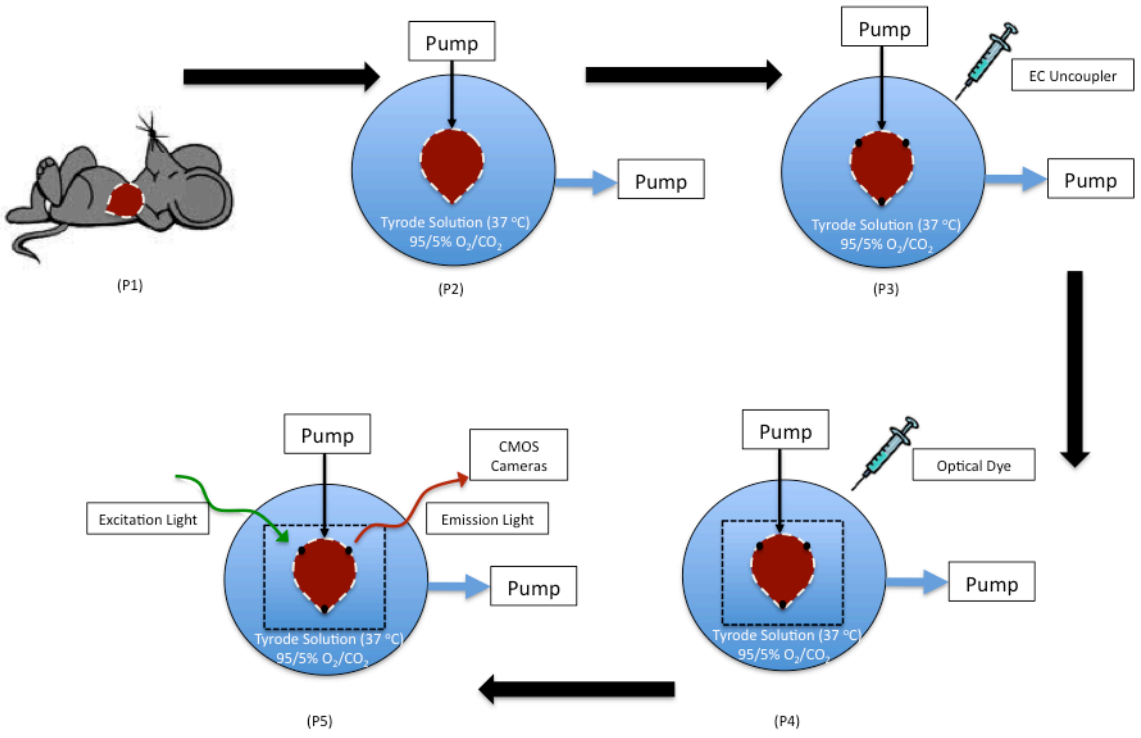

Figure 2.10 Flow chart for experimental protocol.[58]

Part1: Advanced preparation of stock solutions.

1. Prepare stock solutions of Tyrodes' solution (16×) in advance in deionized water and store at 4°C:

    a. Stock I (119.872g/L NaCl, 3.056g/L $CaCl_2$ ($2H_2O$), 5.6g/L KCl, 2.6274g/L NaH_2PO_4, 3.408 g/L $MgCl_2$ ($6H_2O$), (Fisher Scientific, Fair Lawn, NJ));

b. Stock II (26.88g/L $NaHCO_3$, (Fisher Scientific, Fair Lawn, NJ)).

2. Prepare stock solutions of fluorescent dyes. To avoid repeated freezing and thawing, store 30 μl aliquots of both dyes, which corresponds to one experiment, at -20°C:

    a. Voltage-sensitive dye RH237 (Invitrogen, Carlsbad, CA) stock solution, 1.25mg/ml solution in dimethyl sulfoxide (DMSO, Sigma, St. Louis, MO);

    b. Calcium indicator Rhod-2AM (Invitrogen, Carlsbad, CA) stock solution, 1mg/ml solution in DMSO.

3. Prepare excitation-contraction uncoupler Blebbistatin stock solution (Tocris Bioscience, St. Louis, MO, 2mg/ml solution in DMSO) in advance and store the dissolved blebbistatin frozen at 4°C.

    Blebbistatin is a commonly used EC uncoupler that helps to stop the contraction of the heart while maintaining normal electrical activities. Contraction in optical mapping experiments creates large artifacts that can confound the accurate interpretation of the fluorescent signals. In Figure 2.11, signals on the left were collected while the heart was beating. Multiple humps resulted from contraction were observe. While on the right side, signals from same field of view turned stable and accurate after perfusion of Blebbistatin.

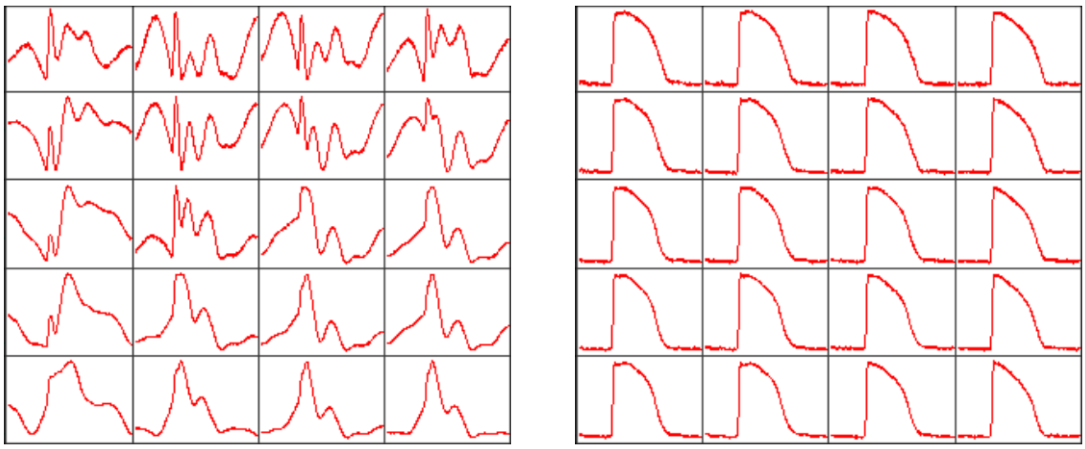

Figure 2.11 Optical mapping signals before and after application of Blebbistatin. Left picture shows membrane potentials with movement artifact from contraction. Right picture is the optical signals from same field of view after application of Blebbistatin.

Part 2: Prepare perfusion solutions and experimental setup [66]:

4. Freshly prepare 2L of Tyrode's solution (128.2mM NaCl, 1.3mM $CaCl_2$ ($2H_2O$), 4.7mM KCl, 1.05mM $MgCl_2$ ($6H_2O$), 1.19mM NaH_2PO_4, 20mM $NaHCO_3$, 11.1mM D-Glucose in distilled water, pH=7.35±0.05). If a stock solution is being used to make 2L of Tyrode's solution (sufficient for one experiment), take 1750mL of deionized water and mix in 125mL of Stock I, 125mL of Stock II, and 4g of glucose.

5. Turn on the two pumps of the perfusion systems. Set the peristaltic pump (Peri-Star, WPI, Sarasota, USA) that retrogradely perfuses the heart. Set the other peristaltic pump (Cole-Parmer Masterflex Peristalic Pump L/S, Cole-Parmer Instrument Company, Vernon Hills, Illinois) that is used for superfusion and to return of the perfusate back to the holding and oxygenating reservoir to 80 ml/min.

6. Wash the perfusion system with 70% ethanol for 30 min and then with 2L deionized water.

7. Once all of the deionized water is evacuated from the chamber, circulate the Tyrode's solution and pass it through a 5-μm filter (Millipore, Billerica, MA, USA). Warm the perfusate to 37°C with a water jacket and circulator (ThermoNESLAB EX7, Newtown, USA), maintain the temperature by implementing a heating system in the perfusion chamber[67], and oxygenate the perfusate by bubbling O_2/CO_2 (95% / 5%) gas into the solution. Monitor the pH of the solution with a pH meter (Oakton Instruments, Vernon Hills, IL) and adjust the rate of O_2/CO_2 bubbling to keep the pH at 7.35 ± .05. Continue monitoring the pH and temperature during experiment.

Part 3: Harvest the mouse heart; cannulate, and set up Langendorff perfusion.

8. Anesthetize the mouse with ketamine/xylazine (ketamin, 80mg/kg bodyweight; xylazine, 10 mg/kg bodyweight) and Heparin (100 units) by intraperitoneal injection. Assure appropriate level of anesthesia by the lack of pain reflex.

9. After a mid-sternal incision, quickly remove the heart and wash it in oxygenated (95% O_2, 5% CO_2), maintain constant-temperature (37±1°C) Tyrode's solution.

10. Using dissection microscope, rapidly identify the aorta and make a clean cut across the ascending aorta below the right subclavian artery. A short section of the aorta is then attached to a custom made 21-gauge cannula with extra edge for silk fitting around its tip. 4-0 black-braided silk (Surgical Specialties Corporation, Reading, PA) is used to fix the heart onto the cannula. After cannulation, the heart is retrogradely perfused and superfused with Tyrode solution. The retrograde perfusion rate is adjusted in the range of 2-5 mL/min to keep the aortic pressure between 60 and 80 mmHg (Pressure transducer, World precision instruments Inc (WPI), Sarasota, USA; Bridge Amplifier TBM4M, WPI, Sarasota, USA).

11. After the heart is cannulated, lung, thymus, and fat tissue are then removed.

12. The isolated heart is pinned (Fine Science Tools) at the apex to the bottom of the perfusion chamber (Sylgard coated) to prevent stream-induced movement. The right and left atrial appendages are also stretched and pinned (Fine Science Tools, Inc, Foster City, CA) to the bottom of the chamber, which provides maximal surface area for optical measurements of the atria in the up-right configuration.

    A small silicon tube is inserted into the left ventricle through the pulmonary veins and fixed by silk to nearby connective tissue. This prevents solution congestion and acidification of the perfusate trapped in the left ventricle, which is especially important after the suppression of ventricular contractions with an excitation-contraction uncoupler.

13. A custom made electrode is placed on the surface of the heart to conduct the pacing stimulations, which is generated by Mater-8 (A.M.P Instruments Ltd, Jerusalem, Israel) or PowerLab 26T (AD Instruments, Sydney, Australia).

14. A small cover glass is fixed on the surface of the solution over the heart to reduce motion artifact from the vibrating solution.

15. Focus the excitation light on the heart. In addition, adjust the distance between the dual camera apparatus and the heart so that maximum resolution will be obtained.

16. Turn off all lights in the room and commence electrical recordings using PowerLab 26T.

Part 4: Load voltage and calcium sensitive dyes and excitation-contraction uncoupler.

17. Warm-up 0.6 ml of blebbistatin (10 μM). Mix 0.5 ml of the blebbistatin with the perfusate in the holding reservoir. Dilute the remaining 0.1ml of blebbistatin in 1 ml of Tyrode's solution

and slowly inject it (over a 20 minute period) through a drug port located near the cannula. Observe as blebbistatin gradually reduces the motion artifact.

18. Dilute 30μL of voltage sensitive dye RH237 stock solution in 1mL Tyrode's solution and slowly inject over 5-7 minutes into the same injection port as blebbistatin.

19. 30μL calcium indicator Rhod-2 AM is 1:1 mixed with Fluronic F127 (Invitrogen, Carlsbad, CA, 20% solution in DMSO) and then diluted in 1mL Tyrode's solution and slowly applied over 5-10 min to perfusion system to the heart through the same injection port.

20. Wait for 5-10 minutes for Blebbistatin and dyes to reach the cell membrane and cytosol. Continue with the protocol when motion is completely suppressed.

21. Continuously monitor ECG recordings over the entire procedure to assure normal electrical function of the heart.

22. Commence fluorescent signal recordings using the SciMedia custom software (SciMedia, Costa Mesa, CA).

2.4 Representative Results

Mouse heart experiment results suggest the accuracy and reliability on V_m and CaT morphology, time scale and the time relations between these two dynamic parameters from designed system.

2.4.1 Typical experimental preparation and optical mapping signals

A photo of a typical cannulated intact mouse heart with Langendorff-perfusion as described in the protocol section is presented in Figure 2.12. Optical mapping signals of action potential and Ca are collected from the black dots labeled in the image. Dramatically distinct morphology of both signals are observed from the right atrium and left ventricle. Atrium signals have a shorter APD compared to ventricular signals. The presence of fluorescence scattering is one of the limitations of optical mapping. In the atrium signals, I observed small humps that are the results of the fluorescent signal scattering coming from the ventricles. Since the signals are collected during ventricular pacing, the hump precedes to atrium activation.

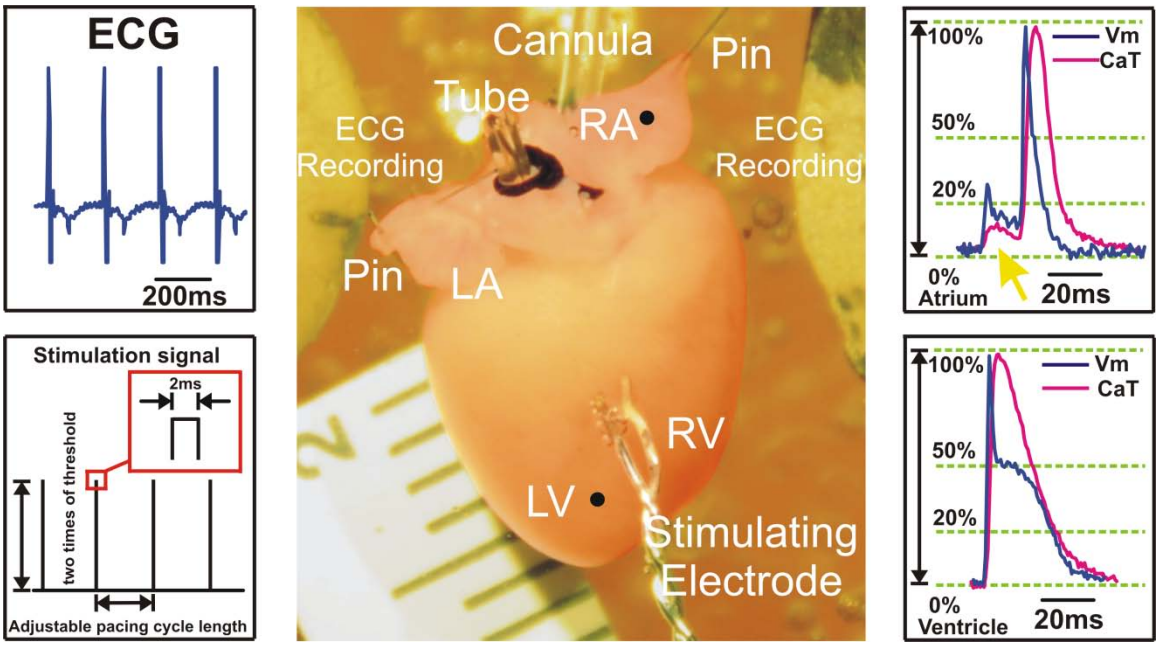

Figure 2.12 Experimental preparation and signal examples recorded during ventricular pacing. Left: ECG signals are collected from $Ag/AgCl_2$ disk electrodes (Top) and an example of S1S1 stimulation protocol is shown (Bottom). Center: Langendorff mouse heart preparation. Right: Representative optical action potentials and calcium transient signals from atria (Top) and ventricles (Bottom) are shown. The yellow arrow (Top) points to the fluorescent signal scattering coming from the ventricles, which is seen in the atrial recordings.[58] LV=left ventricle; RV=Right ventricle; LA=left atrium; RA=right atrium.

2.4.2 High Temporal-Spatial Resolution of Optical Mapping

Optical mapping provides electrical and Ca fluorescent signals with high temporal-spatial resolution. Typical signals were presented from an array of adjunct locations in Figure 2.13. High spatial resolution allows for imaging precise details of electrical property of the cardiac tissue as slight distinctness can be differentiated from locations with tiny distance. Propagation pattern can be reconstructed by plotting the activation time point at each pixel.

Time relation between V_m and CaT can be studied with high temporal resolution of the system. During normal contraction, activation of membrane potential precedes the release of Ca. The time scale between the activation of AP and Cat varies with different species due to different ionic basis. This time difference can be precisely detected in the dual mapping system as the sampling frequency can go quite high up to 1,650 frames per second, which is sufficient for this parameter.

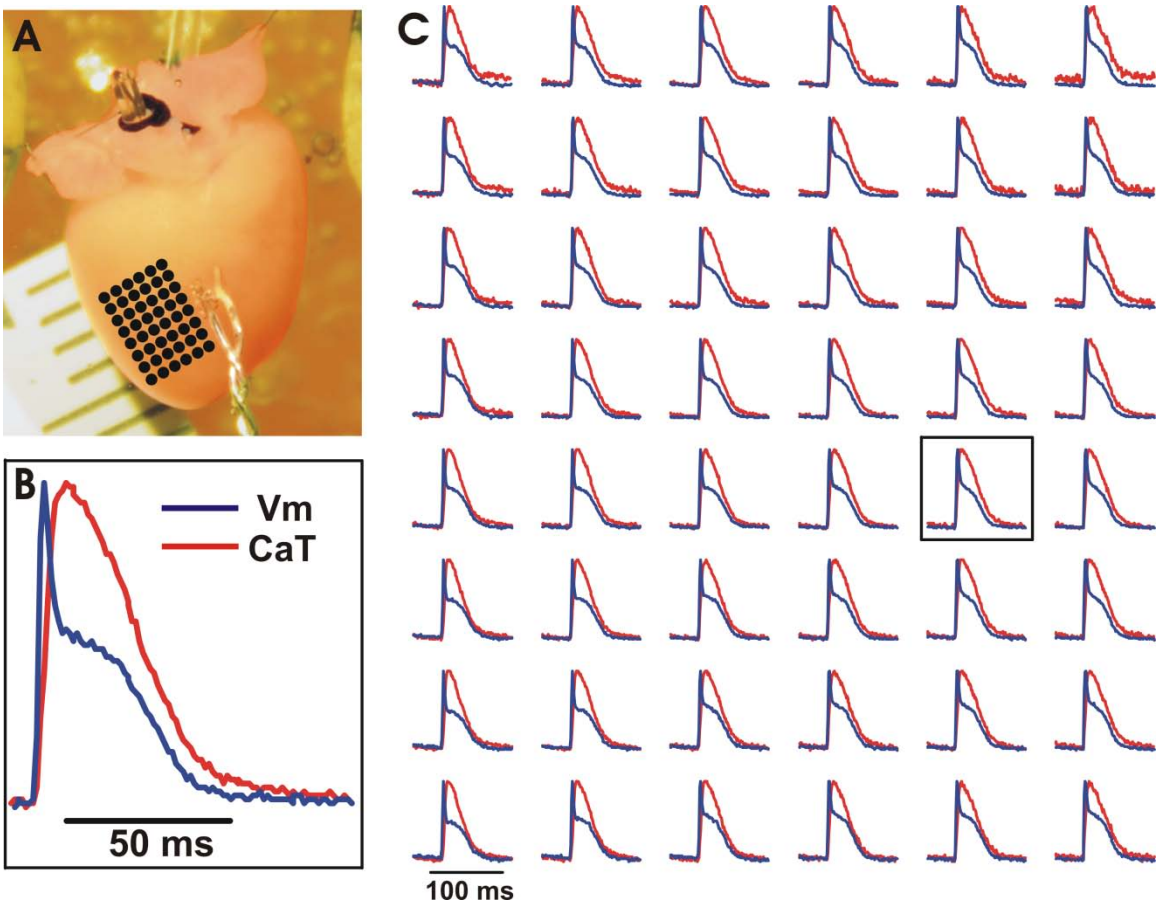

Figure 2.13 Representative optical recordings of V_m and calcium transients (CaT) from the ventricles of a wild type mouse heart. V_m (blue) and calcium transients (red) are shown (C) from an array of evenly spaced locations marked by the black dots (A). (B) Example tracings of V_m and CaT from a central on the array. Signals were binned 3x3. CMOS camera system allows up to 10,000 pairs of recordings of V_m and CaT.[58]

2.4.3 Mapping of Activation and Repolarization: Conduction

Optical mapping has made significant contributions to functional studies of the fundamental mechanisms of impulse generation (activation) and transmembrane potential recovery (repolarization). Activation time can be determined by calculating the maximum first derivative of the upstroke: dV/dt (Figure 2.14B). Alternatively, this time can also be determined when the upstroke reaches 50%. Time points of dV/dt from different pixels over whole surface of the

preparation can be plotted out and used to reconstruct the conduction pattern called activation map. Activation map of mouse heart with ventricular pacing is depicted in Figure 2.14A. It is observed that conduction along longitudinal directions (Labeled as L) is faster than that along transverse directions (Labeled as T).

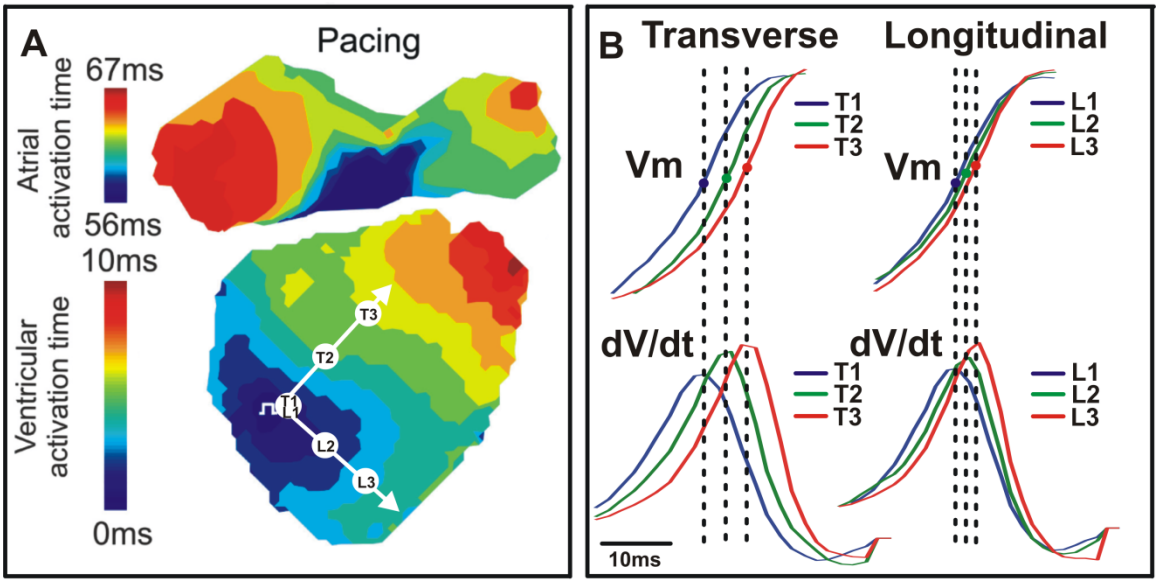

Figure 2.14 Action potential conduction. A. An example activation map from a wild type mouse heart with transverse (T) and longitudinal (L) directions indicated by white arrows. B. V_m signals (Top) and dV/dt (Bottom) corresponding to the three points seen in A (T1, T2, T3; L1, L2, L3).[58]

2.4.4 Mapping of activation and repolarization: APD and CaD

AP represents the net activities of a group of membrane ion channels. Different channels contribute distinctly during disparate phase of action potential. APD at different repolarization levels offers information regarding the contribution of different ion channels. Dysfunction of ion channels in HF underlies the appearance of APD remodeling at different repolarization level. An experiment of isoproterenol (ISO) was applied to validate the sensitivity and reliability for detection on time scale of different phase of action potential (Figure 2.15).

Accordingly, CaT represents Ca handling in the myocytes and is mediated by various Ca handling proteins as described in Chapter 1. Dysfunction in Ca handling due to those proteins results in remodeling on CaT morphology and can be quantified by CaD.

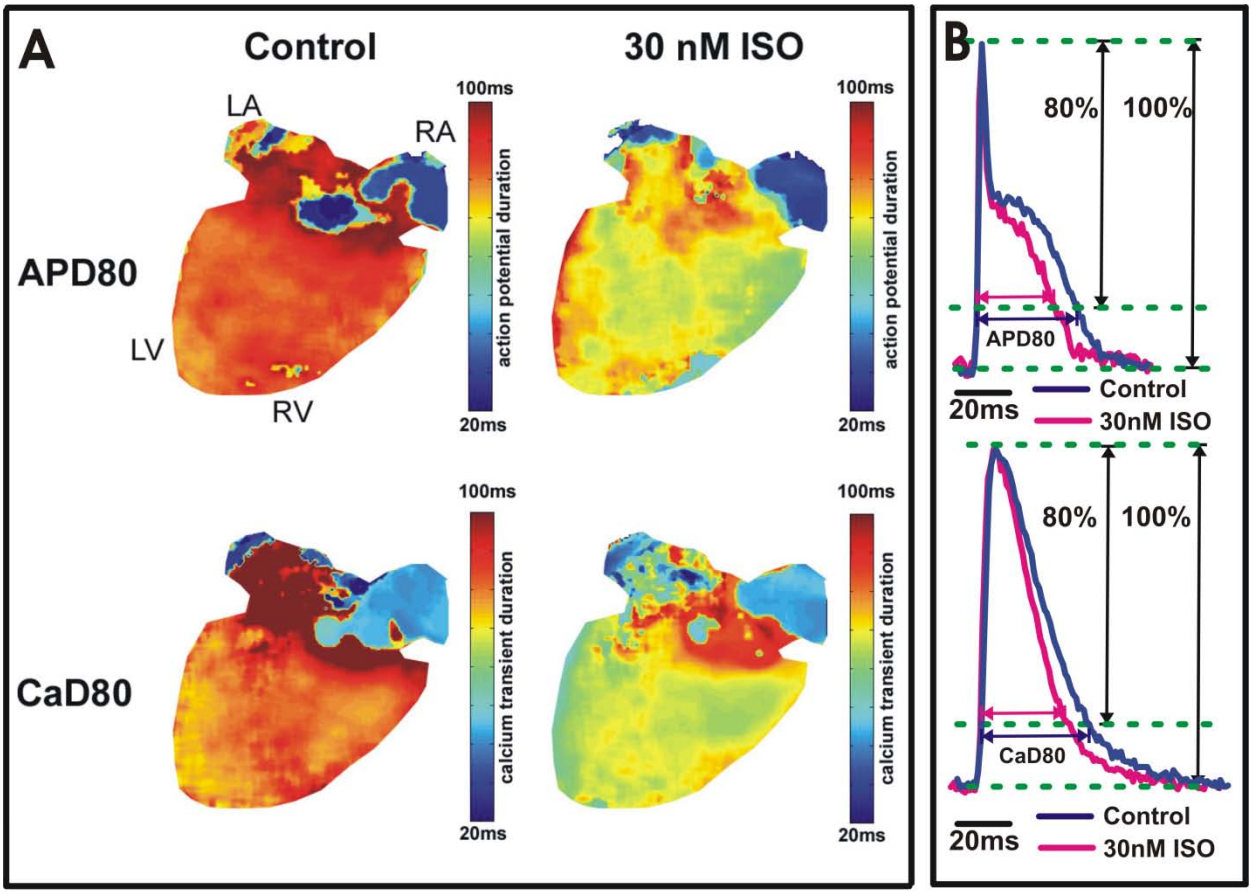

Figure 2.15 Action potential and calcium transient duration analysis. A. APD_{80} and CaD_{80} maps are shown from a heart under control conditions (Left) and after 30nM isoproterenol application (Right). The yellow/green color in the ventricles (Right) indicate isoproterenol shortened APD_{80} and CaD_{80}. B. Action potential duration at 80% repolarization (APD_{80}) and calcium transient duration at 80% relaxation (CaD_{80}) from a wild type mouse heart.[58]

2.5 Discussion

In this chapter, I described the design of a dual optical mapping system. This system has proven its accuracy and reliability in probing action potential and Ca transients. Both signals are

recorded simultaneously, so that time relation between them can be thoroughly investigated, such as how much is action potential activation preceding Ca release. Thus, this mapping system provides a reliable tool to visualize the dynamics of both electrical activity and Ca handling, especially on their association.

In the experimental method, I modified the Langendorff perfusion method by adding a small but important silicon tube. It is used to prevent solution congestion, subsequent endocardial LV ischemia after suppression of ventricular contractions, acidification of the perfusion solution and development of ischemia in the left ventricle. The mouse heart is very sensitive to hypothermia and temperature variations, which can both, cause artificial variations in action potential durations. It is imperative to maintain temperature at 37 ^{o}C during the whole experiment by implementing a heating system in the perfusion chamber as previously described [67]. Since Langendorff model does not retain innervations of the heart, one needs to consider adding neurotransmitters to the perfusates in order to maintain normal sympathetic and parasympathetic tone [68]. Addition of superfusion of the heart to Langendorff perfusion helps to maintain environment parameter like pH and temperature. In this method, the Langendorff perfused heart was placed horizontally. Vertical Langendorff perfusion setup can also be used [69], which may result in slightly different cardiac mechanics [70]. Application of CMOS cameras of high spatio-temporal resolution ensures the accuracy of recordings. However, optical mapping signals are not from a single cell but from hundreds or thousands of cells, depending on optical magnification. Alternative detectors are also available and could be applied to mapping V_m and CaT simultaneously [71]. Optical scattering could distort atrial signals by the presence of much higher ventricular fluorescence; therefore careful interpretation of the optically recorded signals is required. Another limitation of the mouse preparation in this protocol is the signal distortion and noise induced by the curvature of surface due to the small size of the mouse heart [72]. Conduction velocity measurements can also be distorted by electrode

polarity and virtual electrode in addition to the curvature of the heart. To increase accuracy for conduction velocity, activation anisotropy and repolarization maps, correct focus at the surface of the heart is very important. In this method, real time ECG recording could potentially supplement optical investigation of cardiac electrophysiology. Because of the fast response, similar excitation and distinctly different emission spectra of the two dyes, voltage-sensitive dye (RH237) and calcium indicator (Rhod-2AM) are used in the protocol [25, 66]. There are alternative combinations of dyes that can be used to measure Vm and CaT other than RH237 and Rhod-2AM [25]. A novel voltage sensitive dye, PGHI, with a large Stoke's shift (>200nm) was found to generate better Vm and CaT signals because of the greater separation of the emission wavelengths between PGHI and Rhod-2AM[73]. Future improvements may focus on exploration of novel fluorescent probes, which may improve the quantitative measurements achieved using optical mapping, development of new imaging sensors, and improved image processing software. Higher resolution and novel optical imaging modalities for 3D optical mapping are also important directions for optical mapping in future developments [61].

Chapter 3

The Role of Pyk2 in Cardiac Arrhythmogenesis

3.1 Abstract

Proline-rich tyrosine kinase 2 (Pyk2) is a non-receptor protein kinase regulated by intracellular Ca^{2+}, CaMK, and PKC, and can be activated by different stress signals involved in ventricular hypertrophy and heart failure. However, Pyk2 has not been investigated in the human heart, and cardiac function of Pyk2 signaling at the whole heart level has not been elucidated. I hypothesize that Ca-dependent activation of Pyk2 is involved in cardiac autonomic regulation, conduction, repolarization and arrhythmogenesis. I examined expression of Pyk2 in non-failing versus ischemic and non-ischemic failing human hearts (n=6/group) by Western blot. To investigate Pyk2 function, I optically mapped Langendorff-perfused hearts from wild type (WT, n=7) and Pyk2 knockout ($Pyk2^{-/-}$, n=8) mice in control and during autonomic stimulation. I used Illumina beadarray approach for transcriptional profiling of WT and $Pyk2^{-/-}$ mouse ventricles. Western blot using phospho-specific antibodies revealed a doubling of Pyk2 activation in non-ischemic failing human hearts compared to non-failing hearts. In mouse hearts, I observed a much higher probability of ventricular tachyarrhythmia during ACh perfusion in $Pyk2^{-/-}$ vs WT mice. Parasympathetic stimulation resulted in a dose-dependent decrease of atrial action potential duration (APD) in both WT and $Pyk2^{-/-}$ mice, while in ventricles it induced APD shortening in $Pyk2^{-/-}$ but not WT mice.

Deficiency of Pyk2 abolished prolongation of AV-delay induced by ACh in $Pyk2^{-/-}$ mouse but did not affect heart rate. Lower mRNA and protein levels of SERCA2 and higher mRNA level of Na^+/Ca^{2+} exchanger 1 (NCX1) were detected in $Pyk2^{-/-}$ hearts compared with WT hearts. My results suggest a protective role of Pyk2 with respect to ventricular tachyarrhythmia during parasympathetic stimulation by regulation of gene expression related to calcium handling. I hypothesize that activation of Pyk2 in the human heart during heart failure may contribute to protection against arrhythmia.

Contents of this chapter were published in Am J Physiol Heart Circ Physiol[74] and reprinted with the permission of the publisher.

3.2 Introduction

Stress signaling is dramatically remodeled in HF. Not only functional responses are affected, but also gene expression is rapidly modified when cardiac mycotyes are subjected stresses such as injury, ischemia. Such stress can be mimicked experimentally by UV light, heat shock, osmotic shock.[75] Proline-rich tyrosine kinase 2 (Pyk2) mediates a typical stress activated signaling pathways along with c-Src, P38 and regulates a broad range of key biological responses. In this chapter, I investigated the role of Pyk2 in cardiac arrhythmogenesis.

Cardiac arrhythmias account for the majority of the sudden cardiac death, which comprises 11% to 15% of all deaths in developed countries [76]. Many arrhythmias result from an underlying pathology and are characterized by aberrant signal transduction mechanisms. A dysfunction of calcium handling, due to the abnormalities of various signaling regulatory pathways, is widely recognized as the mediator of certain forms of cardiac arrhythmias [77]. Therefore, a better understanding of the signaling pathways that mediate and regulate cardiac calcium handling is

increasingly important for elucidating the mechanisms as well as new treatment targets of cardiac arrhythmias.

Pyk2 is a non-receptor protein tyrosine kinase closely related to focal adhesion kinase (FAK). Pyk2 activity is induced by G protein coupled receptor (GPCR) agonists, hormones, growth factors, inflammatory cytokines, integrin-mediated cell adhesion, membrane depolarization, and stress signals[78], via a mechanism that involves an increase in intracellular calcium levels and activation of protein kinase C (PKC) [79]. Pyk2 activation is mediated by intermolecular autophosphorylation of tyrosine 402 (Y^{402}), resulting in an increase in the activity of Pyk2 and the recruitment of Src-family tyrosine kinases, which in turn phosphorylate several other tyrosine residues of Pyk2 and Pyk2 interacting proteins [79-82]. These phosphorylation events are important for enhancing activation of Pyk2 and signaling to downstream targets. And this activation can be medicated by Acetylcholine (ACh) stimulation. [83] Acting at a crossroads of multiple intracellular signaling pathways [79, 84], Pyk2 has been shown to regulate a broad range of key biological responses, including cell proliferation, differentiation, apoptosis, survival, cell motility and polarity, cytoskeletal regulation and calcium homeostasis, in a cell context- and stimulus-dependent manner (Figure 3.1).

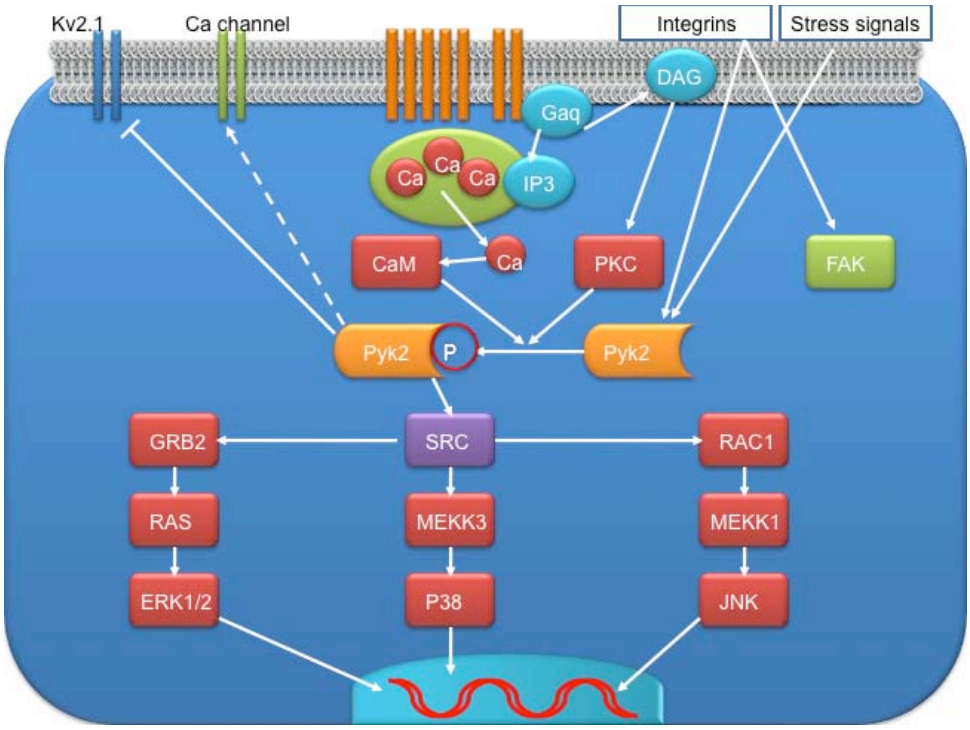

Figure 3.1 Pyk2 signaling pathway. After its phosphorylation activated by stress signals, Pyk2 mediates a typical signaling pathway upstream of c-Src, P38, and regulates several ion channels.[74]

Pyk2 is expressed in cardiomyocytes, cardiac fibroblasts, vascular smooth muscle and vascular endothelial cells [85-89]. Pyk2 signaling has been implicated in the induction of pressure overload-induced left ventricular hypertrophy (LVH) and the transition to heart failure (HF) [90]. Pyk2 expression and phosphorylation are increased in a mouse genetic model of dilated cardiomyopathy [91]. Pyk2 over-expression in neonatal rat ventricular myocytes (NRVM) results in down-regulation of sarco(endo)plasmic reticulum Ca^{2+} ATPase (SERCA2) mRNA level, indicating a potential role for Pyk2 signaling in abnormal cardiac calcium handling in LVH and HF [92]. Studies in cultured neonatal and adult rat ventricular myocytes suggest the roles for Pyk2 in cytoskeletal remodeling and in mediating both cardioprotective and proapoptotic pathways [93-96]. Adenoviral-mediated expression of a dominant-negative inhibitor of Pyk2 signaling following myocardial

infaction (MI) in rat results in improved survival, increased LV function, and altered expression of MHC isozymes, indicating an attenuation of LV remodeling post-MI [97]. These data implicate Pyk2 in promoting deterioration of LV post-MI. However, the role of Pyk2 has not been investigated in human heart, and function of Pyk2 signaling, especially the relationship between Pyk2 and arrhythmias, has not been elucidated.

Therefore, I aimed to study expression of Pyk2 in the failing and non-failing human hearts. I also aimed to study electrophysiology of isolated Langendorff-perfused mouse hearts from wild type (WT) and Pyk2 knockout ($Pyk2^{-/-}$) mice in control condition and during autonomic stimulation.

3.3 Materials and Methods

3.3.1 Patient Groups

Failing human hearts (n=12, Table 1) with cardiomyopathy of different etiologies were obtained during transplantation at the Barnes-Jewish Hospital, Washington University in Saint Louis, MO. Non-failing donor hearts (n=6, Table 1) that were rejected for transplantation due to various reasons including age, atrial fibrillation, or mild coronary disease, were used as non-failing controls. Donor hearts were provided by the Mid-America Transplant Services (Saint Louis, MO). The clinical data that are known regarding each specimen is shown in Table 1. Usage of human hearts for research was approved by the Institutional Review Board at Washington University.

Group	Heart	Age	Sex	Diagnosis
Non-failing	1	34	F	Brain death
	2	56	M	Intracerebral hemorrhagic stroke
	3	66	F	Brain death from hemorrhaging
	4	52	F	Death from stroke after surgery
	5	55	M	Death from stroke
	6	59	M	Anoxic brain injury
Ischemic failing	7	44	M	MI
	8	50	M	MI
	9	65	F	MI
	10	62	M	MI
	11	53	F	MI
	12	49	F	MI
Non-ischemic failing	13	35	F	Restrictive cardiomyopathy
	14	50	M	Hypertrophic cardiomyopathy
	15	54	F	Idiopathic dilated cardiomyopathy
	16	36	F	Post partum cardiomyopathy
	17	47	M	Idiopathic dilated cardiomyopathy
	18	49	M	Idiopathic dilated cardiomyopathy

Table 3.1 Clinical information Clinical information of patients from whom heart tissue was collected and used for western blot experiment. Information of age, gender and clinical diagnosis were listed according to heart number.

Human hearts were harvested as described in the published paper [66]. Briefly, explanted hearts were cardioplegically arrested and cooled to 4-7°C in the operating room following cross clamping of the aorta. Cardioplegic perfusion (in mM: NaCl 110, $CaCl_2$ 1.2, KCl 16, $MgCl_2$ 16, $NaHCO_3$ 10, 4°C) washed out the blood and protected the hearts during the subsequent period of wedge isolation. Arrested heart was maintained at 4-7°C to preserve tissue during 15-20 minutes delivery from the operating room to the research laboratory.

3.3.2 Western Blot Analysis

Tissue samples from human left ventricles were flash frozen in liquid nitrogen and pulverized, then lysed in RIPA buffer (1% NP-40, 1% Na Deoxycholate, and 0.5% SDS) and homogenized, followed by centrifugation at 14,500 rpm for 10 min. The protein content of the samples was quantified using the BCA Protein Assay (Pierce, Thermo Scientific, Rockford, IL), and 40μg total protein was loaded per well. Then proteins were separated by SDS-PAGE electrophoresis, followed by transfer onto nitrocellulose. Primary antibodies (Anti-Pyk2, Poly6053, Biolegend, San Diego, CA; Anti-SERCA2, MA3-919, Thermo Scientific, Rockford, IL) incubations were performed overnight at 4°C and were carried out in 5% dry milk, for anti- Pyk2 (Anti-Pyk2[pY^{402}], 3291S, Biosource, Carlsbad, CA; Anti-Pyk2[pY^{580}], ST1021, Biosource, Carlsbad, CA). Secondary antibody incubations were performed at room temperature for 1.5 hrs. Detection was performed using the SuperSignal West Pico Chemiluminescent Substrate (Thermo Scientific, Rockford, IL), and membranes were exposed using the LAS-4000mini (Fujifilm). Following exposure, membranes were washed and stripped using Restore PLUS Western Blot Stripping Buffer (Thermo Scientific, Rockford, IL). Membranes were reprobed using an antibody against GAPDH (Anti-GAPDH, Sigma, MO) as a loading control. Images were processed using Multi Gauge software (Fujifilm).

3.3.3 Mice and Genotyping

All procedures complied with the standards for the care and use of animal subjects as stated in the Guide of the Care and Use of Laboratory Animals, and protocols were approved by the Animal Studies Committee at Washington University School of Medicine. Pyk2 knockout mice have been previously described [98]. The animals were maintained in C57BL/6 genetic background.

Genomic DNA samples were extracted from ear biopsies according to standard techniques. Genotyping PCR was performed as described [99]. PCR products were separated on a 2% agarose

gel and visualized by ethidium bromide staining. PCR primers used in this study were: 5'-GGAGGTCTATGAAGGTGTCTACACGAAC-3' (forward, WT), 5'-GCCAGCTCATTCCTCCCACTCAT-3' (forward, targeted), 5' CCTGCTGGCAGCCTAACCACAT-3' (reverse, targeted or WT). Genotyping PCR using genomic DNA samples purified from WT, $Pyk2^{-/-}$ and $Pyk2^{+/-}$ mice is shown in Figure 3.2.

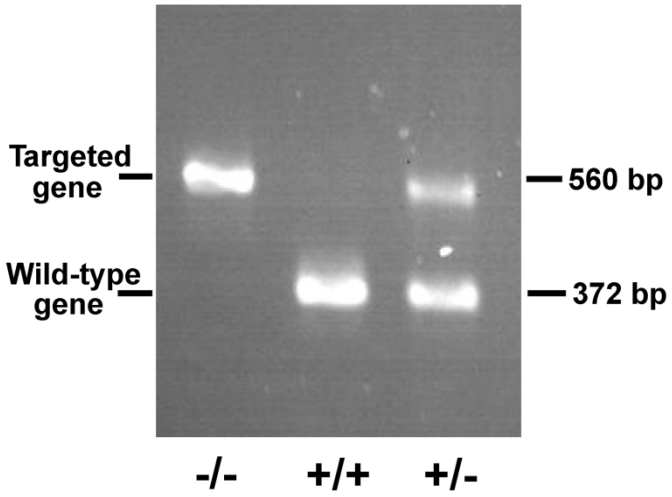

Figure 3.2 PCR analysis of genomic DNA isolated from ear biopsy samples. Inserted gene was detected at 560 bp, while corresponding gene piece in WT mouse is at 372 bp. The mouse with only targeted gene is the knockout mice, with only WT gene is WT mouse and with both bands are heterozygous mouse which are used for breeding.

3.3.4 Isolated Heart Preparations

Fifteen Langendorff-perfused hearts from adult (aged 11 to 20 weeks) mice were separated into two groups (WT, n=7; and $Pyk2^{-/-}$, n=8) and used in this study. The isolated heart preparation was according to a Langendorff perfusion protocol modified for murine hearts [66]. Mice were anesthetized using mixture solution of Ketamine and Xalazine. 100 Units of Heparin was applied used to treat and prevent blood clots in the veins and arteries. After mid-sternal incision, heart was removed and washed in oxygenated (95% O_2, 5% CO_2) constant-temperature (37±1°C), modified

Tyrode solution (in mM: NaCl 128.2, KCl 4.7, NaH_2PO_4 1.19, $MgCl_2$ 1.05, $CaCl_2$ 1.3, $NaHCO_3$ 20.0, and glucose 11.1 (pH=7.35±0.05)). Lung, thymus, and fat tissue were then dissected and removed. A short section of aorta was attached to a custom made 21-gauge cannula. After cannulation, the heart was superfused and retrogradely perfused with Tyrode solution passed through a 5-μm filter (Millipore, Billerica, USA) and warmed (37°C) through a water jacket and circulator (ThermoNESLAB EX7, Newtown, USA). Perfusion was performed using a peristaltic pump (Peri-Star, WPI, Sarasota, USA) under constant aortic pressure of 60 to 80 mm Hg measured by pressure-amplifier (TBM4M, WPI, Sarasota, USA).

The isolated heart was pinned at the apex to the Sylgard bottom of the chamber to prevent stream-induced movement. The right and left atrial appendages were stretched and pinned to be flat that allows optical measurements from maximal surface of the atria. A small silicon tube, fixed by silk to the nearby connective tissue, was inserted into the left ventricle through the pulmonary vein, left atria, and tricuspid valve to prevent solution congestion and subsequent ischemia after suppression of ventricular contractions. This also prevented acidification of the perfusion solution and development of ischemia in the left ventricle (Figure 3.3).

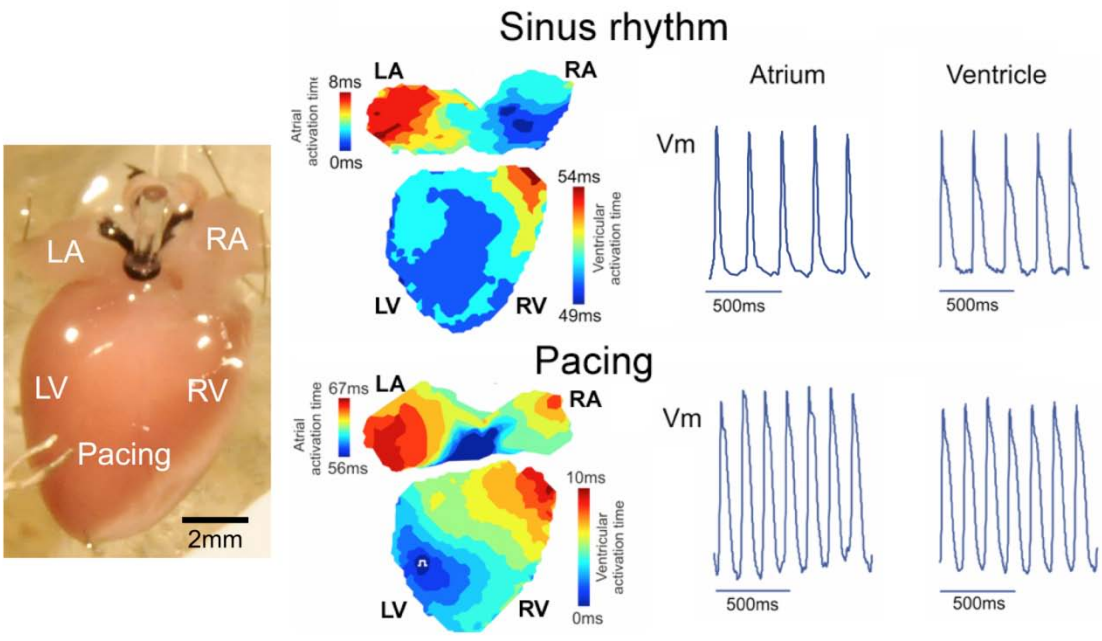

Figure 3.3 Membrane potential signals from atrium and ventricle during sinus rhythm and pacing condition. A photo of intact mouse heart preparation is shown at left. Typical membrane potential signals are collected from atrium and ventricle during sinus rhythm and pacing condition, based on which, activation map was conduced and depicted in the model.[74]

Excitation-contraction uncoupler blebbistatin (10 μM, Tocris Bioscience, USA) was used to prevent the effect of motion artifact on the action potential duration estimation. Application of blebbistatin induced a transient (5-10 min) increase of cycle length. However, blebbistatin did not induce any shifts of leading pacemaker location or action potential duration changes induced by other contraction blockers.

3.3.5 Imaging System

Coronary perfused hearts were stained by perfusion with voltage-sensitive dye (RH-237, Invitrogen, Carlsbad, CA, 5μL of 1 mg/mL dimethyl sulfoxide, DMSO in Tyrode solution), for 5-7 minutes. Excitation light was generated by a 250-W xenon arc lamp with a constant-current, low-noise, power supply (Oriel Instruments, Stratford, CT). The light was passed through a heat filter, a shutter, and excitation filter (530/540 nm). A flexible light guide directed the band-pass-filtered light onto the preparation, and a shutter was used to ensure that the preparation was exposed to light only during image acquisition. The fluorescent light emitted from the preparation was long-pass (>700 nm) filtered using an edge pass filter (Thorlabs, NJ) before reaching the camera. Emitted light was directed towards a MiCAM Ultima-L CMOS camera (SciMedia, CA) with high spatial (100x100 pixels, 230±20 μm per pixel) and temporal (1,000-3,000 frames/sec) resolution. Fluorescent signal acquired was digitized, amplified, and visualized by the custom software (SciMedia, CA) (Figure 3.4).

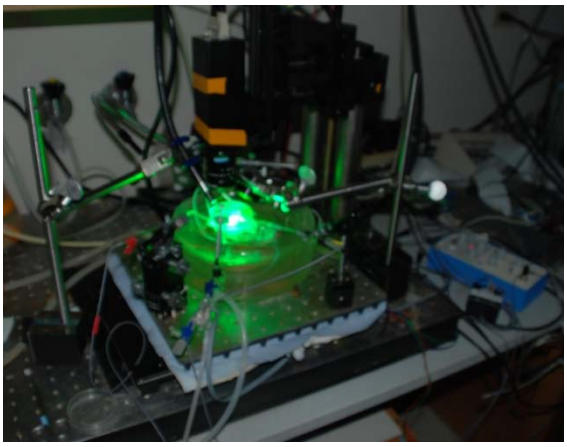

Figure 3.4 Experimental imaging setup for Pyk2 knockout and WT mice.[74]

3.3.6 Experimental Protocols

After isolation and cannulation, motion suppression, and dye staining, preparations were equilibrated for 5-10 min before imaging. To estimate the effects of Pyk2 in the cardiac system, three different concentrations of acetylcholine (ACh, 1μM, 3μM and 10μM) were applied to the heart through perfusion. Atropine (2μM), a competitive antagonist for the muscarinic acetylcholine receptor, was used to block the action of ACh, after which isoproterenol (ISO 1μM) was applied. Details are depicted in Figure 3.5.

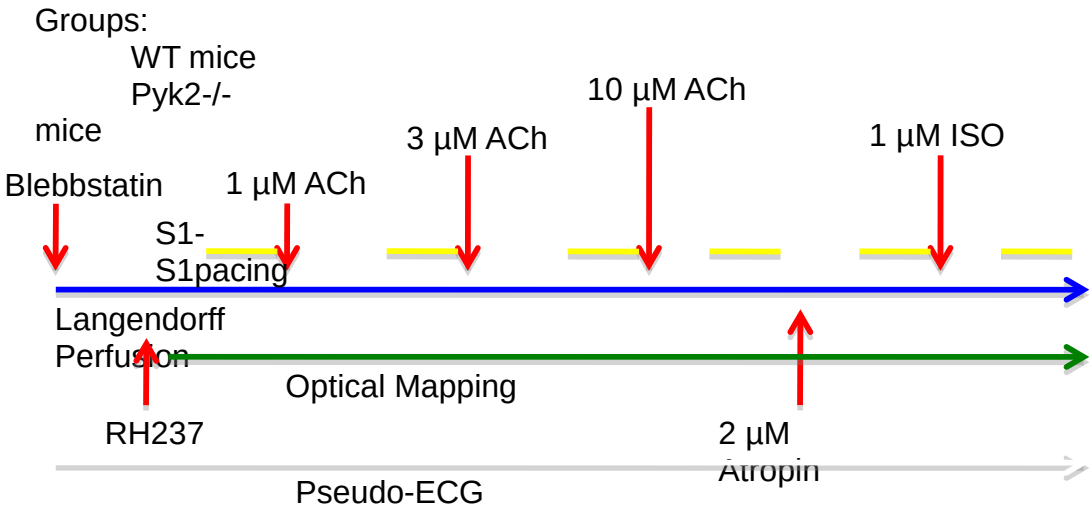

Figure 3.5 Experimental protocol for Pyk2 knockout mice investigation. [74]

I optically mapped the heart during both spontaneous rhythm and ventricular pacing under control and 10 minutes after applying autonomic interventions. Typical signals from both conditions were depicted in Figure 3.3.

Pacing was induced by the electrode located on the anterior ventricular epicardium midway between apex and base. Current value was set as twice of the threshold. The S1-S1 restitution protocol was applied to induce ventricular tarchyarrhythmia (VT). Hearts were paced with a basic cycle length from 150 to 40 ms in steps of 10 ms until 1:1 capture failed or ventricular tarchyarrhythmias, including ventricular fibrillation, occurred.

3.3.7 Classification of Fast Pacing-Induced Arrhythmia

Due to small size of the mouse hearts as compared with the wavelength sustained VT/VF was not readily induced. I defined occurrence of one or more extra beats as fast pacing-induced arrhythmia, which can be further divided into sustained or non-sustained arrhythmia. In agreement

with Fabritz *et al.* [100], I define fast pacing-induced arrhythmia as sustained if 6 or more irregular extra beats were observed.

3.3.8 Data Processing

A custom-built Matlab computer program [101] was used to analyze optical mapping signals. The signals captured were filtered using a low-pass Butterworth filter at 256 Hz. All action potentials were averaged and normalized to a range from −85 to +15 mV. Action potential duration was calculated at 80% of repolarization (APD80). Activation maps were constructed from activation time sequence that was determined using the dV/dt_{max} definition. AV-delay was measured based on PR interval from pseudo-ECG signals. Local conduction velocities were calculated from the gradient of activation times along both longitudinal (CV_L) and transverse (CV_T) directions. Recordings near the stimulating electrode and at a distance from the electrode were excluded to remove virtual electrode artifacts and the effects of 3-dimensional propagation. Anisotropy is defined as the ratio between longitudinal and transversal conduction velocities (CV_L /CV_T).

3.3.9 RNA Microarray

Isolation of total RNA from mouse left ventricles was performed using RNeasy Fibrous Tissue Min Kit. Integrity of total RNA samples was estimated by the RNA integrity number (RIN) comparing to RNA Integrity Database (RINdb) before RNA level measurement using MouseWG-6 v2.0 Expression BeadChip Kits (Illumina). The intensity of the fluorescence from beadchip was normalized and revealed the mRNA level. I analyzed calcium handling proteins mRNA level in this study.

3.3.10 Transverse Aortic Constriction

The constriction of the transverse thoracic aorta was performed on 10 to 12 week-old mice by the Mouse Cardiovascular Phenotyping Core in Washington University in St.Louis as described.[102, 103] In brief, mice was anesthetized and incubated. Following blunt dissection through the intercostal muscles, the aorta and pulmonary artery was identified and freed by additional blunt dissection. 7.0 silk suture was place around the great vessel of interest and tied around a blunt needle. The blunt needle was rapidly removed. The surgical incision was closed in two layers with an interrupted suture pattern.

3.3.11 Statistical Analysis

Group data were represented as mean ± SEM. Comparisons between groups of data were performed using ANOVAs analysis with Scheffe test. A value of $P<0.05$ was considered statistically significant.

3.4 Results

3.4.1 Pyk2 Activation is Increased in Non-Ischemic Failing Human Hearts

I first assessed the expression levels and the activation status of Pyk2 in non-failing and failing human hearts of different etiologies: ischemic and non-ischemic cardiomyopathy. Immunoblot analysis using Pyk2-specific antibody (Anti-Pyk2, Poly6053, Biolegend, San Diego, CA) showed that Pyk2 protein is expressed at comparable levels in the tissue samples from non-failing control and diseased human left ventricles (Figure 3.6A, top panel). Pyk2 kinase activity was assessed by tyrosine phosphorylation. Notably, phosphorylation of Pyk2 on Y^{402}, a major site of Pyk2 autophosphorylation upon activation, is significantly increased in non-ischemic failing hearts,

compared with non-failing hearts and ischemic failing hearts, as measured using phospho-Y^{402}-specific antibody (Anti-Pyk2 [pY^{402}], 3291S, Biosource, Carlsbad, CA) (Figure 3.6A, B). Phosphorylation of Pyk2 on Y^{580} (Anti-Pyk2 [pY^{580}], ST1021, Biosource, Carlsbad, CA) in the kinase domain activation loop was also elevated and observed increased activation in non-ischemic failing hearts (Figure 3.6A, B). These data show that Pyk2 is expressed in human ventricles and is activated in non-ischemic cardiomyopathy, indicating a potential involvement of Pyk2 signaling in this pathology.

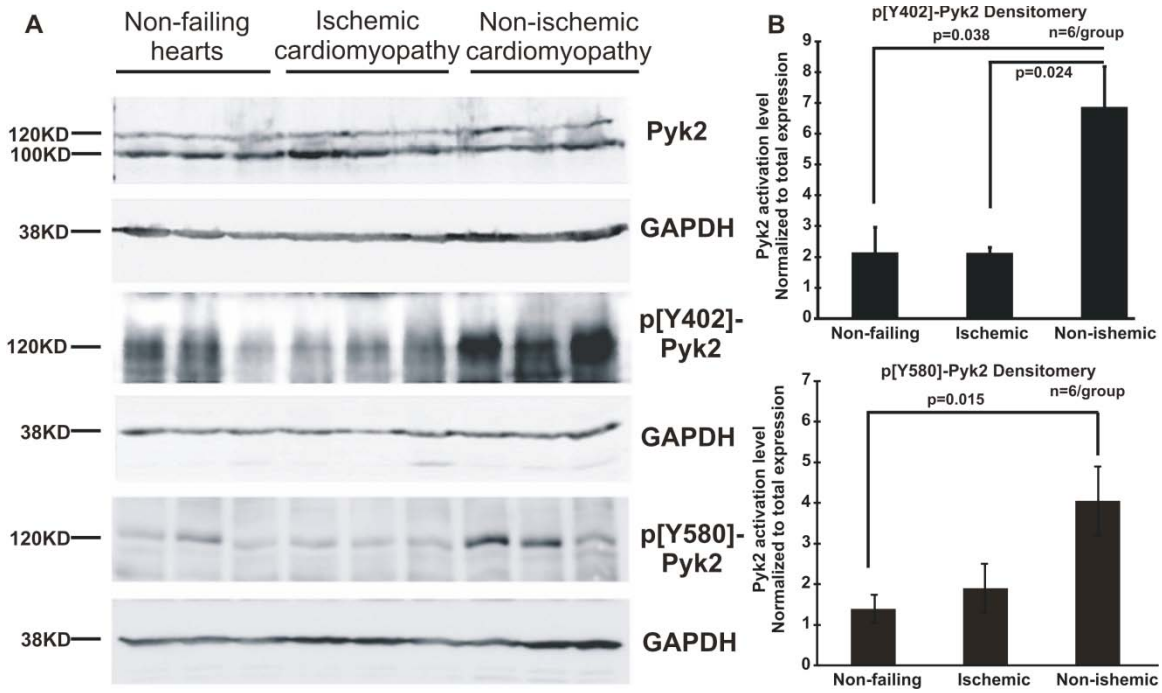

Figure 3.6 Pyk2 is activated in non-ischemic failing human ventricle. (A) Pyk2 expression and activation in non-failing, ischemic failing and non-ischemic failing human ventricle. Pyk2 activation was assessed using phosphorylation on tyrosine 402 (Y^{402}) and tyrosine 580 (Y^{580}). (B) Statistical analysis of Pyk2 activation levels. Pyk2 activation by phosphorylation on tyrosine 402 (Y^{402}) and 580 (Y^{580}) in non-ischemic group is significantly higher than in non-failing and ischemic failing groups.[74]

3.4.2 Autonomic Regulation of Spontaneous Heart Rhythm in WT and Pyk2$^{-/-}$ mice

First, I explored the effect of Pyk2 deletion on the sino-atrial nodal (SAN) function. Both WT and Pyk2$^{-/-}$ mice showed an ACh dose dependent decrease of spontaneous heart rate, which was abolished by atropine. ISO accelerated the heart rate in both WT and Pyk2$^{-/-}$ mice (Figure 3.7A). In WT and Pyk2$^{-/-}$ mice, respectively, after normalizing to control group, heart rate decreased to 75.1% and 79.2%; 63.7% and 61.9%; 50.9% and 50.4% under 1, 3 and 10 μM ACh, then went back to 116% and 101% under atropine. However, no significant difference was observed between the two groups under all conditions (Figure 3.7A). During the measurements of heart rate, both ECG and optical maps showed clear 1:1 conduction, excluding the possibility of AV-junction rhythm playing any role in heart rate under our experimental conditions.

I next assessed the atrio-ventricular (AV) nodal function. AV-delay showed a markedly different response to autonomic stimulation in Pyk2$^{-/-}$ mice versus WT. As expected, an ACh dose dependent prolongation of AV-delay was observed in WT mice (value normalized to control group: ACh 1μM: 1.24±0.05 versus ACh 10μM 1.93±0.23, p=0.024), which was completely abolished by deficiency of Pyk2 in Pyk2$^{-/-}$ mice (ACh 1μM: 1.06±0.04 versus ACh 10μM 1.16±0.05, p=0.19) (Figure 3.7B). No significant change of AV-delay was detected during the application of autonomic stimulation in Pyk2$^{-/-}$ mice at all (Figure 3.7B). Significant differences of AV-delay were observed between WT and Pyk2$^{-/-}$ mice during perfusions of three different ACh concentrations (P=0.021, 0.043, and 0.0035 for 1, 3 and 10 μM ACh respectively).

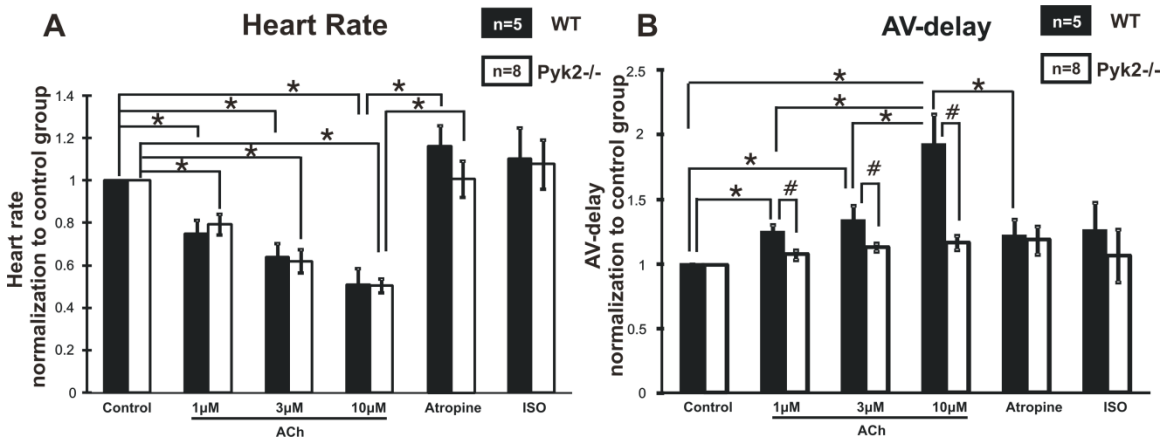

Figure 3.7: Functional change of heart rate and AV-delay in mouse hearts. (A) Heart rate was normalized to control condition. Values of both WT and Pyk2-/- mice showed ACh dose-dependent decrease, which was abolished by Atropine. No significant difference in heart rate was detected between WT and Pyk2-/- groups under autonomic stimulations. (B) Ach-induced increase in AV-delay was detected in WT, but not in Pyk2-/- mice. * - $p<0.05$ between same group; # - $p<0.05$ between WT and Pyk2-/-.[74]

These data suggest that Pyk2 deficiency did not have any effect on SAN function, but had a significant effect on AVN: it abolished the sensitivity of AV conduction to cholinergic stimulation. This observation indicates that Pyk2 expression and activation is involved in AVN function, and not involved in SAN function in the mouse.

3.4.3 Fast Pacing Induced Reentrant Tachyarrhythmia in Pyk2$^{-/-}$ Mice after ACh Application

Next we assessed a possible role of Pyk2 deficiency in vulnerability to the ventricular tachyarrhythmia. I applied a rapid pacing to induce ventricular tachycardia or fibrillation (VT/VF) in both groups of mice. As shown in Table 3.2, Pyk2$^{-/-}$ mice had a significantly higher vulnerability to pacing induced tachyarrhythmia during high concentrations of ACh (3 μM and 10 μM), compared to the WT group (37.5% versus 14.3% and 75% versus 0% ($p<0.001$), respectively). Arrhythmia was

not readily inducible in WT mice at any concentration of ACh, nor in Pyk2$^{-/-}$ mice at low concentration of ACh (1 μM). In this experiment, I observed that spontaneous arrhythmia occurred in three Pyk2$^{-/-}$ mice (indicated by # in Table 2), after which the application of rapid pacing also induced arrhythmia. In contrast, no spontaneous arrhythmia was observed in WT mice.

Pyk2$^{-/-}$	Control	ACh1μM	ACh3μM	ACh10μM	Atropine2μM	ISO1μM
#1	-	-	-	VT/VF*#	-	-
#2	-	-	VT/VF	VT/VF	NA	-
#3	-	NA	VT/VF *#	VT/VF	NA	-
#4	-	-	VT/VF	VT/VF	NA	-
#5	-	VT/VF	-	VT/VF	-	-
#6	-	-	-	VT/VF *#	NA	NA
#7	-	-	-	-	-	-
#8	-	-	-	-	-	-
VT/VF induced	**0/8**	**1/7**	**3/8**	**6/8**	**0/4**	**0/7**
WT						
#9	-	-	-	-	-	-
#10	-	-	-	-	NA	NA
#11	-	-	VT/VF	-	NA	NA
#12	-	VT/VF	-	-	-	VT/VF*
#13	-	-	-	-	-	NA
#14	-	-	-	-	-	-
#15	-	-	-	-	-	-
VT/VF induced	**0/7**	**1/7**	**1/7**	**0/7**	**0/5**	**1/4**

* spontaneous termination
\# spontaneous initiation
NA: Not Available
VT/VF: Ventricular Tachyarrhythimas/Ventricular Fibrilation

Table 3.2 Statistics analysis of ventricular tachycardia induced in Pyk2$^{-/-}$ and WT mice.

To investigate the pattern of tachyarrhythmia induced by rapid pacing in the $Pyk2^{-/-}$ mouse heart during autonomic stimulations, I optically mapped the heart during tachyarrhythmia. The activation maps revealed reentrant arrhythmia. Figure 3.8 shows a representative example of the reentry circuit in $Pyk2^{-/-}$ mouse heart that occurred on the anterior ventricular epicardium of the heart with the reentrant cycle length of 38 ms. Five consecutive activation maps illustrate the reentrant arrhythmia during 196 ms, in which dark blue represents the earliest activation time while dark red represents the latest. Most of the observed reentrant arrhythmias were driven by stable reentry circuits lasting more than 4 s, which is the limitation of our data acquisition system. Some of the reentrant arrhythmias terminated spontaneously, as summarized in Table 3.2.

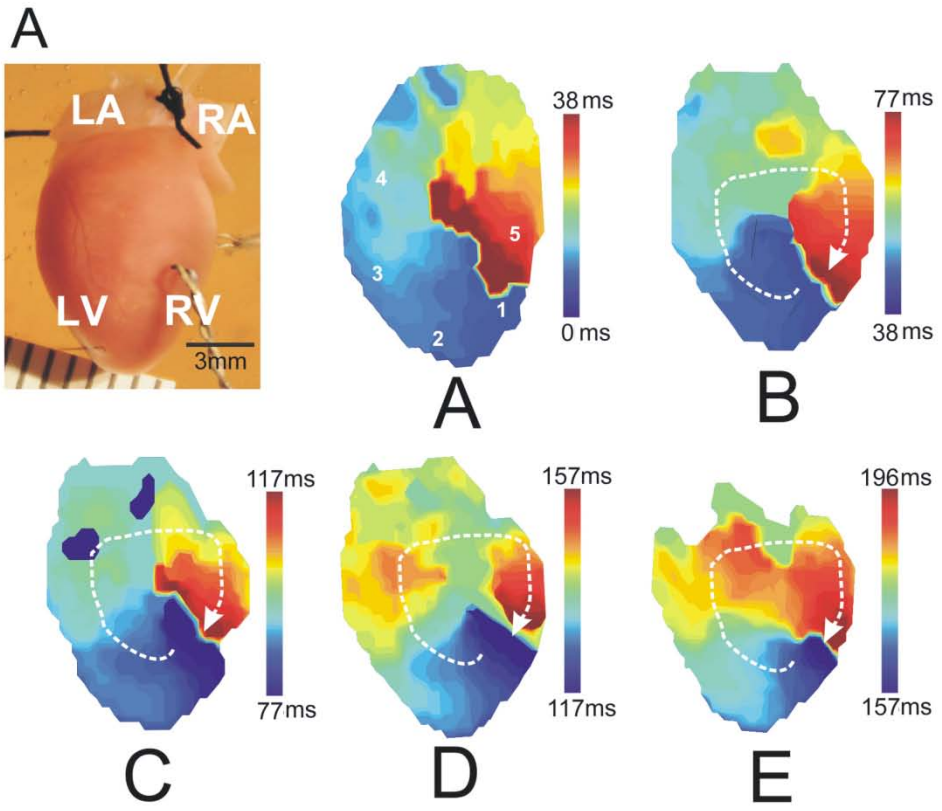
A
LA
RA
LV
RV
3mm
38 ms
0 ms
77ms
38 ms
A
B
117ms
77ms
157ms
117ms
196ms
157ms
C
D
E

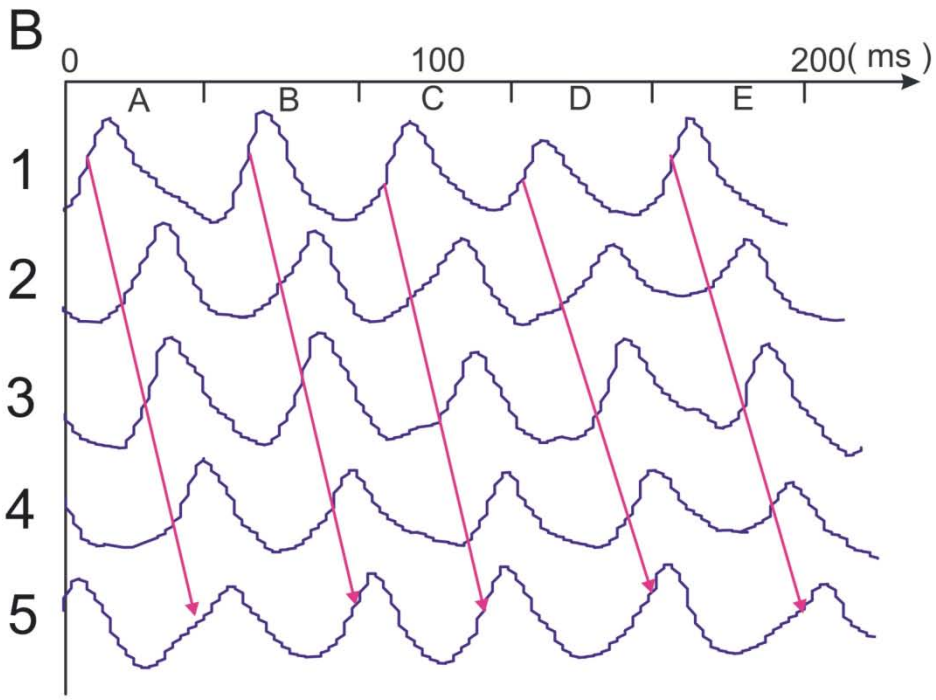
B
0
100
200(ms)
A
B
C
D
E
1
2
3
4
5

Figure 3.8 Typical VT induced in Pyk2$^{-/-}$ mouse heart. (A) Activation map shows 5 cycles (a to e) of clockwise reentrant VT induced by rapid pacing during 10 mM ACh perfusion. The cycle length is 38 ms. The reentrant paths are indicated by white dashed arrow curves. (B) Optical mapping recordings of five points chosen to illustrate reentry (Figure 3.5a) are shown at the same time scale. The pink solid arrows clearly show the direction of action potential propagation that goes from point 1 to 5 in one reentrant arrhythmia cycle.

3.4.4 Spatiotemporal characteristics of activation and repolarization in WT and Pyk2$^{-/-}$ mice

Enhanced arrhythmogenesis in Pyk2$^{-/-}$ mice could be explained by several alternative hypotheses, which are based on abnormalities of conduction and/or repolarization. To explore the underling arrhythmogenesis substrate I characterized repolarization and conduction in both groups of mice. APD at 80% of repolarization levels (APD_{80}) at cycle length of 120 ms pacing were detected in atria and ventricles respectively from both groups of mouse hearts. As expected, ACh decreased atrial APD_{80} in both WT and Pyk2$^{-/-}$ groups (32.3±2.6ms, 18.0±1.5ms, 16.7±2.2ms and 13.4±1.9ms versus 30.1±3.5ms, 20.6±2.2ms, 18.8±1.7ms, and 14.0±2.8ms under control condition, 1, 3 and 10 μM ACh, respectively). Unexpectedly, there was a significant difference in response of WT and Pyk2$^{-/-}$ mouse ventricles to high concentration ACh. As expected, APD_{80} of WT mouse ventricles did not exhibit dependence on ACh. In contrast, ACh significantly decreased APD_{80} in Pyk2$^{-/-}$ group at 10 μM ACh stimulation. APD_{80} was 57.8±2.7ms, 60.7±3.8ms, 65.5±4.6ms and 63.5±5.0ms versus 60.0±3.9ms, 54.9±4.9ms, 51.4±2.8ms and 46.7±2.4ms under control condition, 1, 3 and 10 μM ACh for WT and Pyk2$^{-/-}$ groups, respectively (Figure 3.9B).

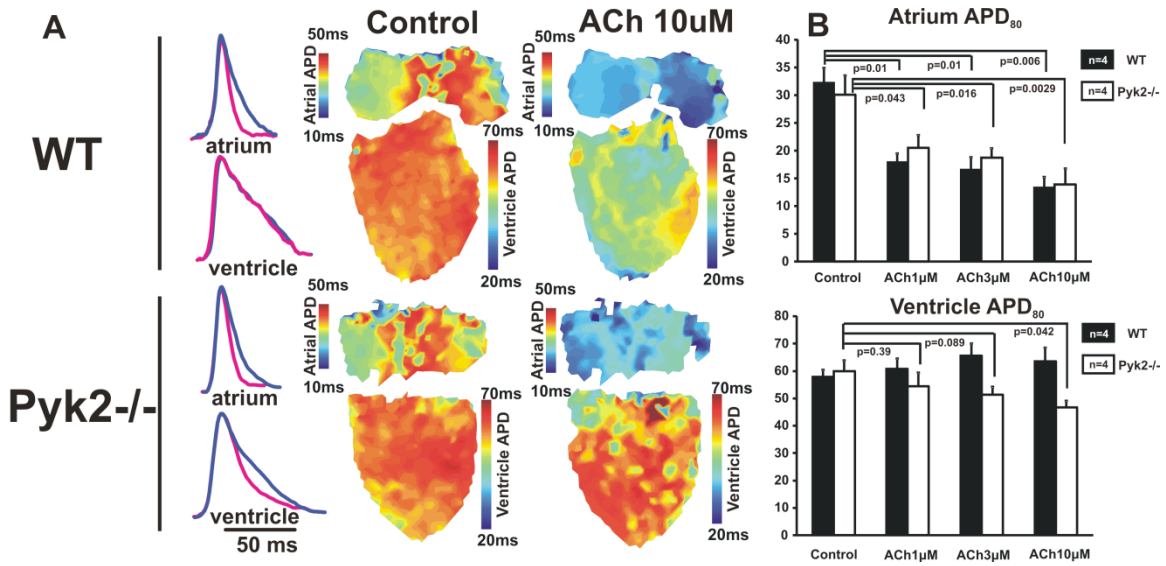

Figure 3.9 Functional change of APD in WT and Pyk2$^{-/-}$ mouse heart mouse heart. (A) Optical signal and APD map of WT and Pyk2$^{-/-}$ mice under control condition and stimulation of 10 mM ACh. (A), Time scale from 20 to 100 ms (20 ms: indicated by dark blue color; 100 ms: indicated by dark red color) was applied to depict the APD80 distribution. ACh significantly decreased APD80 in atrium but not in ventricle. On the contrary, APD80 map of Pyk2$^{-/-}$ mouse heart showed a decrease in both areas after application of 10 μM ACh. (B) Statistical analysis showed that in atria ACh dose-dependently decreased action potential duration at 80% repolarization level (APD_{80}) in both WT and Pyk2$^{-/-}$ mice, while in ventricles ACh did not change APD_{80} in WT mice but decreased it in Pyk2$^{-/-}$ mice.

To explore possible conduction abnormalities, I also measured average transverse and longitudinal conduction velocities (CV), and anisotropy in WT and Pyk2$^{-/-}$ mice. Figure 3.10 illustrates a representative example and summary data for pacing at cycle length of 120 ms. I found no significant differences of CV or anisotropy between WT and Pyk2$^{-/-}$ mice groups. However the Pyk2$^{-/-}$ group showed a trend of higher mean anisotropy values than WT group, which was not statistically significant (p=0.051, 0.084, 0.133, 0.199, 0.613 for control, 1 μM, 3 μM, 10 μM ACh, and 2 μM ISO groups respectively).

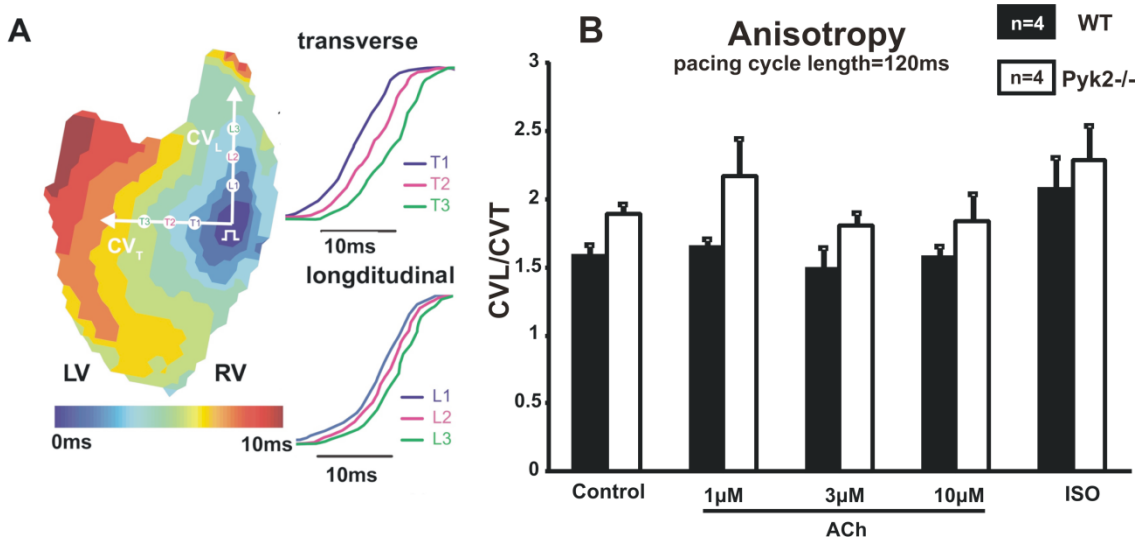

Figure 3.10 Conduction anisotropy in WT and Pyk2$^{-/-}$ mouse heart mouse heart. (A) Optical signals showed different conduction velocity under control condition along transverse and longitudinal direction, which are indicated in the activation map. The fronts of electrical signals from three random places along two directions represented by different colors are shown beside the activation map, which indicates different conduction velocity along the two directions. (B) No significant difference of anisotropy under control condition and autonomic stimulations were detected between WT and Pyk2$^{-/-}$mice.

My data suggests that Pyk2 deficiency resulted in a gain of cholinergic sensitivity of ventricular repolarization. There was no effect on atrial repolarization and on conduction velocity or anisotropy. Therefore, Pyk2 deficiency could account for a significant shortening of ventricular wavelength during cholinergic stimulation, which could explain increased vulnerability of reentrant arrhythmia.

3.4.5 Pyk2-Null Hearts Exhibit Changes in Expression of Calcium Handling Regulators

To investigate the transcriptional changes potentially caused by Pyk2 deficiency, I performed whole genome microarray analysis using RNA samples isolated from left ventricles of WT and Pyk2^{-}

$^{/-}$ mice. I found that SERCA2 mRNA and protein levels were significantly lower in ventricles of Pyk2$^{-/-}$ hearts relative to WT hearts (Figure 3.11). NCX1 mRNA level was also observed significantly higher in ventricles of Pyk2$^{-/-}$ hearts relative to WT hearts (Figure 7). Data from other calcium handling proteins including voltage-gated and other calcium channels (L-type: $Ca_v1.2$, $Ca_v1.3$; T-type: $Ca_v3.1$, $Ca_v3.2$, Inositol-1,4,5-trisphophate receptors ($Ins(1,4,5)P_3R$) and Ryanodine receptor2 (RyR2)), channel regulator (phospholamban (PLN)) and calcium-sensitive enzyme (Ca^{2+}/calmodulin-dependent protein kinase II (CaMKII), protein kinase C alpha (PKCα)) were also analyzed (Figure 3.12). I detected significant increase in Cav1.4 and NCX3 mRNA levels in Pyk2$^{-/-}$ mice; however the functional implications of these findings in the cardiac system remain to be elucidated since neither of these proteins has been reported to be expressed in cardiomyocytes (Figure 3.12 boxed).

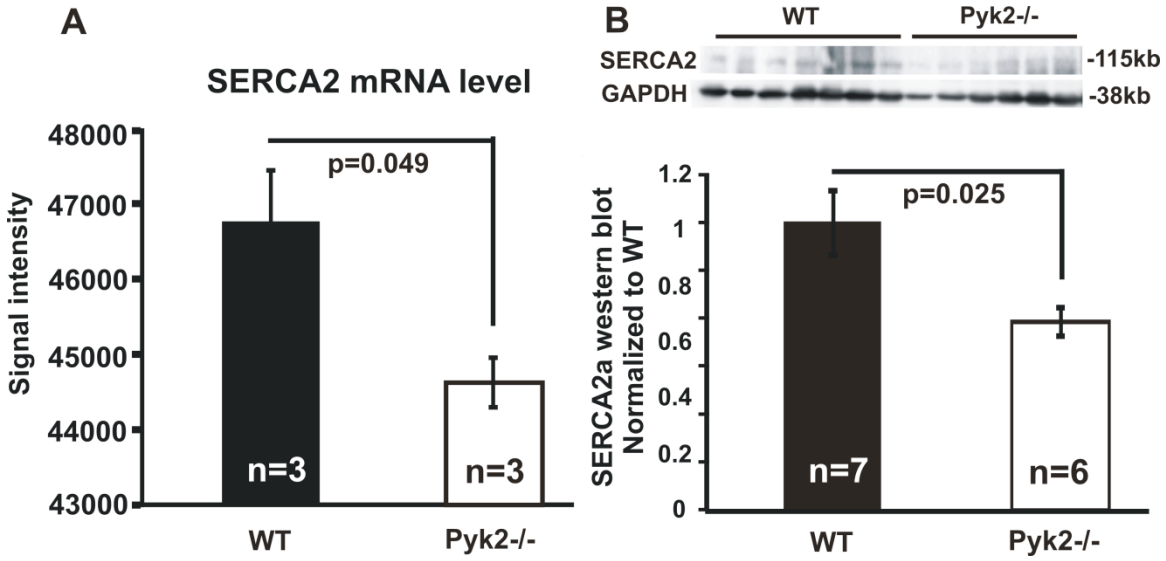

Figure 3.11 SERCA2 mRNA and protein levels in Pyk2$^{-/-}$ mouse heart. SERCA2 mRNA and protein levels are reduced in left ventricles of Pyk2$^{-/-}$ mice. (A) Microarray data using RNA samples isolated from left ventricles show down-regulation of SERCA2 expression in Pyk2$^{-/-}$ versus wild-type counterparts; (B) Western blot shows decreased expression of SERCA2 protein (Anti-SERCA2, MA3-919, Thermo Scientific, Rockford, IL) in Pyk2$^{-/-}$ versus WT group.

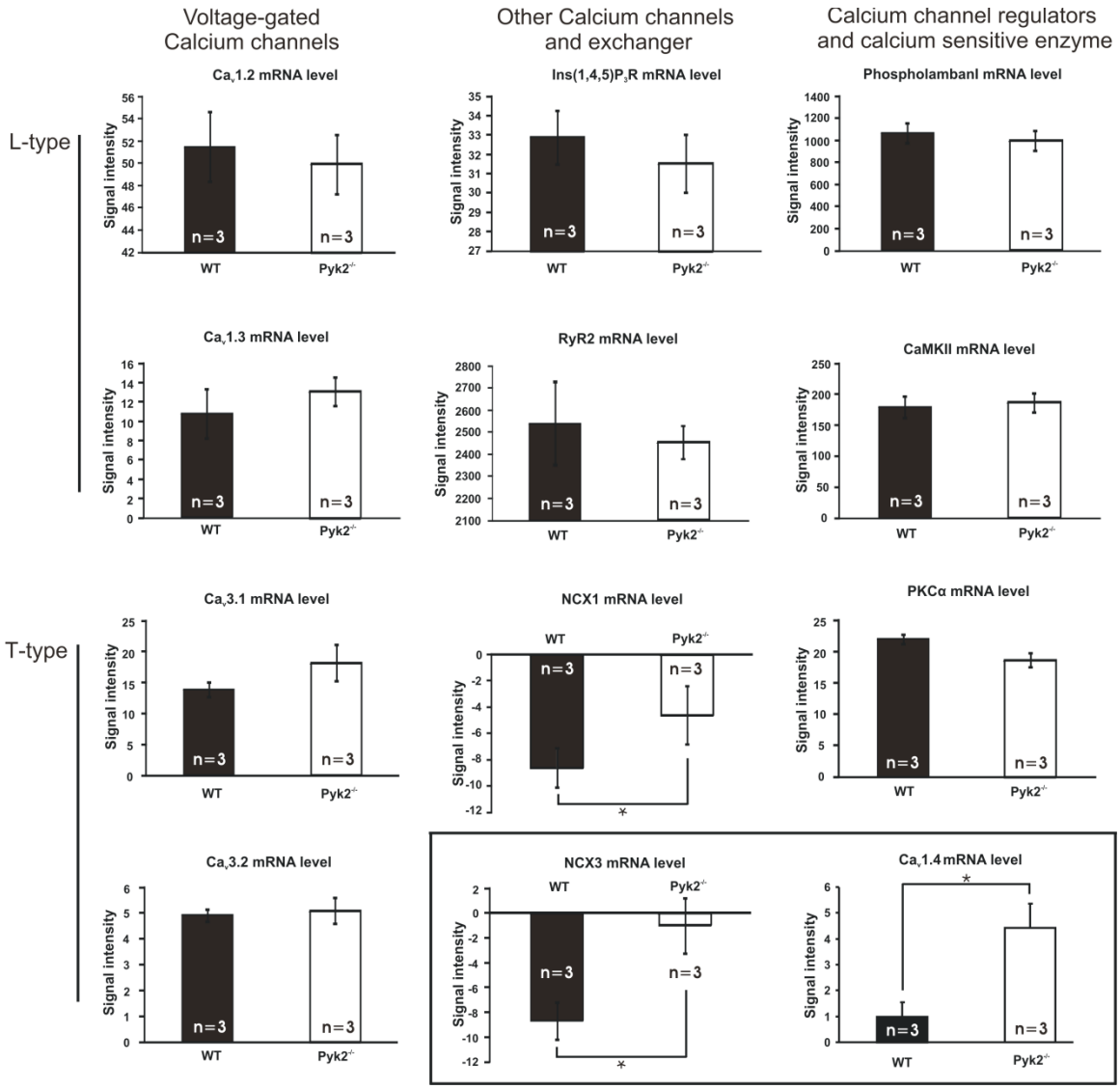

Figure 3.12 Gene expression of calcium handling regulators. Gene expression of calcium handling regulators NCX1, NCX3, and Cav1.4 is altered in Pyk2-null hearts. Microarray data using RNA samples isolated from left ventricles of WT and Pyk2$^{-/-}$ hearts show relative mRNA expression levels for calcium handling proteins including voltage-gated and other calcium channels (L-type: Cav1.2, Cav1.3; T-type: Cav3.1, Cav3.2, Ins(1,4,5)P3R, RyR2 and NCX1), channel regulator PLN, and calcium-sensitive enzymes (CaMKII, PKCα). NCX1 mRNA level is significantly higher in ventricles of Pyk2-/- hearts relative to WT hearts. Cav1.4 and NCX3 mRNA levels (boxed) are also significantly altered in Pyk2-/- hearts compared with WT counterparts.

3.4.6 Pyk2$^{-/-}$ Hearts Display Increased Sensitivity to Ventricular Arrhythmia after Transverse Aortic Constriction

I then hypothesized that pressure overload could further exacerbate disease phenotype in Pyk2$^{-/-}$ mice. I performed a study using transverse aortic constriction model of hypertrophy. Contrary to our hypothesis, both Pyk2$^{-/-}$ and WT mice showed similar phenotype. However, a higher vulnerability to arrhythmia in Pyk2$^{-/-}$ in comparison with WT mice was retained (Figure 3.13).

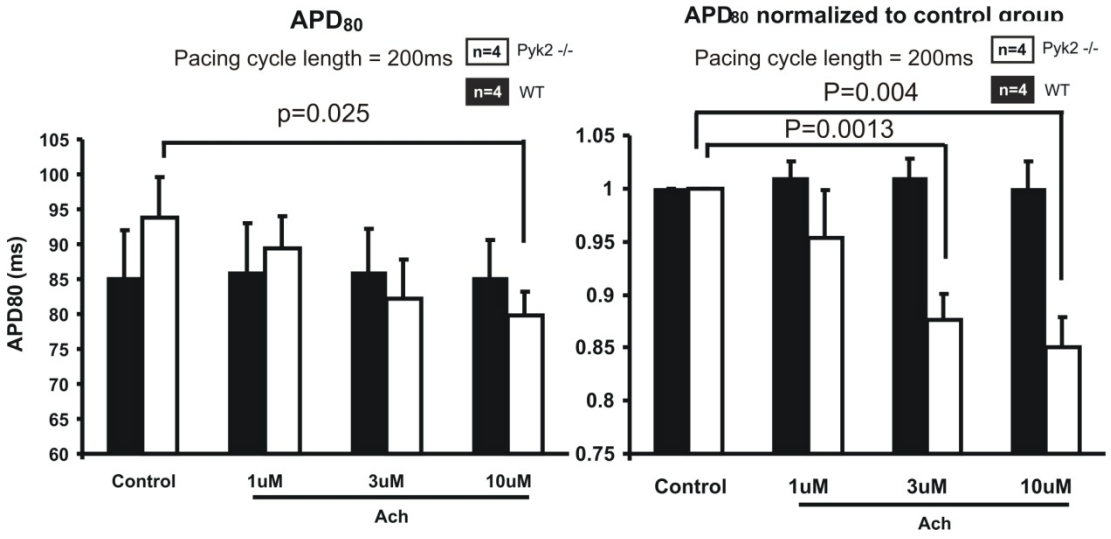

Figure 3.13 APD analysis of TAC mice. APD_{80} was statistically analyzed. Significant drease of APD was observed at high concentration ACh application, as being accord to mice without TAC surgry.

3.5 Discussion

This study presents evidence of expression of Pyk2 in the human heart and its significant activation in end-stage heart failure due to non-ischemic cardiomyopathy, but not in ischemic cardiomyopathy.

Pyk2 function has been investigated in a variety of cell types (reviewed in[79, 84]), including neuronal [79, 104] and immune system cells [98], in which Pyk2 has been shown to act as a key integrator of multiple signaling pathways and play important roles in cell migration, cytoskeletal remodeling, cell proliferation, survival, differentiation, pH regulation and calcium homeostasis. Recent studies have begun to focus on Pyk2 function in cardiomyocytes [85] as well as cardiac fibroblasts, vascular smooth muscle and vascular endothelial cells.[75, 87-89] In this study I investigated the *in vitro* functions of Pyk2 on whole heart level using mice with germline deletion of Pyk2 gene.[98]

Previous studies have reported that Pyk2 is activated by vagal stimulation through acetylcholine receptor [80, 89]. I explored this phenomenon in the whole heart in order to probe its possible role in arrhythmogenesis. I found that Pyk2 deficiency leads to two distinct phenotypes related to cholinergic system. On the one hand, Pyk2 deficiency leads to a loss of cholinergic function in the AV node. On the other hand, $Pyk2^{-/-}$ mice exhibit a significant shortening of ventricular APD80 during cholinergic stimulation in a dose-dependent fashion, which results in increased vulnerability to pacing induced ventricular arrhythmogenesis. These results suggest that Pyk2 plays an important role in patterning vagal control of the heart structures and may play a role in protecting ventricular myocardium against tachyarrhythmias in the settings of vagal stimulation.

The mechanisms of arrhythmogenesis in the $Pyk2^{-/-}$ mice are related to ACh-sensitive APD shortening and not due to conduction abnormalities. I did not explore the mechanisms of APD

shortening in this study, but it is likely due to a gain of function of potassium channels or a loss of function of calcium currents. Previous studies showed that Pyk2 is involved in the calcium-induced regulation of ion channels including potassium channels and calcium channels. For example, Pyk2 was shown to regulate the delayed rectifier-type potassium channel (Kv1.2) [80], calcium-activated potassium channels (BK_{Ca}) [105] and voltage-gated calcium channels that mediate their response by and are sensitive to intracellular calcium concentration [80, 92]. These ion channels may contribute to the observed shortening of APD in the $Pyk2^{-/-}$ mouse ventricles.

In addition to acute functional consequences induced by deficiency of Pyk2 in the mouse heart, I also found a chronic remodeling of calcium handling proteins using gene expression profiling. I found that SERCA2 mRNA level is decreased in $Pyk2^{-/-}$ ventricles compared with WT ventricles. In contrast to our findings, Pyk2 overexpression has been reported to downregulate SERCA2 mRNA level in neonatal rat ventricular myocytes [92]. Interestingly, overexpression of catalytically inactive (kinase-dead) and phosphorylation-site mutant forms of Pyk2, which are known to exert dominant-inhibitory effect on the endogenous Pyk2 signaling, has also resulted in reduction in SERCA2 mRNA levels.[92] It should be noted that the study by Heidkamp et al.[92] utilized a "gain-of-function" approach to overexpress various forms of Pyk2 via adenoviral gene transfer in cultured neonatal rat cells, whereas our study uses a knockout mouse model approach. The differing results between our study and that by Heidkamp et al. may therefore reflect the differences in the experimental approaches and/or the experimental systems employed in each study. Remodeling of NCX1 related with Pyk2 has not been reported. Microarray results indicate that Pyk2 signaling regulates calcium handling on transcriptional level. Additional studies are needed to elucidate the mechanisms underlying the Pyk2-dependent regulation of SECRA2 and NCX1 gene expression.

Previous cardiac studies of Pyk2 were mainly focused on ventricular cells; therefore its role in the SAN, atria or AVN has not been explored. In this study, I measured heart rate and AV-delay

to estimate the effect of Pyk2 on SAN and AVN. I found that Pyk2 deficiency does not alter autonomic regulation of heart rate and atrial APD. However, autonomic regulation of AV conduction is significantly altered. Unexpectedly, AVN lost sensitivity to cholinergic stimulation in $Pyk2^{-/-}$ mice. This data indicates that Pyk2 may participate in patterning of cholinergic control of the mammalian heart.

Pyk2 expression in cardiomyocytes was first reported by Bayer et.al in 2001,[85] but it has not been reported in the human hearts until this report. I show for the first time a robust expression of Pyk2 in human ventricles with a constant level of expression across disease states including end stage heart failure of ischemic and non-ischemic etiologies. Furthermore, I also found that Pyk2 is significantly activated in non-ischemic but not in ischemic cardiomyopathy. Overall, our findings suggest that Pyk2 activation could be involved in cardiac protection against arrhythmia in non-ischemic cardiomyopathy. Pyk2 has been shown to be expressed at much higher levels in cultured neonatal compared to adult cardiomyocytes.[85] Therefore, a possibility needs to be considered that at least some of the electrophysiological effects observed in the $Pyk2^{-/-}$ mice might be potentially due to Pyk2 ablation in non-cardiac cell types (i.e. neuronal, vascular endothelial, immune cells, all of which normally express abundant levels of Pyk2). Additional studies, using conditional tissue-specific *Pyk2* gene targeting, are needed to elucidate the mechanisms underlying this important issue.

Chapter 4

Regional Calcium Mishandling in Aged *mdx* Mouse during Ventricular Stretch Conditions

4.1 Abstract

Cytoskeletal signaling allows cell deformation and mechanical stress to adapt form to function mediated by cytoskeletal proteins. Duchenne Muscular Dystrophy (DMD) is a clinical syndrome due to recessive dystrophin which an important protein bridges extracellular matrix and actins. Cardiac dysfunction is a primary cause of patient mortality in DMD, potentially related to deleterious effects of elevated cytosolic calcium. However, the regional versus global functional consequences of cellular calcium mishandling have not been defined in the whole heart. Here, we sought to elucidate potential regional dependencies between calcium mishandling and myocardial fiber/sheet function as a manifestation of dystrophin-deficient cardiomyopathy. Isolated-perfused hearts from 16 month-old mdx and wildtype were experimentally used to detect myocardial sheet architecture by MRI and optically mapped to evaluate Ca handling. Compared to WT, mdx hearts exhibited normal systolic sheet architecture but a lower diastolic sheet angle magnitude ($|\beta|$) in the basal region. The regional diastolic sheet dysfunction was normalized by reducing perfusate calcium concentrations. Optical mapping of calcium transients in isolated hearts suggested deficiency of distrophin is not enough to induce Ca handling at baseline, thus a mechanical stretch stimulation setup was designed. Result of optical mapping on mdx hearts with this setup revealed a stretch–

inducible regional defect of intracellular calcium reuptake, reflected by a 25% increase of decay times (T50) and decay constants, at the base of mdx hearts. The basal region of mdx hearts also exhibited greater fibrosis than did the apex, which matched the regional sheet dysfunction. We conclude that myocardial diastolic sheet dysfunction is observed initially in basal segments along with calcium mishandling, ultimately culminating in increased fibrosis. The preservation of relatively normal calcium reuptake and diastolic/systolic sheet mechanics throughout the rest of the heart, together with the rapid reversibility of functional defects by reducing cytosolic calcium, points to the significance of regional mechanical factors in the progression of the disease.

Part of the contents of this chapter were published in Am J Physiol Heart Circ Physiol[106] and reprinted with the permission of the publisher.

4.2 Introduction

Cardiac myocytes possess a complex cellular architecture, which is maintained by a protein framework called the cytoskeleton. Cytoskeletons perform structural functions in the cell, such as organizing functionally related proteins and facilitating mechanical interactions with adjacent cells and the extracellular matrix (ECM). In addition, cytoskeletal structures also regulate proliferation through pathways activated by cytoskeletal signaling. Cytoskeletal signaling allows cell deformation and mechanical stress to adapt form to function by modifying the size, shape and even molecular composition of the heart. This role is especially important in HF where cytoskeletal signaling contributes to various responses leading to functional remodeling in myocytes. Mechanical dysfunction remains one of the best predictors of sudden cardiac death in HF. However, the relationships between mechanical dysfunction and electrical instability are not fully understood.[107, 108]

The mechanical and signaling functions of the cytoskeleton stem fromthe interactions of dozens of proteins. One of these proteins, dystrophin, anchors the actin microfilaments to dystroglycan, which spans the plasma membrane to bind such ECM proteins such as fibronectin and laminin. Within the cytosol, dystrophin and dystroglycan form a signaling complex with dystrobrevin and syntrophins to participate in cytoskeletal singaling (Figure 4.1). Mutations in dystrophin can cause dilated cardimyopathies by destabilizing cell-matrix linkages and increase chances of HF. Duchenne muscular dystrophy (DMD) is a typical disease of such underlying pathology.

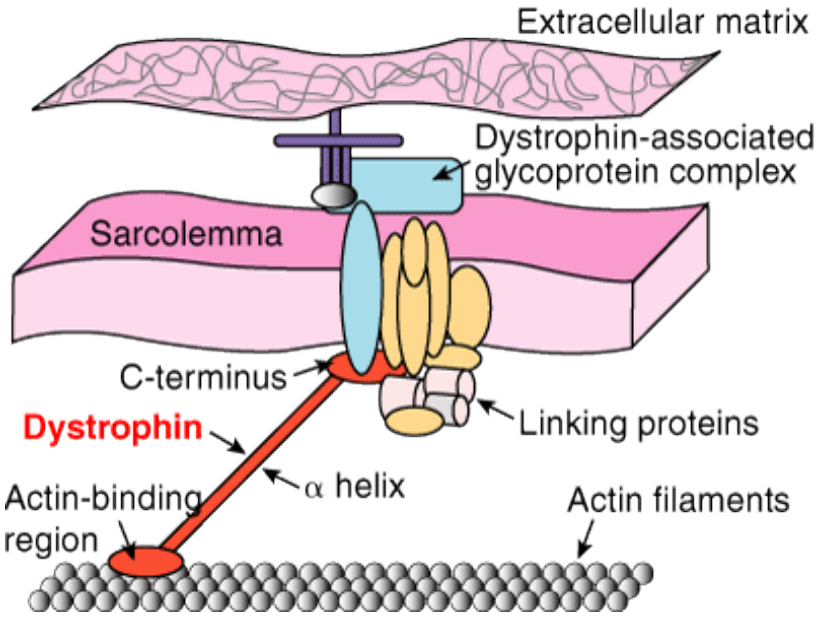

Figure 4.1 Structure diagram of Dystrohin. From McGavin group.[109] Dystrophin formed complex bridges sarcolemma and actin.

DMD is a fatal X-linked genetic disease that affects 1 in 3500 of newborn boys who manifest unremitting deterioration of all muscle groups over time. Cardiac dysfunction accounts for 10~20% of all mortality in DMD, making it the second leading cause of patient death following respiratory failure [110]. Advances in respiratory support and patient care allow many patients to

survive into their late 20s and 30s.[110-118] Accordingly, cardiac complications now are commanding closer scrutiny in the management of advanced disease in DMD patients.[117, 118]

The clinical DMD phenotype reflects the absence of normal dystrophin due to mutation of the dystrophin-encoding gene on the X-chromosome. Dystrophin is a key component of the transmembrane dystrophin-associated glycoprotein complex (DGC) that bridges intracellular actin and the ECM to facilitate mechanical coupling and signal transduction, and to stabilize the sarcolemma membrane.[119, 120] Previous studies using MR tagging uncovered, abnormal wall strains occurring regionally at the base of heart in DMD patients. A subsequent report by Li *et al* has also suggested that cardiac mechanical strain abnormalities are more prominent in the basal segments of hearts in *mdx* mice.[121] These observed regional dependencies for DMD cardiac mechanical dysfunction remain to be explained as the mutation is present homogeneously in all cardiomyocytes.[122-126]

With respect to pathophysiological features of dystrophin deficiency potentially responsible for mechanical dysfunction, several recent studies using isolated cardiomyocytes from *mdx* mouse have suggested that $[Ca^{2+}]_i$ mishandling is a key causative factor.[127-129] How calcium mishandling influences cardiac mechanical dysfunction in whole heart preparations has not been clarified, especially when considering cellular and mechanical events that are spatio-temporally distributed (e.g., excitation-contraction coupling) and regionally heterogeneous (stress and strain).[130, 131] Given the known abnormal and regionally heterogeneous wall strains in DMD hearts[132], the present work will evaluatethe hypothesis that the functional consequences of dystrophin deficiency are played out *regionally* in DMD hearts over time, despite there being genetic abnormality in all cardiomyocytes.

Accordingly, I sought to elucidate such regional mechanical consequences of the disease on local myocardial fiber-sheet function using diffusion tensor MRI, in concert with whole heart optical calcium mapping. Complete global 3D information set acquired from isolated, perfused, and beating *mdx* hearts should allow the delineation of cycle dependence (diastole vs. systole) of principle cardiac defects in dystrophin-deficiency and potentially shed light on whether these defects might be reversible (i.e. functional) consequences of calcium mishandling or be nonreversible consequences of fibrosis (i.e., remodeling).

4.3 Part I. MRI Reveals Focal Diastolic Sheet Dysfunction in *mdx* Mouse Heart

MRI experiment was conducted were performed by Ya-jian Cheng as a collaboration with Dr. Samuel Wickline's group.

4.3.1 Material and Methods

4.3.1.1 Animals

Adult male *mdx* (C57BL/10ScSn-Dmdmdx/J, N=14) and age matched male wild type (WT: C57BL/10SnJ, N=10 and C57BL/6, N=3) mice were purchased from Jackson Laboratory (Bar Harbor, ME, USA) and the National Institute on Aging (NIA, MD, USA)[133] and housed under a AAALAC-approved facility to 16-month of age. All mice were housed in the same animal facility and cared for under approval by Washington University's animal study committee.

4.3.1.2 Isolated Heart Preparation for diffusion tensor MRI

Ten *mdx* mice and ten WT mice (C57BL/10SnJ) were used for diffusion tensor MRI (DTI) measurement. Mice were heparinized (1000 U/kg) and anesthetized with 0.05 isoflurane. Hearts were excised and cannulated for retrograde perfusion using a procedure modified from Chen *et al.*[134] Briefly, hearts were first perfused with Krebs buffer at 60 mmHg constant pressure for approximately 5 min to wash out the residue blood. Five *mdx* hearts and five WT hearts were perfusion-arrested in diastole (perfusion pressure = 60 mmHg) with the regular St. Thomas' cardioplegic solution containing normal [Ca^{2+}] of 1.2 mmol/L (denoted as *mdx*-NC and WT-NC, respectively) under room temperature. DTI of diastolic arrested hearts were performed for 1.5 hours. After that, hearts were reperfused with 37 C Krebs buffer to resume beating. Upon stabilization of cardiac work (~6 min, up to 300 beats per min), 2.5 mmol/L $BaCl_2$ was introduced to induce cardiac contracture.[134-136] All solutions were equilibrated with 95% O2 plus 5% CO2 (PH 7.4) and contained adenosine (45μmol/L) to maximally dilate the coronary vessels.[137] Bovine serum albumin (BSA; 61 μmol/L) was added to the perfusate to minimize interstitial edema. [138, 139] DTI of systolic hearts were imaged for ~1.5 hours. Upon the completion of MRI, all hearts were perfused with 10% formalin to fix in diastole or systole for histological study.

To evaluate the effect of [Ca^{2+}] on the cardiomyocyte architecture in dystrophin-deficient mice, another five *mdx* hearts and five WT hearts were perfusion-arrested in diastole with the a modified cardioplegic solution containing low [Ca^{2+}] of 0.078 mmol/L (denoted as *mdx*-LC and WT-LC, respectively). The 0.078 mmol/L [Ca^{2+}] was chosen over the calcium-free condition to minimize the risk of complete depletion of intracellular calcium, which can cause calcium overload upon reperfusion with solutions containing normal [Ca^{2+}], thereby exerting unfavorable effects on certain ion channels. [135, 140]

A dedicated MRI-compatible retrograde mouse heart perfusion system was used to acquire high signal to noise (SNR) diffusion tensor MR images. This system provides a quantitative and

non-destructive assessment of diastolic and systolic myocardial architecture from the same heart. The system includes: (1) a custom-built 15 mm-diameter solenoid coil, which provides high SNR: 65 for non-diffusion weighted images; and 40 for diffusion weighted images; (2) a Langendorff constant-pressure perfusion apparatus that allows arrest of a viable heart sequentially in diastole and then in systole.

4.3.1.3 DTI

All MRI experiments were performed on a Varian 11.7-T small animal MR scanner (Varian Associates; Palo Alto, CA) and a custom-built 15mm-diameter solenoid coil was used to acquire images. Long-axis scout images were acquired as previously described.[134] A multislice spin-echo sequence with diffusion-sensitizing bipolar gradient were used to acquire short-axis, diffusion weighted images. Diffusion-sensitizing gradients were applied in six noncolinear directions. Imaging parameters are as follows: echo time, 46 ms; time interval between diffusion-sensitizing gradients, 30 ms; b-value, 0 and 800 s/mm^2; in-plane resolution, 125 × 125 μm^2, repetition time, 3 s; and image-acquisition time, 1 h. For diastolic arrested hearts, eight contiguous slices (thickness = 0.7 mm) extending from the base to apex were acquired. For systolic arrested hearts, eight contiguous slices were acquired with slice thickness adjusted to 0.55–0.65 mm based on the fraction of longitudinal shortening after barium induced contracture. Attention was paid to keep the slice selection and the heart orientation the same between diastole and systole imaging.

All MR images were processed using custom-developed software written in Matlab (The MathWorks Inc., M.A. USA.) as described previously [134]. Fiber helix angle (α) and sheet angle (β) are calculated from the tensor according to literature [134]. Briefly, the fiber helix angle (α) was calculated as the angle between the circumferential cardiac axis and the projection of the first

eigenvector of the diffusion tensor onto the circumferential-longitudinal plane; the right-handed helix was set as positive [141]. Sheet angle (β) was determined as the angle between the secondary eigenvector and the radial axis; the sheet inclined toward the base from endocardium to epicardium was set as positive (Figure 4.2) [141, 142]. Because regional wall thickening is accompanied by a reduced magnitude of the sheet angle (|β|) despite the sign of sheet angle [134, 143], the |β| was used to analyze regional diastolic and systolic sheet function. LV wall thickness was calculated as the mean distance between epicardial and endocardial borders. The through-wall difference of α, defined as the difference in endocardial and epicardial helix angles, i.e., $\Delta\alpha = \alpha_{endocardium} - \alpha_{epicardium}$, was used to quantify transmural changes of fiber orientation.

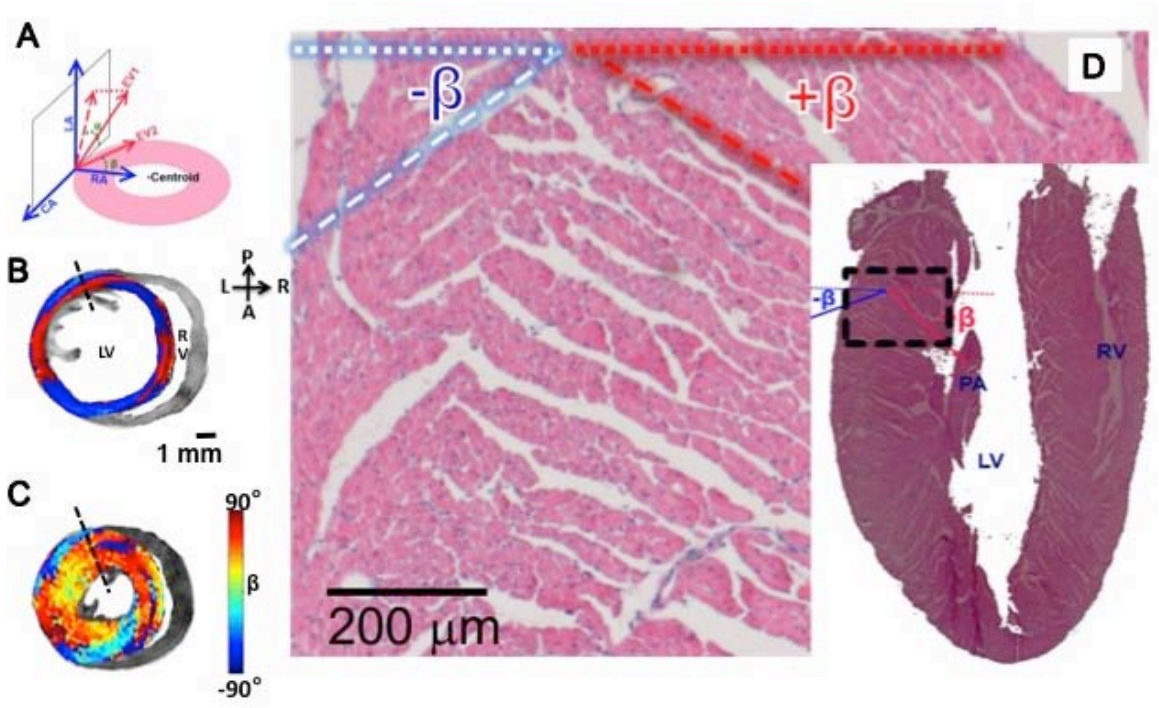

Figure 4.2 Representative DTI and histology images of sheet architecture in WT mouse hearts. A, A local cylindrical coordinate system was used to determine LV myocardial structures. The primary eigenvector of the diffusion tensor is characterized by helix angle (α), which is the angle between the circumferential axis and the projection of the first eigenvector onto the circumferential-longitudinal plane; the α shown in A is set as negative. The secondary eigenvector is characterized by sheet angle (β), which is the angle between the secondary eigenvector and the radial

axis; the β shown in A, toward base and toward endocardium, is set as negative. B & C, short-axis views of DTI determined sheet angle (β) in a basal slice of WT heart that was sequentially arrested in diastole (B) and systole (C). The posterior-lateral wall of LV manifested two populations of β, exhibiting positive (red) and negative (blue) values. D, Histology of sheet organization in a WT heart. Images were acquired from the basal-lateral wall, which is highlighted on the H&E stained image (insert). Two populations of β were observed.

4.3.2 Results

4.3.2.1 mdx Hearts Manifest Abnormal Regional Diastolic Sheet Function

DTI defined two populations of b with opposite signs in the LV wall of WT and mdx mice, as confirmed by several previous reports [134, 142, 144-147]. The $|\beta|$ value is decreased in systole (Figure 4.2 B&C, Figure 4.3 A&B), reflecting the reorinetation of myocardial sheets, which contributes ~50% of systolic focal wall thickening [134, 143, 145, 148]. Under conditions of barium-induced systolic arrest, at each short-axis location, the systolic $|\beta|$ was comparable among all groups of hearts (p = N.S.). However, the diastolic $|\beta|$ of mdx hearts (mdx-NC) was ~10° lower than that of WT hearts (WT-NC) at the base when perfused with regular cardioplegic solution ($p < 0.05$, Figure 2). The $|\beta|$ at the apex of mdx-NC hearts appeared normal (p = N.S. compared to WT-NC at each corresponding short axis imaging slice), demonstrating that sheet diastolic dysfunction in mdx hearts occurred focally at the base. By reducing the $[Ca^{2+}]$ of the cardioplegic solution to 7% of its regular concentration, a complete and rapid restoration of diastolic $|b|$ in mdx hearts (mdx-LC) to normal values was observed. No effect of calcium manipulation on WT cardiac sheet function was observed (WT-LC, p = N.S. compared to WT-NC at each corresponding short axis imaging slice), indicating that the diastolic sheet dysfunction in mdx hearts was substantially calcium dependent. These data suggest that even at this advanced age, a principle mechanical

abnormality in mdx mice likely is associated with incomplete sarcomere relaxation that is regionally dependent.

At the base, further regional analysis indicated that the maximal decrease of diastolic |β| in mdx-NC hearts occurred in the endocardium and in the posterior-lateral wall. Compared to WT-NC, mdx-NC exhibited 13° lower |β| (75°± 2°vs. 62°± 3°) in the endocardium (inner 1/3 wall-depth in transmural direction); 10°lower |β| (74°± 1°vs. 64°± 2°) in the midcardium (middle 1/3 wall-depth in transmural direction); and 8° lower |β| (68°± 2°vs. 60°± 2°°) in the epicardium (outter 1/3 wall-depth in transmural direction) (Figure 2C). In the posterior-lateral wall, the diastolic |β| was 51°± 6° in mdx-NC (Figure 2F). This value was approximately 20° lower than that of mdx-LC (70°± 4°), as well as that of WT-NC (72° ± 4°) or WT-LC (72°± 6°) groups ($p < 0.05$ for all comparisons). Together these findings indicate a clear regional and transmural dependence of incomplete relaxation, despite the ubiquitous dystrophin mutation.

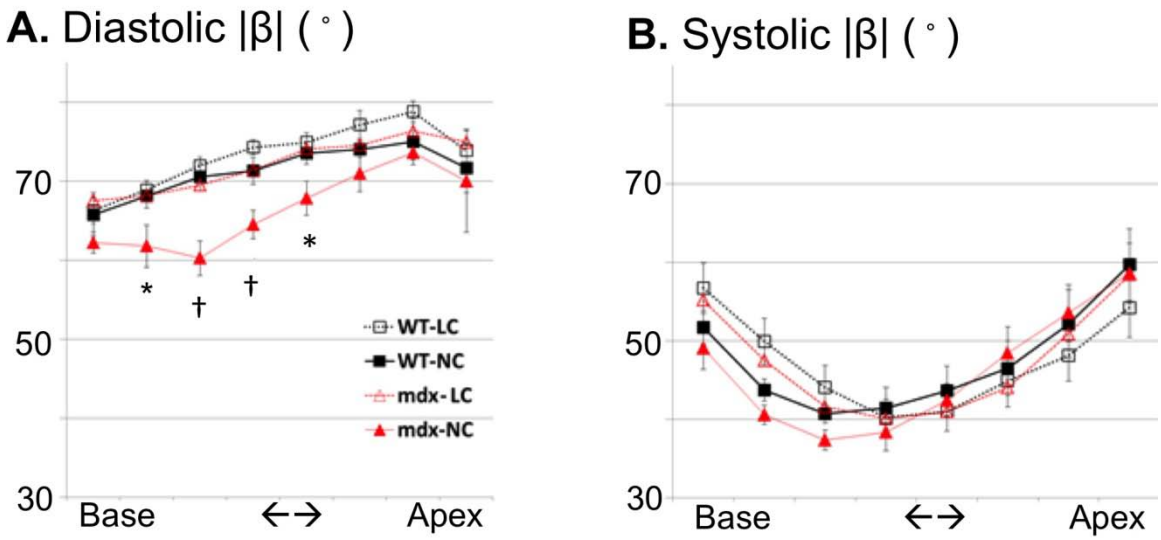

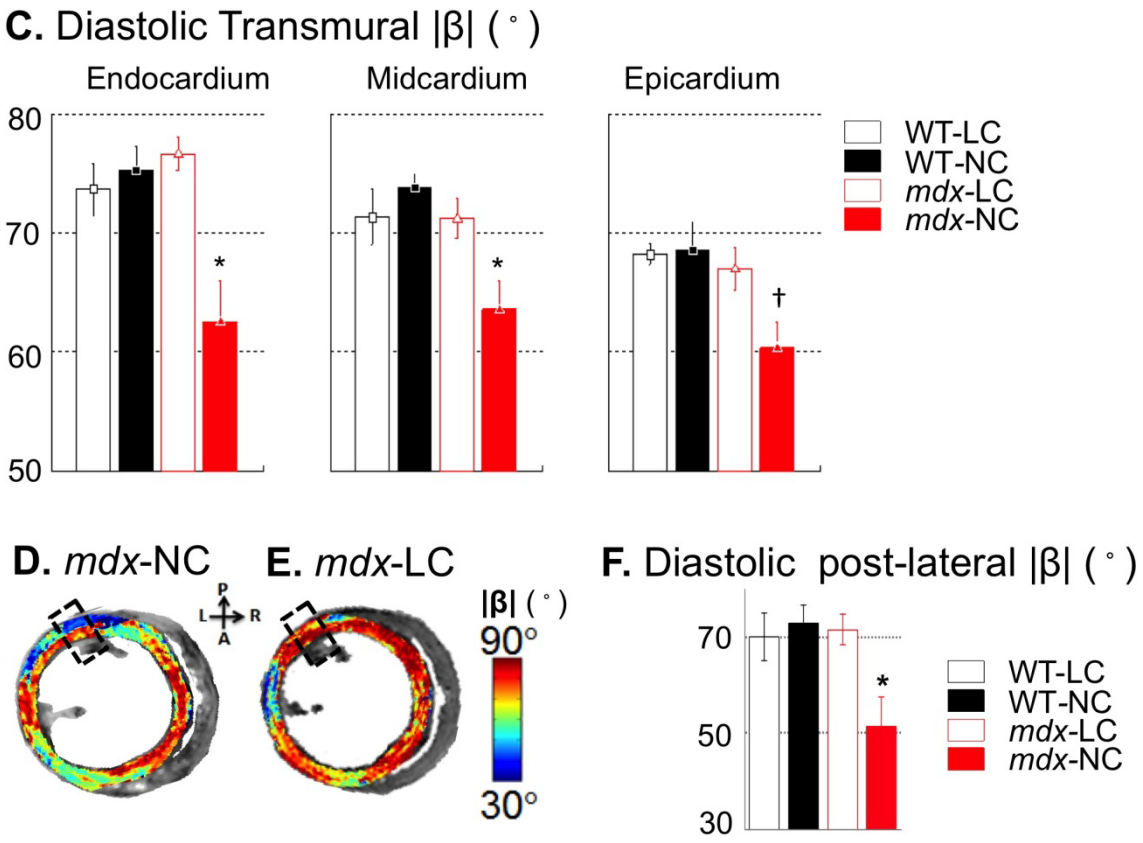

Figure 4.3 DTI-determined diastolic and systolic |β| in short-axis slices. A, mdx hearts exhibited abnormally lower diastolic |β| that was recovered to normal value after reducing [Ca2+] in the perfusate. For hearts perfusion-arrested in diastole with normal calcium solution, mdx hearts (*mdx*-NC) exhibited lower |β| than did WT (WT-NC) hearts with the maximal ~10° difference occurred at the basal region. In contrast, mdx hearts perfused with the low calcium solution (mdx-LC) exhibited normal diastolic |β|. Varying [Ca^{2+}] had no effect on diastolic |β| in WT hearts (WT-LC). B, systolic |β| exhibited no difference among four groups of hearts. C, diastolic |β| in the epicardium, midcardium, and endocardium at the base of WT and *mdx* hearts. In all regions, diastolic |β| of mdx-LC hearts were comparable to that of WT-LC and WT-NC hearts, but all are higher than that of mdx-NC hearts. The largest difference in diastolic |β| between mdx-LC and mdx-NC was observed in the endocardium. D & E, representative DTI-determined diastolic |β| maps on short-axis slices at the base of mdx-NC and mdx-LC hearts. The lower |β| in mdx-NC heart, indicated by fewer regions with red color, was visually appreciable. F, in the posterior-lateral region (the areas enclosed by dashed line in D & E), the diastolic |β| of mdx-NC hearts was approximated 20° lower than that of mdx-LC hearts and of all WT hearts. Data represent mean ± SEM. N = 5 for each group. *, $p < 0.05$; †, $p < 0.005$ for the indicated short axis location.

4.4 Part II Mechanical Stretch Induced Regional Ca Mishandling underlies Sheet Dysfunction

Dysfunction of sheet angle indicates dysregulation of cardiac contractions, which is mainly mediated by Ca signaling. To explore the mechanism underlying the dysfunction of sheet angle, I conducted optical mapping of intact *mdx* mouse hearts. Experiments were designed to: 1) evaluate the relationship between Ca dysfunction and mechanical stretch (relation experiment) and 2) investigate several parameters of Ca release and Ca reuptake to evaluate Ca dysfunction from mechanical stretch (dysfunction experiment).

4.4.1 Material and Methods

4.4.1.1 Animal

Animal information is the essentially the same as described in section 4.3 except with the addition of young WT and *mdx* mice in the experiment. Two aged WT and 3 aged *mdx* mice are used in baseline experiments.

Four groups of mice are used in the relation experiment: aged WT (n=5); aged *mdx* mice (n=5); young WT (n=5); young *mdx* mice (n=5). Another 4 aged WT and 4 aged *mdx* mice are used in the dysfunction experiment.

4.4.1.2 Isolated Heart Preparation and Ca Dye Loading

Langendorff-perfused hearts from 16 months and 12 weeks old mice were separated into four groups (aged WT, n=5; aged *mdx*, n=5; young WT, n=5; young mdx, n=5 and aged WT, n=4 and aged mdx, n=4 for relation and dysfunction experiment respectively). The isolated heart was

prepared according to a Langendorff perfusion protocol modified for murine hearts [74]. Briefly, after anesthesia and heart excision, a short section of aorta was attached to a 21-gauge cannula. After cannulation, hearts were superfused and retrogradely perfused with oxygenated (95% O_2, 5% CO_2) and modified Tyrode solution (in mmol/L: NaCl 128.2, KCl 4.7, NaH_2PO_4 1.19, $MgCl_2$ 1.05, $CaCl_2$ 1.3, $NaHCO_3$ 20.0, and glucose 11.1 (pH=7.3)) that was passed through a 5 μm filter (Millipore, Billerica, USA) and held at a constant-temperature (37±1°C). Perfusion was performed using a peristaltic pump (Peri-Star, WPI, Sarasota, USA) under a constant aortic pressure of 60 - 80 mm Hg.

The isolated heart was pinned at the edge of ventricular apex to a Sylgard base in order to prevent stream-induced movement. A small silicon tube was inserted into the left ventricle through the pulmonary vein, left atria, and tricuspid valve to prevent solution congestion and subsequent ischemia. A small black tape was used to cover the atria to prevent fluorescence scattering from the atria (Figure 4.4). Excitation-contraction uncoupler blebbistatin (10 μM, Tocris Bioscience, USA) was used to prevent the effect of motion artifact when estimating action potential duration. The heart was then stained with a calcium indicator (Rhod-2 AM, Invitrogen, Carlsbad, CA, 30μL of 1 mg/mL dimethyl sulfoxide, 1:1 mixed with Fluronic F127, Invitrogen, Carlsbad, CA in Tyrode's solution), for 5-7 minutes.

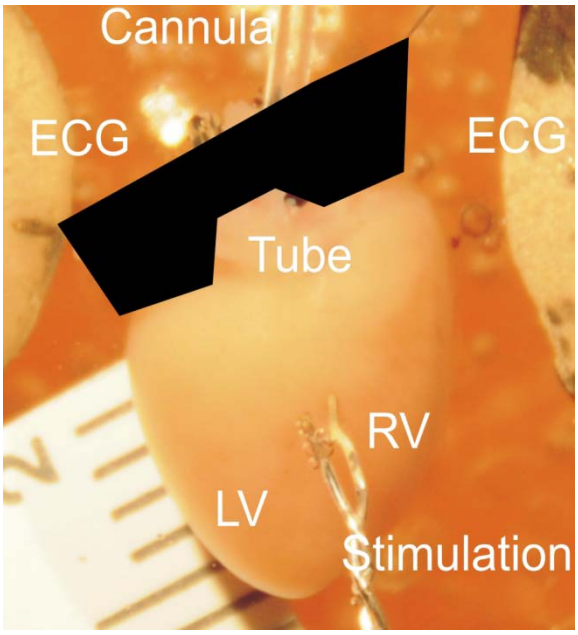

Figure 4.4 Intact mouse heart preparation. Small black tape covered the atria to prevent fluorescence scattering from the atria thus making it is possible to accurately analyze the regional difference of CaT over the ventricle.

4.4.1.3 Optical Imaging System

The excitation light was generated by a halogen lamp (Newport Oriel Instruments, Stratford, CT; SciMedia, Costa Mesa, CA) and passed through a heat filter, shutter, and excitation band-pass filter (520 ± 45 nm). A flexible light guide directs the band-pass filtered light onto the heart preparation. The optical mapping apparatus comprised an MiCAM Ultima-L CMOS camera (SciMedia, Costa Mesa, CA) with high spatial (100x100 pixels, 230±20 μm per pixel) and temporal (1,000-3,000 frames/sec) resolution. A band-pass filter (590±15 nm, Thorlabs, Newton, NJ) was fixed in front of the calcium-imaging camera.

4.4.1.4 Mechanical Stretch Setup

A mechanical stretch setup was designed to apply appropriate mechanical stimulation on the heart while normal contraction is suppressed during optical mapping experiments. Mechanical

stretch is induced by manipulation of the inner pressure within left ventricle. As depicted in Figure 4.4, the silicon tube inserted into the left ventricle was used to pump temperature-controlled and oxygenated Tyrode's solution. Left ventricular inner pressure can be quantified and controlled while inflating Tyrode's solution is placed at different height. Real-time monitoring of pressure is conducted by a pressure transducer held at the same level of the heart. For accuracy, the transducer was hooked up at the tip of silicon tube emerging out of the heart.

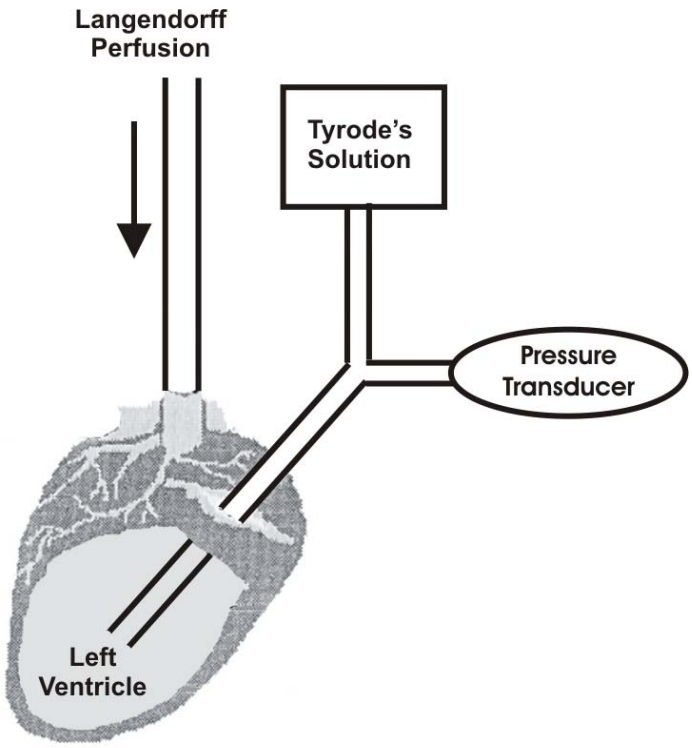

Figure 4.5 Mechanical stretch setup design layout. Left ventricle is filled with Tyrode's solution, and its inner pressure can be manipulated by gravitational effects when solution is place at different heights.

4.4.1.5 Optical Mapping Protocols

After isolation and cannulation, motion suppression, and dye staining, prepared hearts were equilibrated for 5-10 min before imaging. Optical mapping signals were recorded sequentially under

unloaded and stretched conditions. The unloaded condition was achieved by a pressure releasing silicon tube inserted into the LV chamber of the Langendorff heart preparation. The stretched condition was achieved by inflating the LV chamber with the mechanical stretch setup. Mapping of CaT was conducted at different loading conditions including baseline (0 mmhg pressure), 40, 60, 80, 100 and 120-mmhg pressure. Design of pressure point is based on pressure-volume loop of rodent models (Figure 4.5). Physiological ventricular inner pressure ranged from 10 to 100 mmhg. An un-physiological condition at 120 mmhg is chosen to evaluate the response of both WT and *mdx* mice heart under mechanical damage. Baseline recording was conducted to test the reversibility of such damage. The aortic perfusion pressure was increased from 60 to 100 mmHg to maintain the direction of the retrograde perfusion and the viability of the perfused heart. 200 ms and 100 ms pacing were conducted at each stretch condition. In the following experiment when 80 mmhg was chosen to detect the detailed regional dysfunction of Ca handing in aged *mdx* mice, a steady-state restitution (S1-S1)[74] pacing protocol was applied under both conditions. Briefly, hearts were paced with a basic cycle length from 200 to 100 ms in steps of 20ms and from 100 to 40 ms in steps of 10 ms until 1:1 capture failed or ventricular tachyarrhythmia, including ventricular fibrillation, occurred.

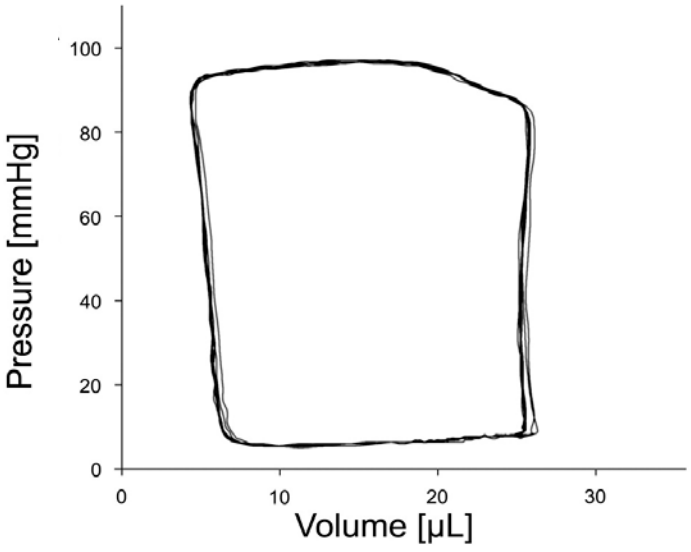

Figure 4.6 Pressure-Volume loop of rodent animals. From Nielsen et al.[149]

4.4.1.6 Optical Mapping Data Processing

A custom-designed Matlab program was used to analyze optical mapping signals. The signals were filtered with a low-pass Butterworth filter at 256 Hz. Regional calcium dynamics were quantified in WT and *mdx* mouse ventricles (base vs. apex) under both unloaded and stretched conditions. Hand-drawn regions of interest were used to define basal (upper 1/3 area of left ventricle) vs. apical regions (lower 1/3 area of left ventricle). Ca relaxation time from the calcium transient peak value to 50% relaxation (T50) was calculated and used to define the calcium reuptake phase. Ca decay constant was calculated using an exponential curve fitting program measuring from 50% calcium peak value to full relaxation. Taken together, the T50 (for the early relaxation phase) and the decay constant (for the late relaxation phase) represent the process of Ca reuptake-dependent relaxation.

4.4.1.7 Statistics

Statistical differences were assessed with the use of analysis of variance (ANOVA) or multivariate analysis of variance (MANOVA) as appropriate. Bonferroni correction was applied to post-hoc comparisons. A value of $p < 0.05$ was considered significant. Data were expressed as mean ± standard error of the mean (SEM). All statistics were analyzed using the IBM SPSS Statistics program.

4.4.2 Results

4.4.2.1 No dysfunction of Ca handling in mdx mouse heart at baseline (unloaded) condition

CaT was optically mapped in aged *mdx* and WT mice hearts without mechanical stimulation. Isolated mouse heart was retrograde perfused by the Langendorff system as described. Under this condition, inner ventricular pressure was maintained at 0 throughout the whole experiment as perfusion solution does not defuse in and flow through heart chambers in Langendorff perfused hearts. CaD at different levels of Ca relaxation (30%, 50% and 80%) evaluates the morphology of CaT and represents Ca handling proteins' function at various phases of CaT. Results showed that no dramatic morphological change was observed in mdx mouse heart compared to WT group, indicating Ca handling was not significantly dysregulated under this condition. Quantification of this data is shown in Figure 4.6.

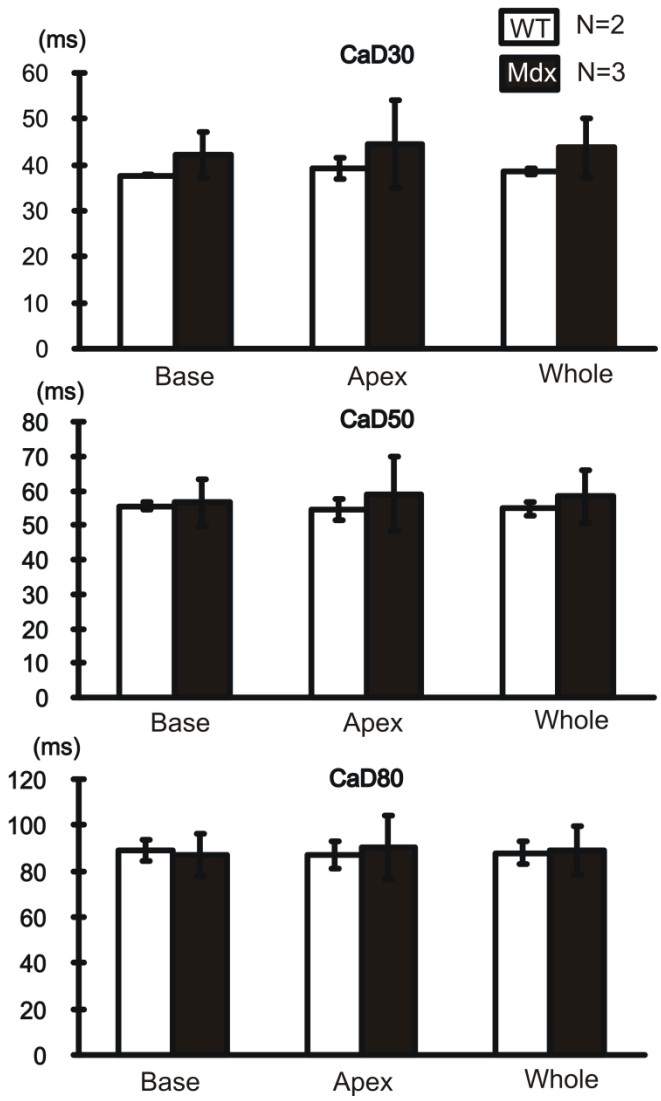

Figure 4.7 CaD at different levels of relaxation suggests no morphological change. CaD at different level of Ca relaxation (30%, 50% and 80%) was calculated to evaluate the morphology of CaT in both *mdx* and WT mouse heart.

4.4.2.2 Mechanical Stretch Stimulation Prolonged Ca Rise Time and CaD in Aged mdx Mouse Heart Following Pressure Dependent Pattern

When the left ventricle was loaded with Tyrode's solution, ventricular myocytes were stretched to different levels according to the inner ventricular pressure. CaD and Ca rise time were calculated under different loading conditions to evaluate the dysfunction of Ca handling. The sheet

angle experiment aimed to reveal whether Ca handling changes based on the region. CaT signals from the ventricular base, mid and apex were averaged and analyzed respectively. CaD values of all three regions from WT mouse hearts did not display a significant difference until the pressure increased to non-physiological pressures. In WT hearts, when the ventricular inner pressure increased to 120 mmhg, CaDs of the base and mid are dramatically prolonged while CaD of the apex is maintained at similar level as other conditions. This remodeling is reversible as CaD values returned to baseline level after pressure was released (Figure 4.7).

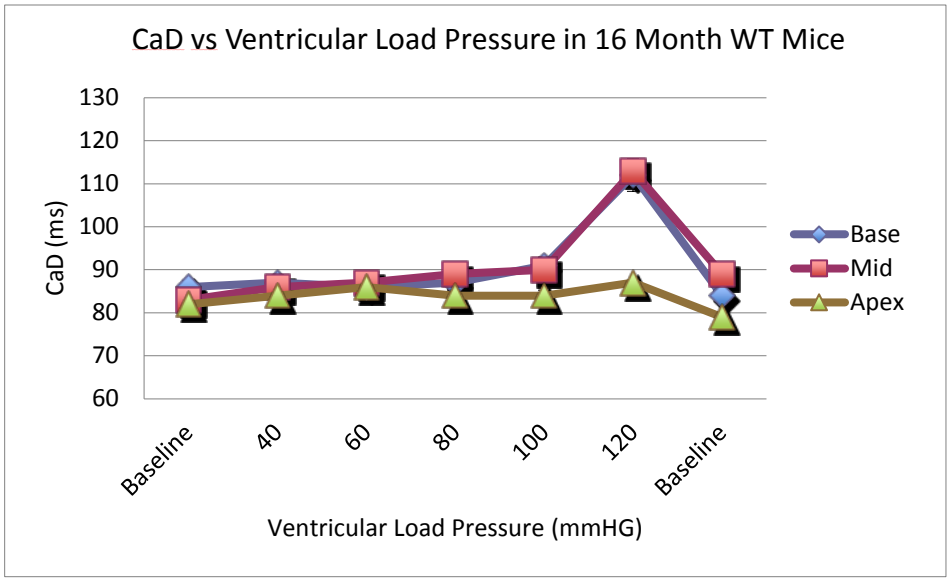

Figure 4.8 CaD-pressure relation curves of aged WT mice. CaD values of the base mid and apex were plotted as the function of pressures. CaD of base and mid maintained similar level until ventricle was stretched to a nonphysiological condition. At 120-mmhg condition, CaD of base and mid regions were significantly prolonged but recovered after the pressure was released. CaD of the apex remains unchanged for all conditions.

In the aged mdx group, prolongation of CaD of base and mid appeared at physiological pressures, even at very low pressure like 40 mmhg. Ca dysfunction evaluated by CaD prolongation aggravated as the pressure increased. This aggravation plateaud around 80 mmhg. In completely reversal of what was seen in WT mice, CaD of the base from added mdx mice did not return to baseline level after pressure was released (Figure 4.17). Similar to WT, CaD of apex remained unchanged under all conditions.

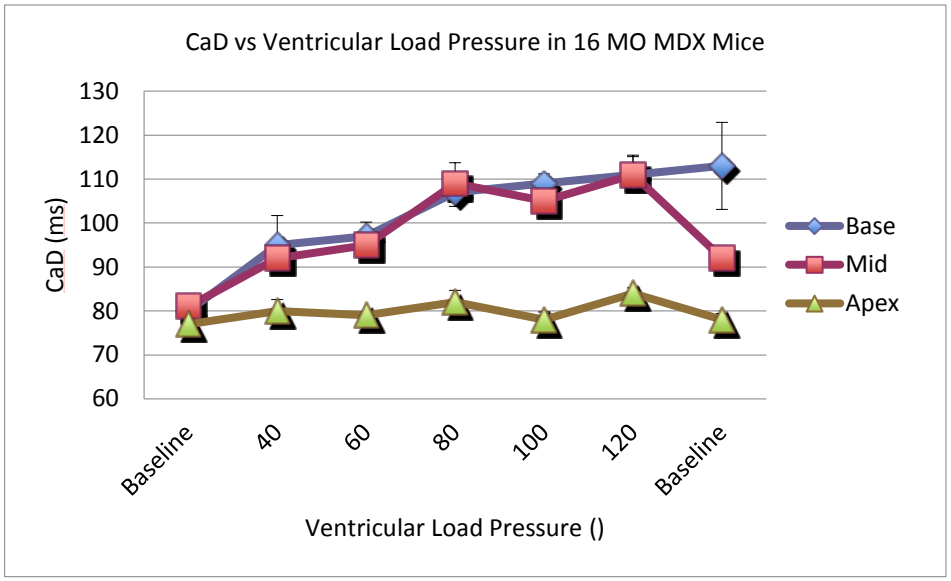

Figure 4.9 CaD-pressure relation curves of aged *mdx* mice. CaD of base and mid prolonged since 40 mmhg inner ventricular pressure. The prolongation aggravated as pressure increased. Prolongation of CaD of base did not recovery after pressure released. CaD of apex maintained unchanged under all conditions.

CaD from young WT and young mdx mice were also calculated. CaD value of all regions remained unchanged for all stretch conditions in both groups of mice (Figure 4.9 and 4.10).

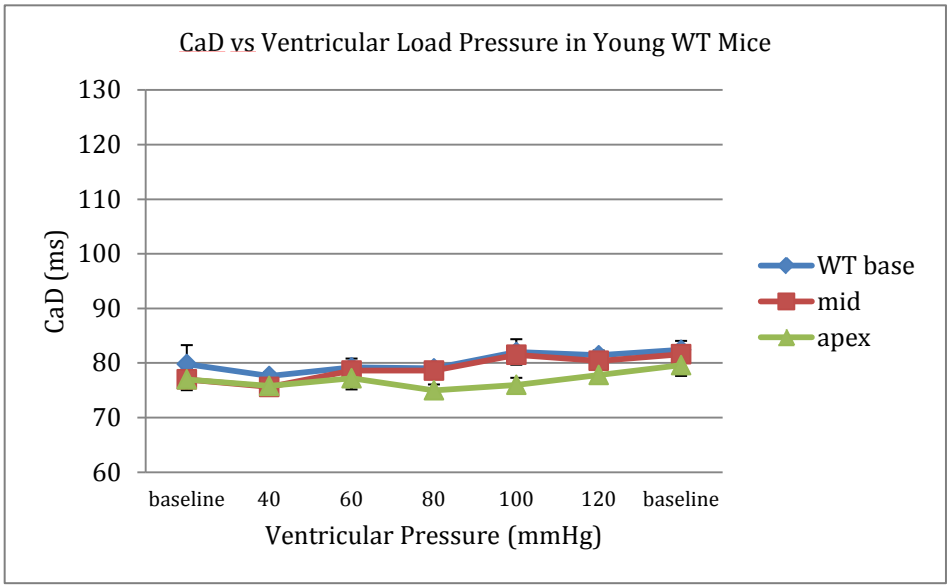

Figure 4.10 CaD-pressure relation curve of young WT mice. CaD maintained no change under all conditions in young WT mice.

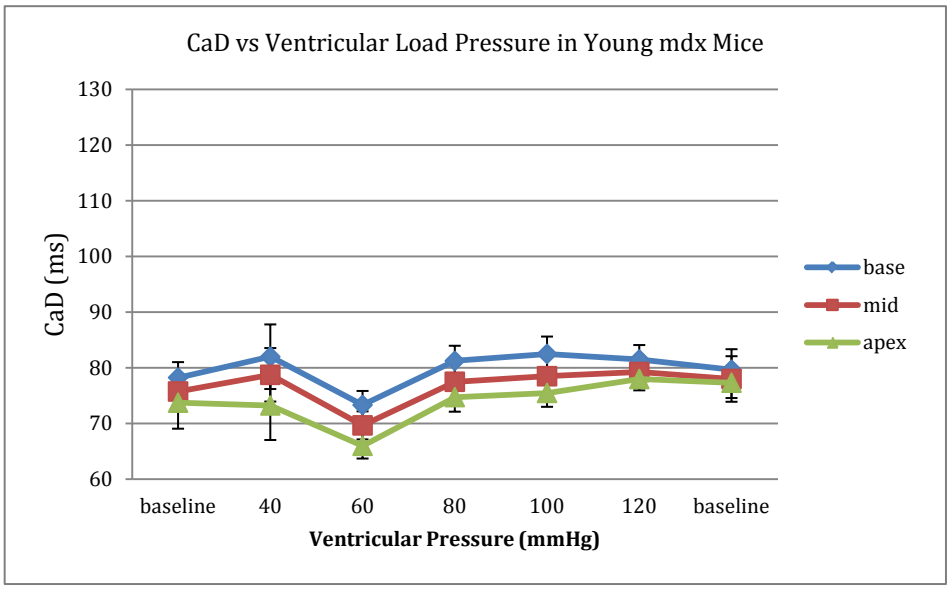

Figure 4.11 CaD-pressure relation curve of young *mdx* mice. CaD maintained no change under all conditions in young *mdx* mice.

CaT rise time is calculated as the time period from 10% peak value of upstroke to 90% peak value of upstroke. This parameter signifies the Ca release process. Similar to what was seen in CaD, rise time of base and mid in aged mdx mice prolonged as inner ventricular pressure increases. This prolongation has a logarithmic curve shape where at lower pressures, the slope is steeper, and after 80 mmhg, the slope decreased. However, the apex of aged mice also displayed slightly prolonged rise time as pressure increased, but not as much when compared to base and mid (Figure 4.11).

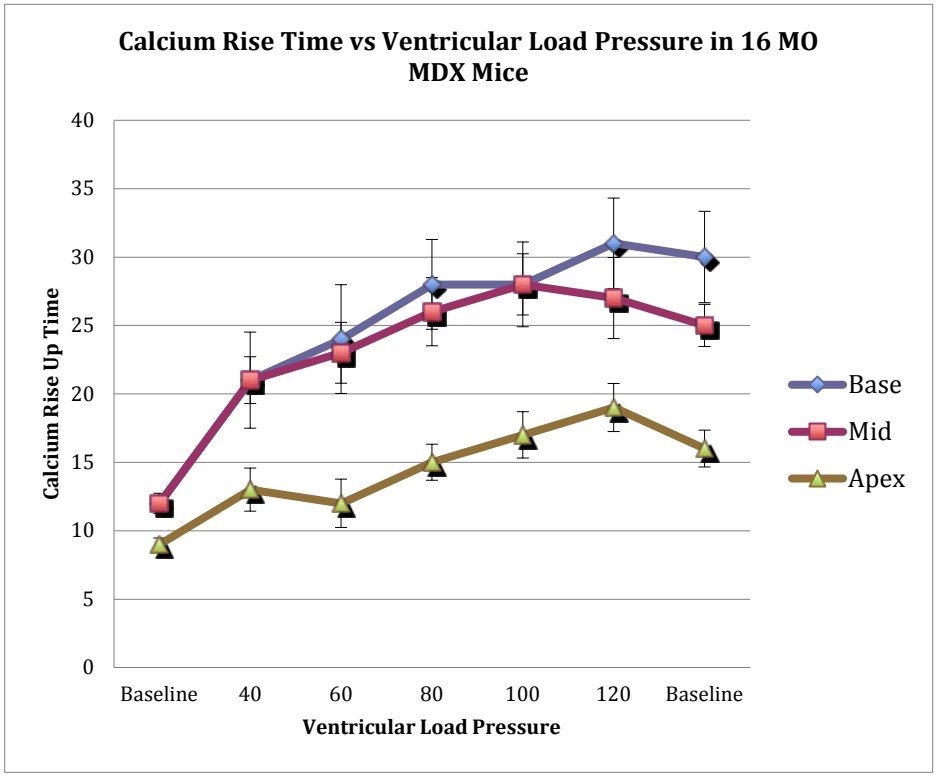

Figure 4.12 Ca rise time-pressure relation curve of aged *mdx* mice.

Ca rise time in aged WT mice was not remodeled (Figure 4.12). In young group, both mdx and WT showed no change, which is similar to the CaD result (Figure 4.13).

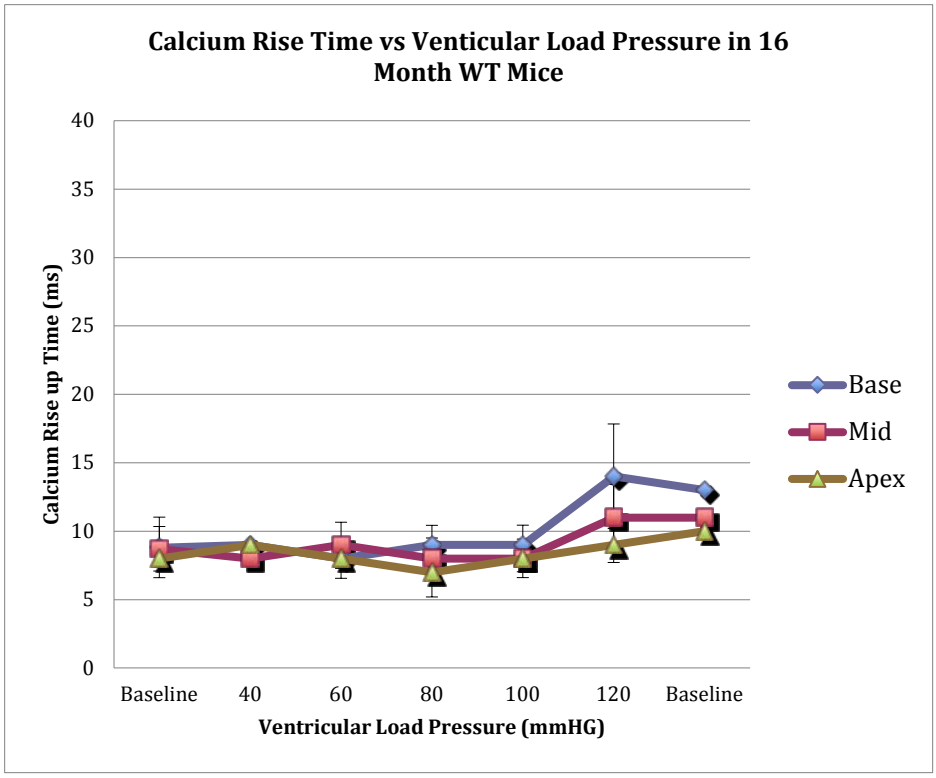

Figure 4.13 Ca rise time-pressure relation curve of aged WT mice.

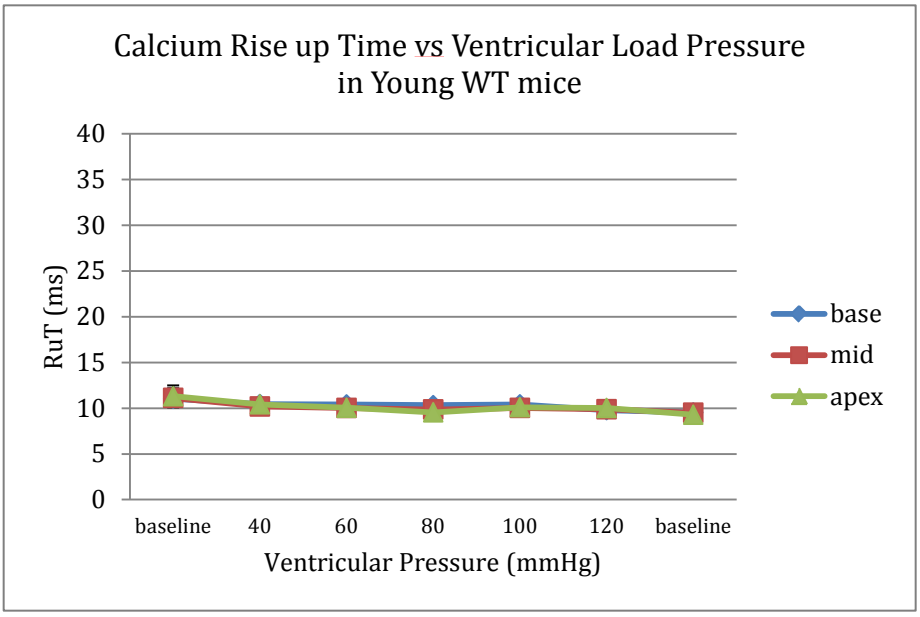

Figure 4.14 Ca rise time-pressure relation curve of young WT mice.

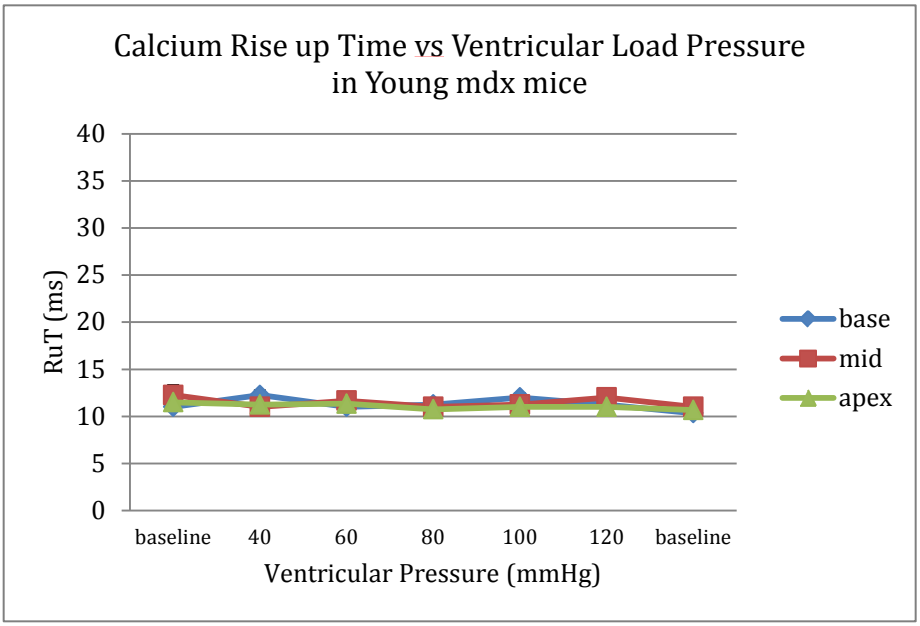

Figure 4.15 Ca rise time-pressure relation curve of young *mdx* mice.

4.4.2.3 Regional Dysfunction of Ca Handling in Aged *mdx* Mouse Associated with Arrhythmogenesis

Experiments investigating Ca handling dysfunction-pressure relation showed that a stretch stimulation could induce Ca handling dysfunction but only in aged mdx mice. The dysfunction does not correspond linearly to inner ventricular pressure. Dysfunction, as evaluated by CaD and rise time prolongation, does not dramatically worsen after 80 mmhg. Thus, detailed Ca dysfunction was evaluated below 80 mmhg.

Dramatic change in CaT morphology was observed in aged mdx mouse ventricular base only (Figure 4.15 A). Prolongation of both Ca release and Ca extrusion were observed. Rise time as described in the previous experiment was calculated to evaluate Ca release. Ca extrusion, which in mouse heart as opposed to human, is mainly the process of Ca reuptake back into SR. The process is assessed by two parameters: T50 describes the time course from CaT peak to 50% relaxation value; Ca decay constant establishes the late phase of Ca reuptake. The decay constant is calculated by exponential curve fitting that the bigger value indicates a shorter process of Ca from 50% of peak value return to baseline.

Similar to the relation experiments, remodeling regarding to Ca release and reuptake phases are observed in aged mdx mouse heart ventricular base. Prolongation of rise time, T50 was observed. Although the late phase of Ca reuptake is shortened from the increase of Ca decay constant, the whole CaD is dramatically increased. Ca dysfunction in aged mdx mouse ventricular base is defined as prolonged Ca release, early phase of Ca reuptake but shortened late phase of Ca reuptake (Figure 4.15, 4.16 and 4.17).

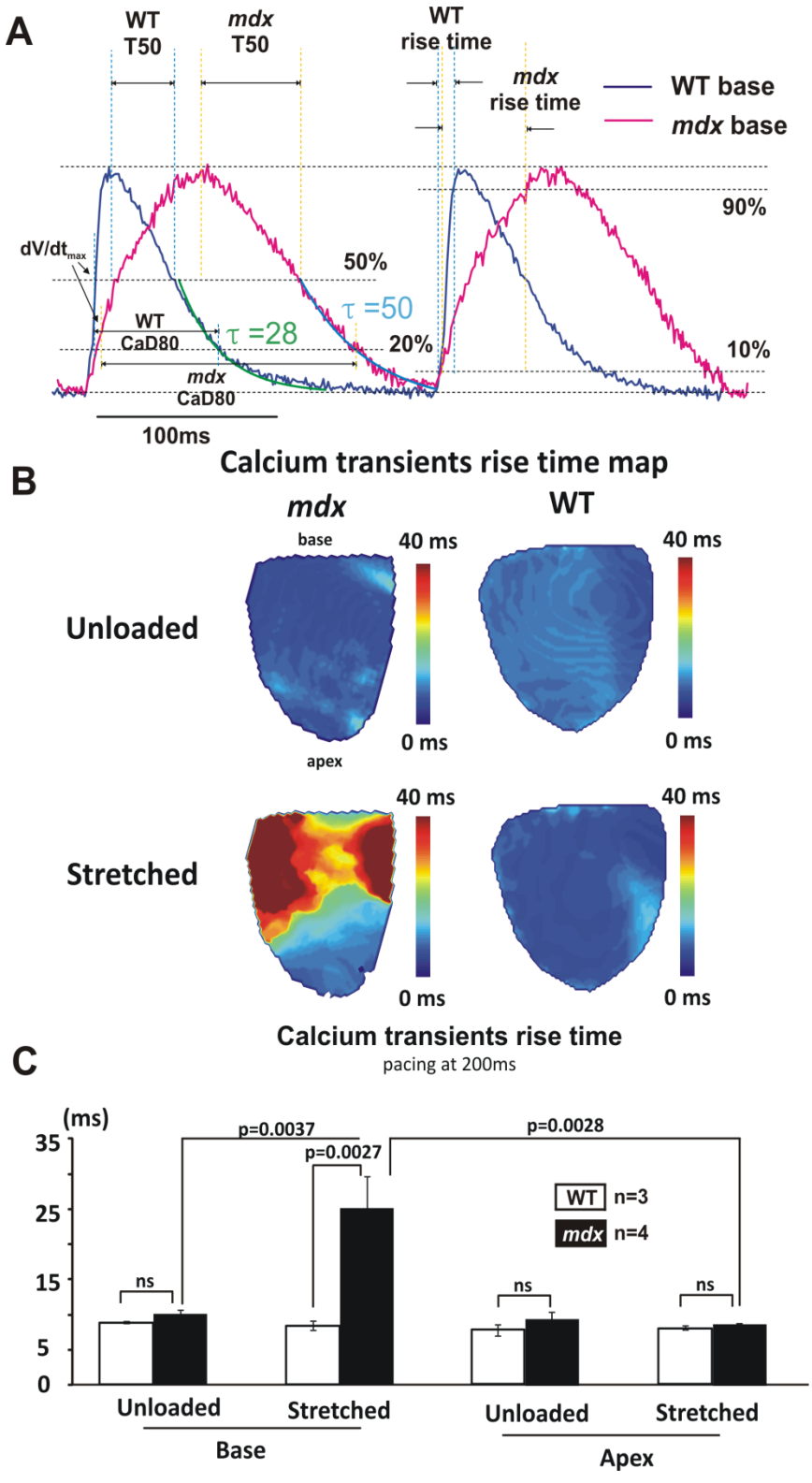

Figure 4.16 CaT signals and rise time under unloaded and stretched conditions. (A) Typical CaT signals from aged WT mouse ventricular base and mdx mouse ventricular base.

(B) Regional prolongation of Ca rise time in mdx ventricular base is appreciated from Ca rise time map. (C) Statistical analysis of Ca rise time.

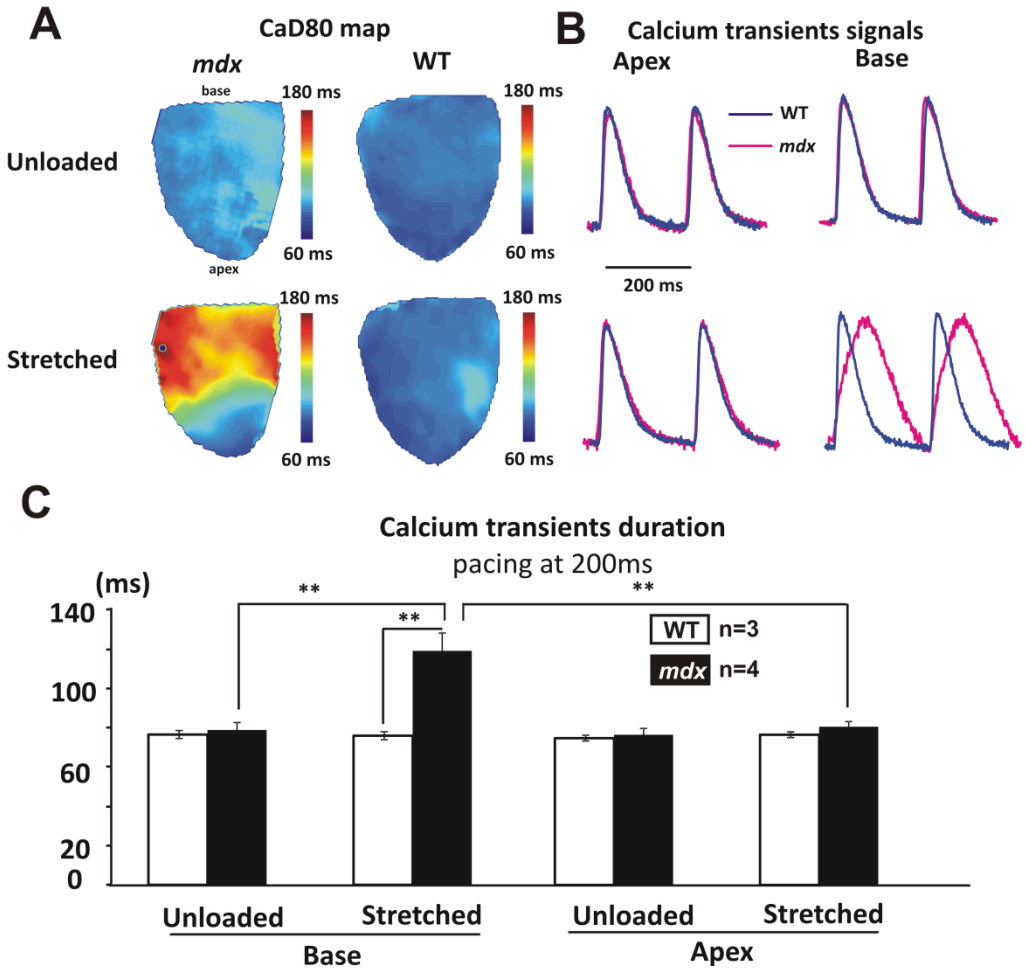

Figure 4.17 CaD_{80} from *mdx* and WT ventricles. (A) CaD_{80} map shows stretch stimulation induced prolongation of CaD in aged mdx mouse ventricular base. (B) CaT signals from both base and apex in WT and mdx are similar under unloaded condition, while after stretch, mdx ventricular base signal morphologically changed. (C) Statistical analysis of CaD from base and apex under different conditions.

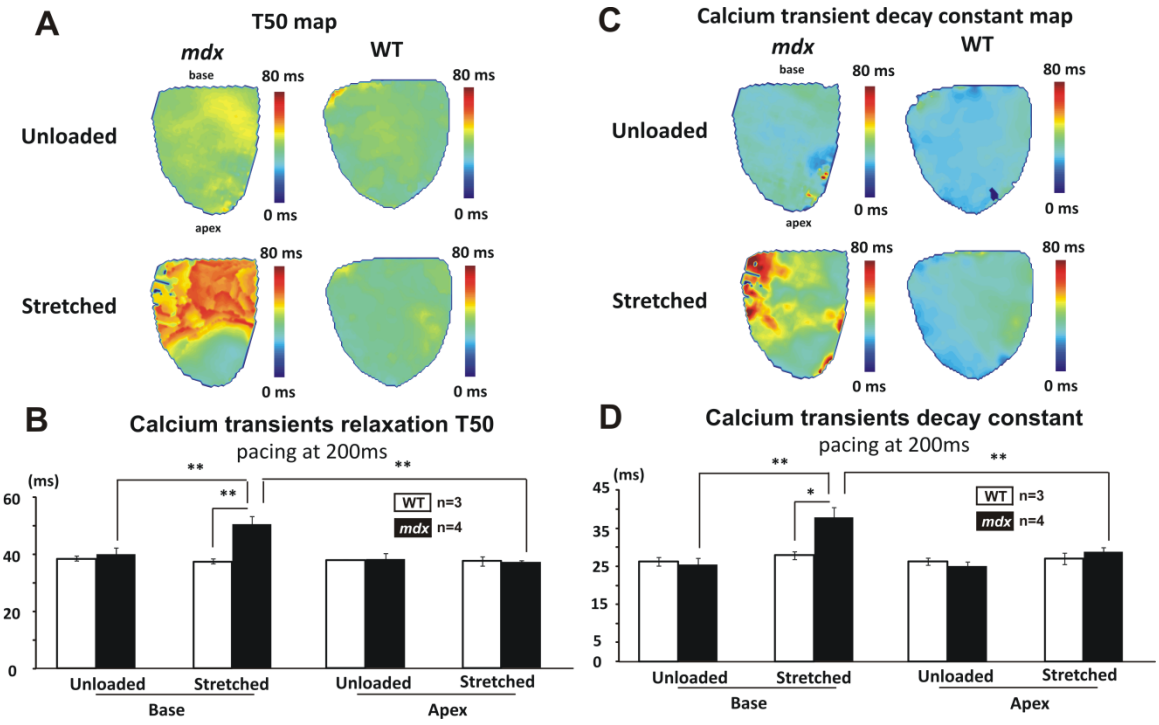

Figure 4.18 T50 and CaT decay constant of *mdx* and WT mice. (A) and (C) are T50 and CaT decay constant map. (B) and (D) are statistical analysis of T50 and decay constant of base and apex from two groups of mice.

Dysfunction of Ca release and reuptake results in remodeling of CaT functional refractory period (FRP). Under stretch conditions, prolonged FRP was observed in mdx mouse heart ventricular base, but in apex (Figure 4.18 A). Heterogeneity of Ca dynamics promotes arrhythmogenesis as discussed in Chapter 1. Resulting from regional dispersion of FRP, Ca alternans appeared in the base and apex at different pacing cycle lengths after stretch stimulation. The ventricular base in mdx mice started to show Ca alternans at a low pacing frequency. Figure 4.18 B shows CaT began to lose 1:1 capture at 90ms pacing in the base after stretch.

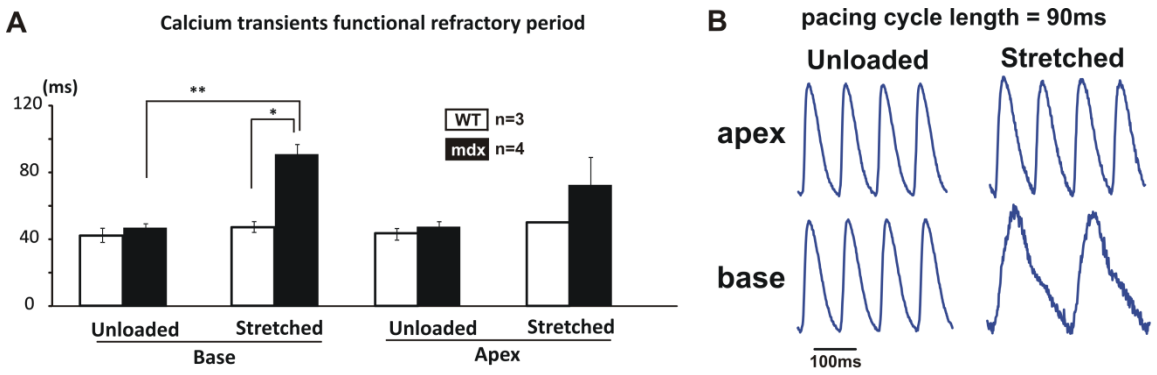

Figure 4.19 CaT functional refractory period analysis and regional occurrence of Ca alternans. (A) CaT functional refractory period was statistically analyzed. (B) CaT began to lose 1:1 capture at 90ms pacing in base after stretch.

4.5 Discussion

Mechanical defect is suggested to be a key factor associated with deficiency of dystrophin. Together the mechanical damage induced dysfunction of Ca handling, which, in turns, results in dysfunction of contraction.

This study shows for the first time that mdx hearts exhibit an abnormal myocardial sheet angle $|\beta|$ during relaxation that is calcium dependent and rapidly reversible. Furthermore, regional gradients of diastolic dysfunction are evident, primarily in the more basal segments where abnormal calcium reuptake was been demonstrated. These colocalized abnormalities in calcium reuptake and diastolic sheet function strongly suggest that features other than the simple absence of dystrophin are critical to the evolution of heart failure in DMD. Indeed, it is well recognized that mechanical defect in the dystrophin encoding gene does not independently elicit DMD cardiac functional defects such as reduced circumferential wall strain,[132] which emerge in a regionally heterogeneous fashion over time, and not at loci where dystrophin is missing. In the baseline condition optical

mapping experiments, this hypothesis has been proved as no dysfunction of Ca handling has been observed in both aged WT and mdx mouse hearts.

Abnormality in the basal region could be due to regionally different contraction load during a heartbeat. During left ventricular ejection, its cavity changes shape and help propel blood superiorly, according to Newton's third Law, which states that for every action there is an equal and opposite reaction, the base of the heart moves inferiorly.[150] This movement, called decent of the base that doesn't occurred at apex.

Prior recognition of stretch induced calcium mishandling in isolated *mdx* cardiomyocytes informs the present work [151]. Specifically, mechanical stretching increases the probability of opening stretch-activated channels (SAC) [151] and developing transient membrane microruptures in *mdx* cardiomyocytes [151]. The resultant leakage of extracellular calcium into the cytosol then compromises calcium clearance during relaxation and renders *mdx* cardiomyocytes vulnerable to stretch induced injury [152]. In experiment with intact perfused hearts, I employed a stretch protocol to mimic cardiomyocyte activity under moderate strain regimes by inflating LV pressure to 80 mmHg, which is similar to that used for investigating fibrillation[151]. Under stretched condition, *mdx* hearts exhibit a regional deficiency in calcium release and uptake, as shown by a prolonged Ca rise time, T50 and decay time constant at the base where the sheet functional defect was observed. Thus, my results indicate a regional correspondence between abnormal diastolic sheet mechanics and disturbed calcium kinetics.

Prolongation of Ca rise time reflects the dysfunction of Ca release, which is induced by small amount of Ca transport through L type Ca channel, but is mainly mediated by SR Ca released through RyR. This finding was not in agreement with previous study on isolated myocytes, which claims Ca release was observed shortened[151]. Despite differences between cellular and whole heart level studies, stretch stimulation which I to be found crucial in evoking Ca mishandling was not

applied in their study. RyR forms a chemically gated, non-energy consuming Ca release channel with relatively low Ca selectivity.[151] When the channel is in its open state, relatively large monovalent cations can be transported. Thus, the force for Ca release through RyR relies mainly on Ca diffusion, which is determined by the difference between SR and cytoplasmic Ca concentration. According to previous studies, this difference is dramatically decreased in aged mdx ventricular myocytes, as SR Ca concentration was observed decreased and cytoplasmic Ca was found increased comparing to normal heart.[151] Thus, prolongation of Ca release may be due to the decrease in force behind it.

The prolonged T50 and decay constant observed in *mdx* mouse hearts may reflect calcium leakage through the destabilized sarcolemma as a direct effect of the lack of infrastructural integrity normally provided by the dystrophin-associated glycoprotein complex. A therapeutic strategy to inhibit calcium leakage during the resting state (i.e., unrelated to the operation of voltage-gated L-type channels for cell excitation), could be effective in restoring cardiac function in myopathic *mdx* heart. Promising results with compounds such as P188 that has been claimed to repair sarcolemma microruptures [151], and S107 that stabilizes RyR2 [151], together with the ineffectiveness of L-type calcium channel blockers as demonstrated in earlier clinical trials,[153] attests to the potential clinical utility of the approach.

All the Ca mishandling shows regional dispersion and eventually results in the Ca alternans occurring ithe n base at a much lower pacing rate compared to the apex. The heterogeneity of Ca dynamics facilitates arrhythmogenesis. Moreover, both mechanical defects and Ca mishandling contribute to the development of HF.

Chapter 5

Arrhythmogenic Remodeling of β_2 versus β_1 Adrenergic Signaling in Human Failing Heart

5.1 Abstract

β-Adrenergic receptor (AR) blockers remain a mainstay of heart failure (HF) therapy. However, the efficacy of β blockers in preventing fatal ventricular tachycardia (VT) remains controversial. I aimed to investigate the electrophysiological and arrhythmogenic implications of differential β_1/β_2 remodeling in patients with HF. Using programmed stimulation and optical mapping of action potentials (AP) and $[Ca^{2+}]_i$ transients (CaT) I assessed β_1 (Xamoterol) versus β_2 (Procaterol) adrenergic response in human donor (D, n=8) and failing (F, n=8) left ventricular wedge preparations. Molecular mechanisms were assessed with quantitative-PCR and Western blot. β_1-stimulation significantly increased conduction velocity (CV), shortened action potential duration (APD) and calcium transient (CaT) duration (CaD) in D but not F hearts, due to desensitization of β_1-AR in HF. β_2-stimulation increased CV both in F and D hearts, while more potently shortening APD in F versus D suggesting switched coupling from G_i to G_s in HF. The transmural gradient of β_2 effect on APD and CaD creates substrate for delayed after depolarization (DAD). Both β_1 and β_2 stimuli augmented vulnerability and frequency of ectopic activity and enhanced substrate for ventricular tachycardia (VT) in F, but not D hearts. Two mechanisms of ectopy induced by β-

stimulation were documented: Purkinje fiber (PF) automaticity and Ca-mediated premature ventricular contractions (PVCs). In human HF, β_1-AR is desensitized, while β_2-AR becomes a dominant player in electrophysiological regulation and arrhythmogenesis. HF remodeled β-AR signaling increases VT/VF vulnerability via Ca-mediated PVCs and enhanced Purkinje fiber automaticity.

5.2 Introduction

Increased sympathetic activity through β adrenergic signaling is common in HF, often leads to ventricular remodeling and, consequently, serious impairments of cardiac contractile function. Up to 50% of HF mortality is sudden, due to tachyarrhythmias.[9] β_1 or non-selective adrenergic blockers are widely used and have been proven to reverse ventricular remodeling and reduce mortality in HF patients.[154-157] However, the efficiency of β blockers of preventing fatal VT in HF patients is controversial.[158-160] Recently, non-selective β-blockers or β_2-blockers were advocated by several clinical trials and studies.[161-164] The mechanisms of subtype-specific adrenergic remodeling and its implications for arrhythmia in humans are not fully understood. Although effects of β_1/β_2 adrenergic system remodeling on contractility have been studied in human trabeculae,[165] the role of β_1/β_2 adrenergic system remodeling in arrhythmogenesis has not been thoroughly investigated in human myocardium.

I hypothesized that differential remodeling of β_1 versus β_2 adrenergic signaling may have important arrhythmogenic effects in end-stage HF. Furthermore, we hypothesized that such molecular remodeling manifests anatomically as endocardial-epicardial gradient, contributing to arrhythmogenesis and dysfunction of excitation-contraction (EC) coupling. I sought to explore β_1

versus β_2 selective adrenergic effects by examining EC coupling using dual optical mapping of AP/CaT in left ventricular (LV) wedge preparations from human F and D hearts.

5.3 Material and Methods

5.3.1 Clinical Information for Human Hearts

Usage of human hearts was approved by the Institutional Review Board of Washington University. Non-ischemic failing human hearts (F, n=8) were obtained during transplantation at the Barnes-Jewish Hospital of Washington University in St. Louis, MO. Donor hearts (D, n=8) that were rejected for transplantation for reasons such as age were used as controls. Donor hearts were provided by Mid-America Transplant Services (St. Louis, MO). Ejection fraction values were obtained from echocardiography, which was conducted at variable times. All donor hearts were characterized as hearts without history of heart failure. The clinical data of patients are shown in Table 5.1.

Heart No.	Geneder	Age	Diagnosis	EF	arrhtymia history
			Donor Heart		
1	M	60	Stroke-Brain death	67%	AFIB
2	M	57	Stroke-Brain death	50%	
3	F	63	Anoxic brain injury	57%	
4	F	55	Stroke-Brain death	45%	Sinus tachycardia
5	F	59	Stroke-Brain death		
6	M	50	Stroke-Brain death	65%	
7	M	40	Gunshot wound	35%	
8	M	65	Stroke-Brain death	57%	
			Failing Heart		
1	M	65	NICM	<10%	AFIB
2	M	63	NICM	26%	AFIB
3	F	35	NICM	20%	
4	M	27	NICM	15%	Aflutter
5	F	61	NICM	36%	
6	M	60	NICM	20%	
7	M	55	NICM	<20%	
8	M	65	NICM	<20%	AFIB & VTACH

Table 5.1 Clinical information. Clinical information including gender, age, diagnosis, ejection fraction and arrhythmia history of the patients were provided. (NICM: non-ischemic cardiomyopathy; AFIB: atrial fibrillation; Aflutter: atrial flutter; VTACH: ventricular tachycardia)

Explanted hearts were cardioplegically arrested in the operating room following cross clamping of the aorta. Immediately after the heart was received, 100 ml 0°C cardioplegic solution (in mmol/L: NaCl 110, $CaCl_2$ 1.2, KCl 16, $MgCl_2$ 16, $NaHCO_3$ 10; pH=7.3±0.05) was perfused through right and left coronary arteries respectively to remove the blood and to protect myocardium from ischemia. The heart was then bathed in 0°C cardioplegic solution for transportation, dissection and cannulation.

5.3.2 Left Ventricular Wedge Tissue Preparation

The arterially perfused left ventricle wedge preparations were made as previously described.[166, 167] Briefly, preparations were dissected approximately from the same area of the hearts to minimize tissue differences. Before dissection, the quality of perfusion was verified by injection of Methylene Blue dye (Sigma, St. Louis, MO). A segment of left ventricular wedge along a posterior marginal artery was isolated based on the blue color in areas supplied by the dye solution. Each wedge contained a section of coronary artery along its length. The wedge was cannulated with a custom flexible plastic cannula. The quality of the perfusion was again tested by the blue dye, and poorly perfused surfaces were trimmed. Major arterial leaks in the wedges were ligated with silk suture to maintain pressure (Figure 5.1).

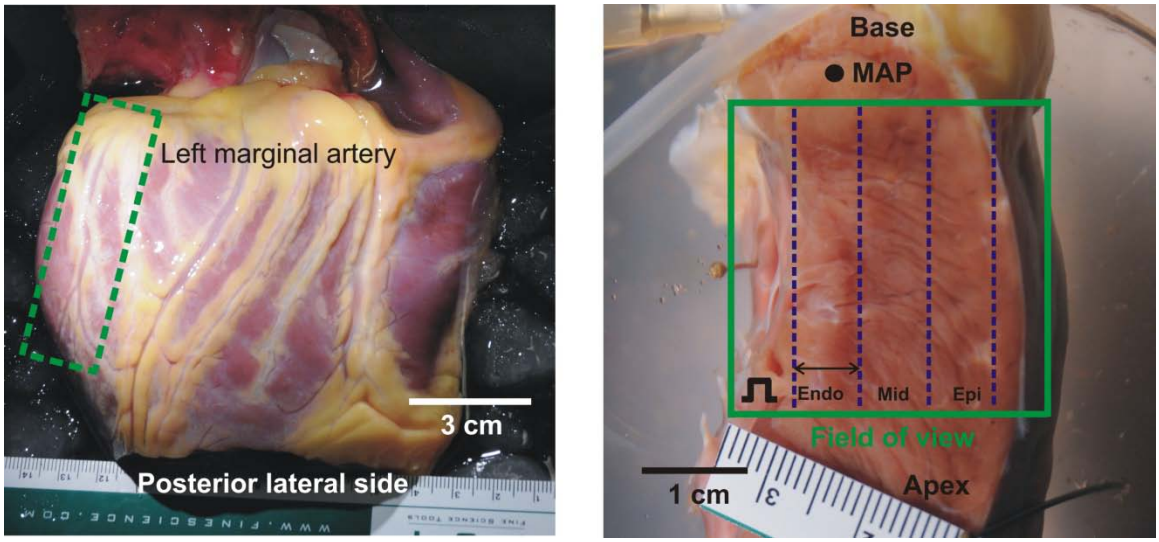

Figure 5.1 Representative photos of human heart and left ventricular wedge preparation. Tissue was selected along left marginal artery as boxed in green dashed line in the left photo. Field of view and definition of different transmural layers are depicted in the right photo.

5.3.3 Simultaneous Optical Mapping of AP and CaT

The isolated tissues were mounted in a warm chamber with the dissection exposed transmural surface up, facing the optical apparatus. The preparation was both superfused and coronary perfused with oxygenated Tyrode solution (in mmol/L: 128.2 NaCl, 4.7 KCl, 1.19 NaH_2PO_4, 1.05 $MgCl_2$, 1.3 $CaCl_2$, 20.0 $NaHCO_3$, and 11.1 glucose, and gassed with 95% O_2-5% CO_2; pH=7.35±0.05). I maintained a solution temperature of 37 °C and an arterial pressure of 60-70 mmHg. Continuous monitoring of pH and temperature was conducted during the experiment. The preparation was fully immersed in the perfusion efflux, which assured proper superfusion.

After 30 minutes of washout to remove excessive fat and blood residues, gradual warming after cold cardioplegia to 37 °C, tissue recovery, and stabilization, Blebbistatin (10 to 20μM; Tocris Bioscience, Ellisville, MO) was perfused into the preparation to suppress motion artifacts. After tissue was completely stabilized, RH237 and Rhod-2 AM were applied as probes for AP and CaT, respectively.

The dual optical mapping apparatus consisted of two MiCAM Ultima-L CMOS cameras (SciMedia, Costa Mesa, CA) that have high spatial (100×100 pixels, with the field of view of 3cm×3cm) and temporal (1,000 frames/sec) resolution. A band-pass filter (590±15 nm, Thorlabs, Newton, NJ) was placed in front of the calcium imaging camera; a long-pass filter (>700 nm, Thorlabs, Newton, NJ) was positioned in front of the voltage imaging camera. The cameras were arranged perpendicular to one another by a holder, which contained a dichroic mirror (635 nm cutoff, Omega Optical, Brattleboro, VT). Immediately below the dual camera holder were a group of lenses (100mm and 50 mm focal length, f 0.95; Navitar), which helped to focus the emission light coming from the heart onto the CMOS sensors with adjustable field of view. The excitation light

was generated by a halogen lamp (Newport Oriel Instruments, Stratford, CT; SciMedia, Costa Mesa, CA) and was passed through a heat filter, shutter, and band-pass filter (520±45 nm). A flexible light guide directed the band-pass filtered light onto the preparation, and a shutter was used to ensure that the preparation was exposed to light only during image acquisition to avoid photobleaching of the dyes.

5.3.4 Experimental Protocols

Specific agonists for β_2-AP and β_1-AR procaterol (1μM)[168, 169] and xamoterol (1μM)[170, 171], respectively, and non-specific β-AR agonist isoproterenol (ISO, 100nM) (Tocris Bioscience, Ellisville, MO) were perfused into the preparation. The agonists were applied at saturate constrations according to previous cardiac studies [168-171] so that the maximum effective activation of the receptors could be achieved. Conclusions are carefully driven based on comparisons between D and F hearts under the effects of different β-AR selective agonists, respectively.

Complete washout evaluated by the recovery of action potential duration (APD) was applied between Xamoterol and Procaterol. Extra blebbistatin and dye were loaded as needed. Programmed electrical stimulation (PES) S1S1 protocol was applied with the pacing electrode placed at subendocarium at twice the diastolic pacing threshold. Pacing cycle length (CL) ranged from 4000 to 400 ms as shown in Figure5.2. Representative mapping recordings were collected during each condition. Real time monophasic action potential (MAP) and pseudo ECG were continuously monitored in parallel with and in validation of optical mapping. 1 ml of Lugol's solution was painted

to the endocardium surface after enhanced automaticity was observed, followed by quick superfusion of Tyrode solution.[172]

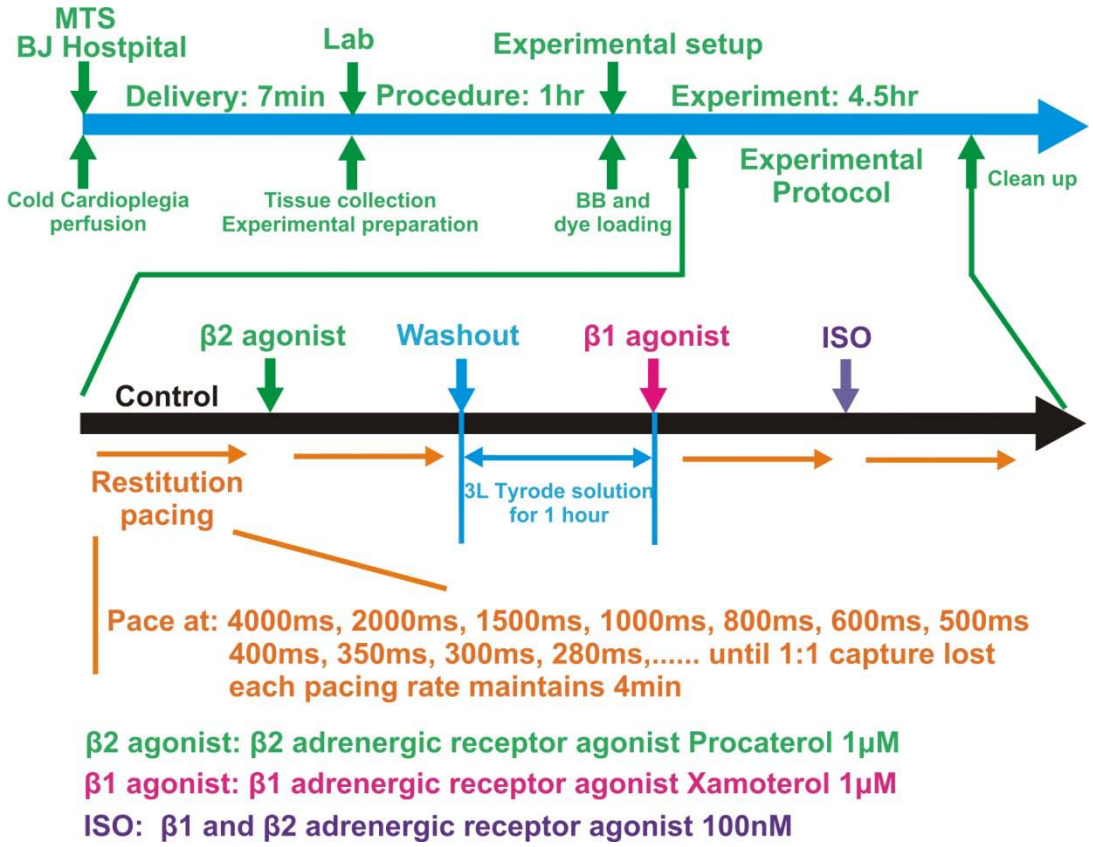

Figure 5.2 Detailed experimental protocol.

5.3.5 Data Analysis

Transmural surface was subdivided into areas of interest: subepicardium (epi), midmyocardium (mid) and subendocardium (endo), as defined in Supplementary Figure 1. Mapping signal was low-pass filtered at 256 Hz. AP duration (APD) and CaT duration (CaD) were measured from time point of upstrokes (dV/dt_{max} and dCa/dt_{max}) to 80% repolarization and Ca relaxation. The

difference between CaD and APD (CaD-APD) was also calculated.[173] Conduction velocity (CV) was measured and plotted as a function of direction with transverse direction defined as zero degree (Figure 5.3 A). Action potential-Calcium delay map (AP-CaT Delay map) shows the time difference between AP activation and Ca release ($dCaT/dt_{max}$ - dV/dt_{max}) with positive value indicating activation of AP precedes calcium release (CaT). CaT rise time was quantified to estimate the Ca release phase, which was defined as the time interval between 10% and 90% CaT upstroke value. T_{50} and Ca decay constant were calculated to evaluate the Ca extrusion fast component and slow component respectively. T_{50} measures the time period from time point of CaT reaching peak value to 50% relaxation. Ca decay constant was investigated by fitting CaT signal from 50% to 100% relaxation with exponential curve (a*exp(-1/b*x)+c), where b was defined as decay constant.

5.3.6 Western Blot Studies

Additional tissue samples from human LVs were flash frozen in liquid nitrogen, pulverized, and lysed. Proteins were separated by SDS-PAGE, followed by transfer onto nitrocellulose membranes. Incubations with primary antibodies (β_2-AR antibody, sc-569; p-β_2-AR antibody (Ser345/Ser346), sc-16718; Santa Cruz Biotechnology, Santa Cruz, CA) were performed overnight at 4°C and were carried out in 5% BSA. Incubations with secondary antibodies were performed at room temperature for 2 h. After exposure, membranes were washed and stripped using Restore PLUS Western Blot Stripping Buffer (Thermo Scientific). Membranes were reprobed using an antibody against GAPDH (anti-GAPDH, Sigma, St. Louis, MO) as a loading control. Images were processed using Multi Gauge software (Fujifilm).

5.3.7 Statistics

Two-way ANOVA was used for the statistical analysis. The statistical analysis of dependent variables (APD, CaD, CV) on the interactions between two fixed factors (group factor: F/D heart, layer factor: tissue layers, condition factor: baseline and β stimulations) was carried out. Bonferroni adjustment was applied as post hoc test. Values of $P<0.05$ were considered as statistically significant.

5.3.8 Quantitative-Polymerase Chain Reaction

Additional tissue samples from human LVs were preserved in RNAlater (Sigma, St. Louis, MO) before RNA extraction. Total RNA extracted was processed using RNeasy Fibrous Tissue Mini Kit and a High Capacity cDNA Reverse Transcription Kit (QIAGEN, Manchester, UK) according to the manufacture's instructions. mRNA quantification for the different targets was assessed by quantitative PCR (q-PCR) using TaqMan gene expression assays by StepOne instrument (Applied Biosystems, Grand Island, NY). The thermal profile for the q-PCR reactions followed manufacturer's instruction. Data analysis for q-PCR data used efficiency-corrected ΔCt method to determine the relative amounts of the gene of interested that were normalized to an endogenous reference RNA of GAPDH.

5.4 Results

The interaction between arrhythmogenic triggers and substrates determines the initiation and maintenance of fatal ventricular arrhythmias. In HF, remodeled β-AR signaling regulates numerous

electrophysiological targets, including ion channels, calcium handling and sarcomeric proteins, which further induce remodeling of conduction, repolarization, calcium handling, and spatial electrophysiological heterogeneities of LV, ultimately providing arrhythmogenic triggers and substrates.

5.4.1 Effects of β_2 versus β_1 AR stimulation on arrhythmic substrates in HF

5.4.1.1 β_2 AR stimulation Increased Longitudinal Conduction Velocity (CV) and Increased Anisotropy in Failing Hearts

We quantified CV along transverse (CV_T) and longitudinal (CV_L) directions. β_2 agonist and ISO significantly increased $CV_{L,}$ but only mildly increased CV_T in both groups of hearts (Figure 5.3). β_1-stimulation enhanced CV in D, but not in F hearts. This differential, orientation-dependent increase of CV leads to significant increase of anisotropy (CV_L/CV_T) by β_2-stimulation, but a decrease by β_1-stimulation in F hearts (Figure 5.3E).

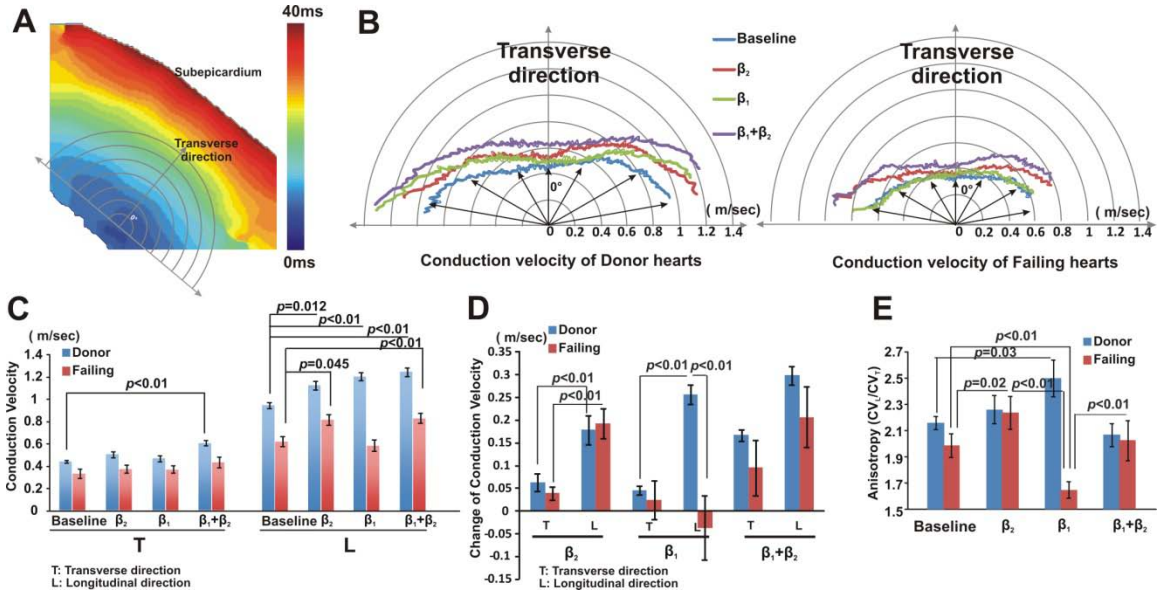

Figure 5.3 Effects of β adrenergic stimulation on conduction velocity and anisotropy. A) CV is measured and plotted out as a function of directions on activation map B) Quantified CV was plotted out in a radial coordinate system. Origin is defined at pacing location and 0° axis is along transverse direction. Averaged CV at each condition from D and F hearts was depicted with different colors (Baseline: blue; β_2 agonist: red; β_1 agonist: green; β_1+β_2 agonist: purple). C) CVs of longitudinal (CV_L) and transverse (CV_T) directions were statistically compared between different conditions. β-stimulation significantly increased CV_L in D hearts but only moderately in F hearts (β_1-stimulation did not increase CV_L in F hearts). D) β_2-stimulation increased CV dramatically in longitudinal direction but mildly in transverse direction in both D and F hearts. β_1-stimulation showed similar effect in D but not in F hearts. E) β_1-stimulation increased anisotropy in D but decreased it in F hearts, while β_2-stimulation increased anisotropy in F hearts.

5.4.1.2 β_2 AR Stimulation Increased Transmural Heterogeneity in Failing Hearts; while β_1 Slightly Affects Repolarization

In agreement with previous studies, APD was significantly prolonged in F hearts[174] (see details in Figure 5.4 and Table5.2).

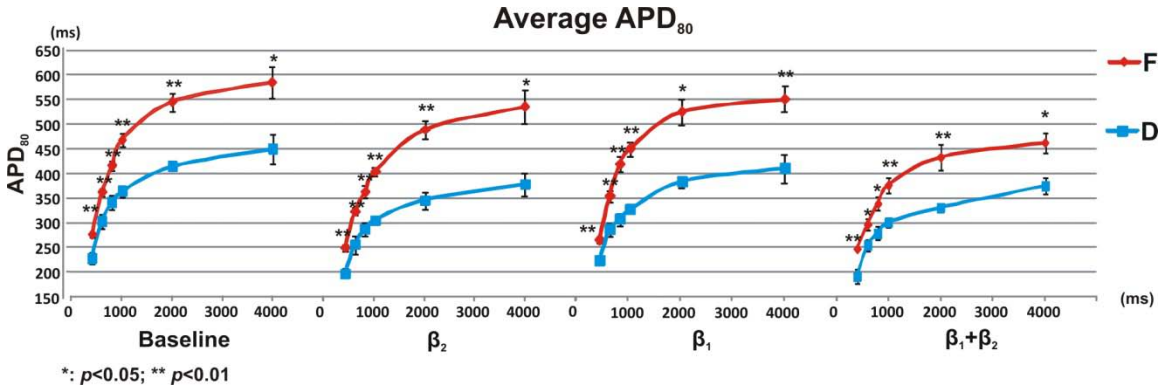

Figure 5.4 Transmural average APD from Failing and Donor human hearts. Average APD_{80} through the whole transmural surface for both D and F hearts were plotted. In F hearts, prolonged APD were observed at every pacing cycle length under all conditions.

APD_{80} (ms)

Condition	layer \ cycle length	4000	2000	1000	800	600	400 (ms)
Donor Heart							
Baseline	epi	414	388	320	307	281	214
	mid	448	411	333	318	291	224
	endo	469	427	348	326	299	241
β_2	epi	359	322	265	250	219	186
	mid	380	346	284	271	242	203
	endo	397	373	303	285	257	214
β_1	epi	394	363	280	263	230	200
	mid	405	379	297	286	257	216
	endo	419	390	313	296	268	229
$\beta_1+\beta_2$	epi	357	315	264	247	227	177
	mid	381	334	282	262	237	193
	endo	398	353	297	277	256	206
Failing Heart							
Baseline	epi	534	504	443	384	338	261
	mid	559	535	464	407	356	272
	endo	580	551	470	433	372	281
β_2	epi	497	460	368	341	305	235
	mid	521	485	392	357	322	254
	endo	557	501	425	378	339	261
β_1	epi	518	497	432	395	328	239
	mid	544	527	446	412	349	261
	endo	570	544	467	437	369	273
$\beta_1+\beta_2$	epi	450	402	357	311	275	235
	mid	457	445	381	346	305	248
	endo	476	468	403	369	317	262

Table 5.2 APD value at different pacing cycle length. Detailed average APD_{80} value under different pacing cycle length is provided for epi, mid and endo under all conditions.

β_2, β_1 and non-selective β agonists all shortened APD at different pacing rates in all three LV myocardial layers, but with varying degrees as evident from the restitution curves (Figure 5.5). β_2-

stimulation resulted in an increase of spatial heterogeneity of APD in F hearts (quantified by APD_{endo}-APD_{epi} at pacing CL=1sec in Figure 5.6) due to unequal transmural reduction of APD. The reduction (ΔAPD) was calculated as the difference of APD values between baseline and after β stimulation, and ΔAPD values were analyzed at pacing CL=1sec. In D hearts, both agonists reduced APD, and this reduction was greater in endo- than epicardium. However, β_2-AR stimulation reversed ΔAPD in F compared to D hearts. Specifically, APD reduction was significantly greater in epi- and mid-, but not in endocardium. β_1-AR stimulation, on the other hand, only mildly reduced APD without a spatial gradient (Figure 5.5C).

Western blot measurements of β_2-AR protein expression showed a clear endo-to-epi gradient in D hearts, which was reversed in F hearts (Figure 5.5F). Thus, the reversal of functional transmural gradient of ΔAPD observed during β_2-AR stimulation is due to β_2-AR protein expression remodeling in F hearts.

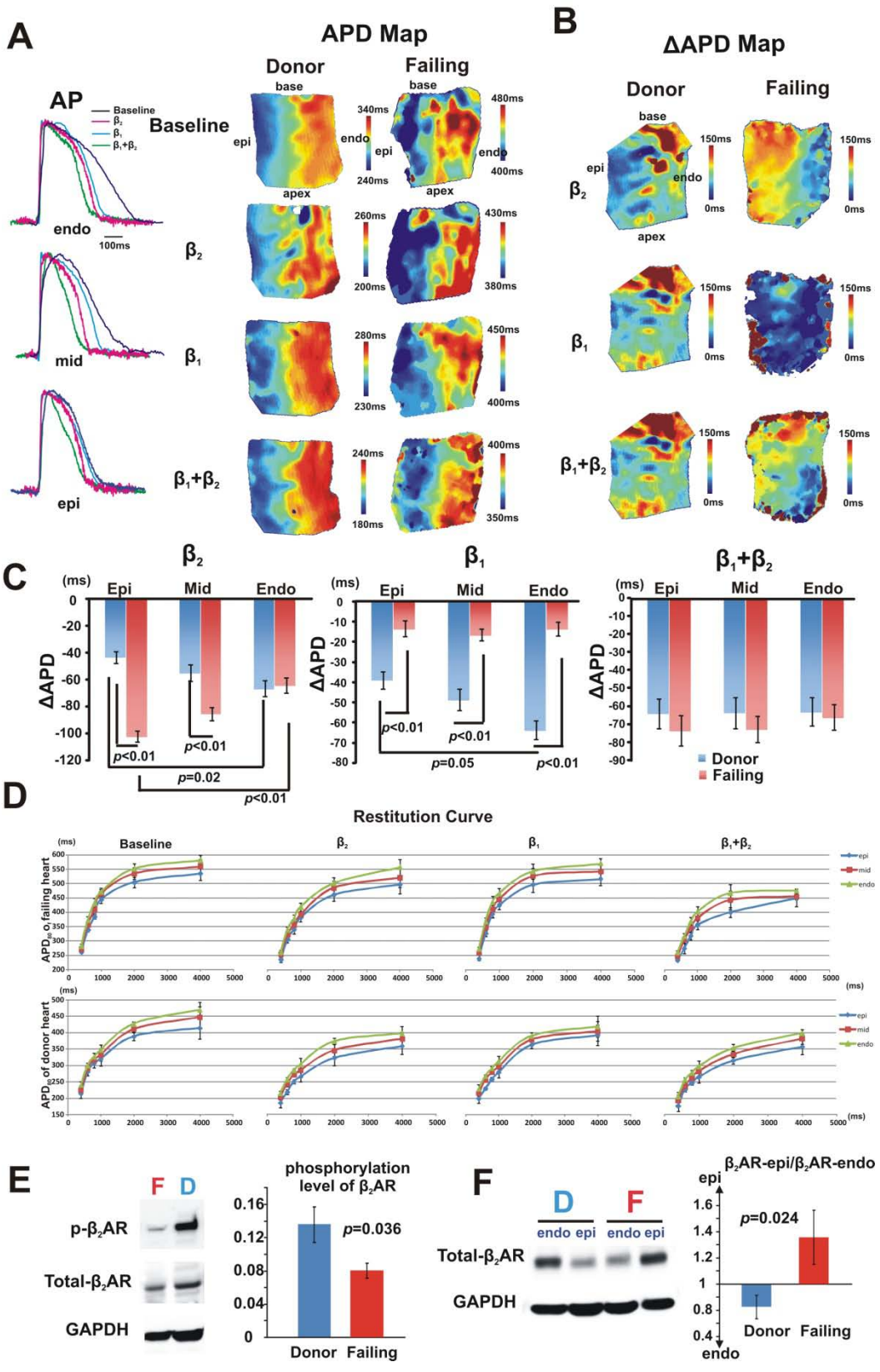
A
APD Map
Donor
Failing
AP
Baseline
β2
β1
β1+β2
endo
mid
epi
100ms
base
apex
epi
endo
340ms
240ms
480ms
400ms
260ms
200ms
430ms
380ms
280ms
230ms
450ms
400ms
240ms
180ms
400ms
350ms
B
ΔAPD Map
Donor
Failing
150ms
0ms
C
β2
β1
β1+β2
(ms)
Epi
Mid
Endo
ΔAPD
p<0.01
p=0.02
p=0.05
Donor
Failing
D
Restitution Curve
Baseline
β2
β1
β1+β2
APD90 of failing heart
APD90 of donor heart
epi
mid
endo
E
F
D
F
p-β2AR
Total-β2AR
GAPDH
phosphorylation level of β2AR
p=0.036
Donor
Failing
β2AR-epi/β2AR-endo
p=0.024

Figure 5.5 Effects of β adrenergic stimulation repolarization and Western blot test. A) Typical AP optical mapping recordings at 60 bpm pacing from endo, mid and epi under different conditions were plotted and labeled with different colors (Baseline: blue; β_2 agonist: red; β_1 agonist: green; β_1+β_2 agonist: purple). APD maps are shown for representative D and F heart. B) APD reduction (ΔAPD) resulting from stimulation by different β-agonists were calculated, and ΔAPD maps of D and F hearts are shown. C) ΔAPD resulting from β_2-stimulation in D hearts showed a spatial gradient, which appeared to be significant in epi and mid but not in endo. β_1-stimulation produced significant differences across the heart. Non-selective stimulation did not produce any significant differences. D) Restitution curves for F and D hearts. E) D hearts showed a significantly higher phosphorylation level of β_2-AR with similar level of total β_2-AR. F). β_2-AR shows transmural differences of expression in F and D hearts, where D hearts had higher β_2-AR in endo; F hearts had higher β_2-AR in epi.

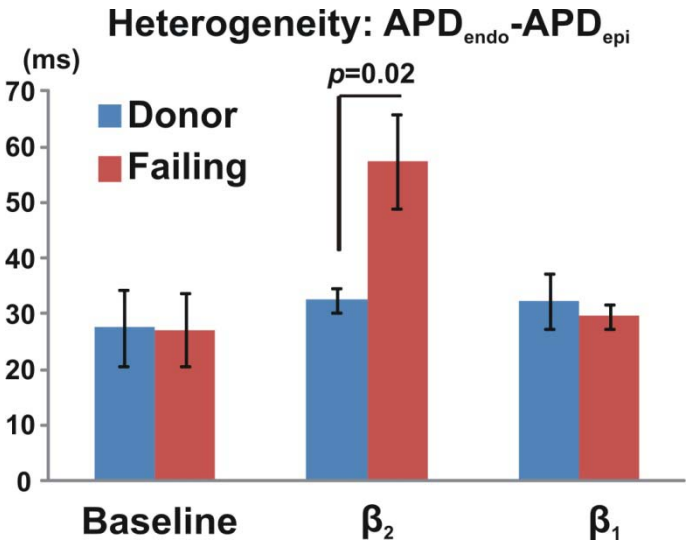

Figure 5.6 APD heterogeneity was evaluated by APD_{endo}-APD_{epi}. No significant difference was observed at baseline condition. β_2-stimulation significantly increased APD_{endo}-APD_{epi}, while β_1-stimulation did not change it.

5.4.1.3 Phosphorylation of β_2 AR by PKA Reduced in Failing human Hearts

Shortening of APD by β-stimulation is mediated by G protein and PKA downstream signaling. Unlike β_1-AR, which only couples to stimulatory G protein (G_s), β_2-AR can couple to either G_s or inhibitory G protein (G_i).[175] The mechanism underlying the increased ΔAPD induced by β_2-stimulation in F hearts may lie in this dual coupling with different G proteins. According to Lefkowitz group, phosphorylation of β_2-AR by PKA can switch its coupling from G_s to G_i (Figure 5.7).[176] I measured β_2-AR phosphorylation level at PKA-phosphorylation site Ser345/Ser346[177] and normalized it to total protein expression. β_2-AR protein phosphorylation was significantly reduced in F hearts, while total β_2-AR protein expression was unchanged (Figure 5.5E), suggesting that β_2-AR coupling to G_i is reduced and coupling to G_s is increased. This switching may augment β_2-AR effects on APD.

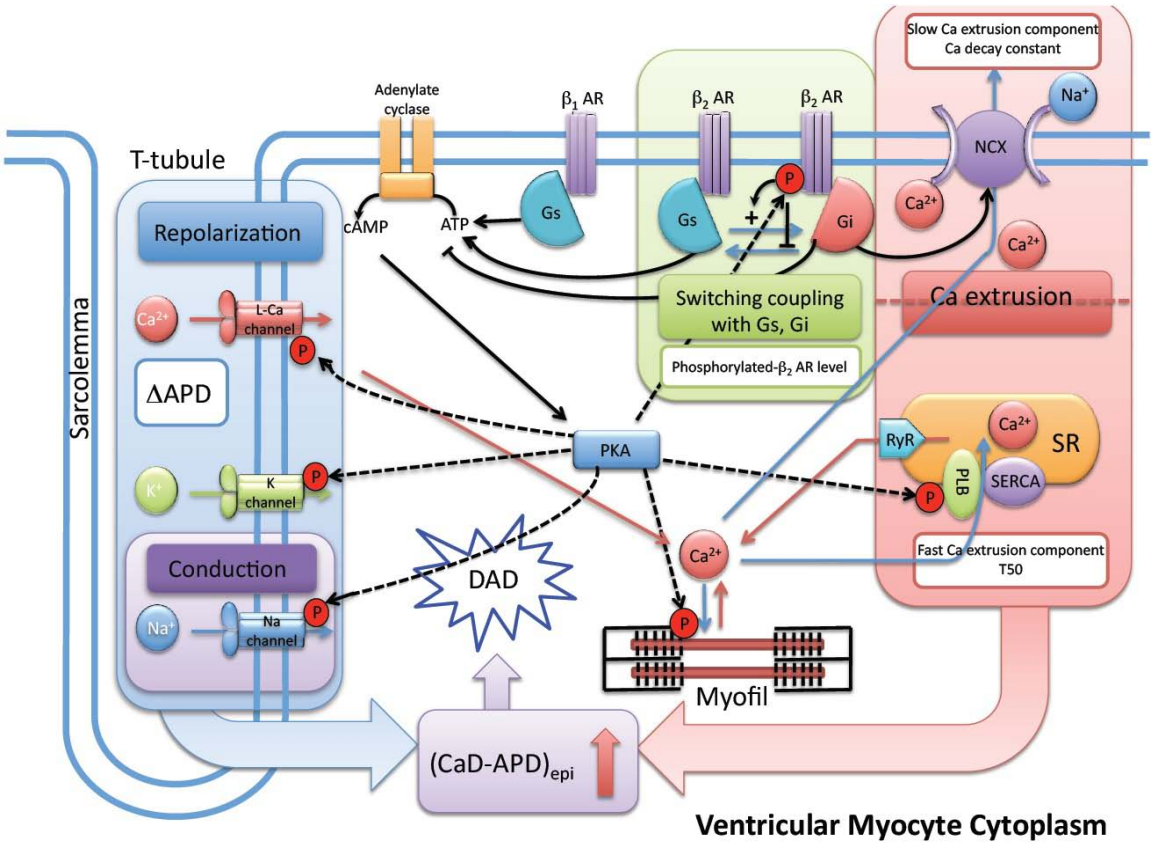

Figure 5.7 Diagram of β adrenergic system signaling in cardiomyocyte. Both β_1 and β_2 adrenergic receptors couple to G_s protein and regulate various membrane ion channels as well as calcium handling proteins. Such regulation is mediated by the activation of PKA signaling pathway.[178, 179] Paradoxically, β_2 adrenergic receptor also couples to G_i protein that not only inhibits the activation of PKA but also regulates proteins that are not shared with G_s signaling such as NCX. By coupling to G_i, β_2 adrenergic stimulation increases the activity of NCX.[180] The phosphorylation of β_2-AR by PKA plays a key role in balancing the coupling of β_2-AR with two types of G proteins. When β_2 adrenergic receptor is phosphorylated by PKA, it switches its coupling from G_s to G_i, which forms a negative feedback control on its coupling with G_s.[176]

5.4.1.4 β_2 AR stimulation Lead to Similar ΔCaD in F and D hearts; while β_1-stimulation produced less effect on CaD reduction in F than D hearts

Along with optical AP, we simultaneously recorded CaT (Figure 5.8A). β_1-agonist treatment shortened CaD significantly less in F vs. D hearts. In contrast, the β_2-agonist shortened CaD to a similar degree in both F and D groups. Unlike with APD, neither agonist exhibited transmural spatial differences (Figure 5.8B).

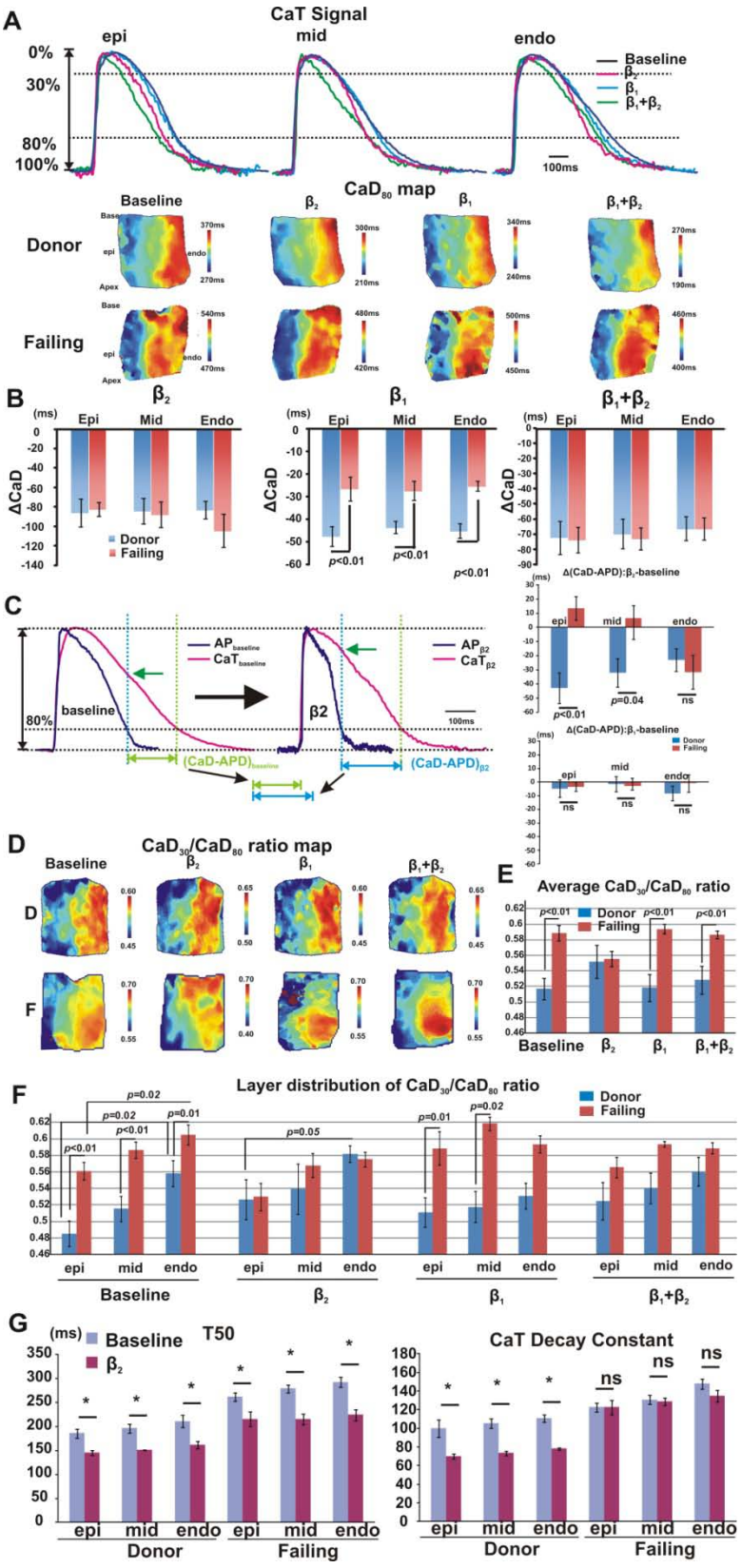
A
CaT Signal
epi
mid
endo
0%
30%
80%
100%
Baseline
β2
β1
β1+β2
100ms
CaD80 map
Baseline
β2
β1
β1+β2
Donor
Failing
B
β2
β1
β1+β2
(ms)
Epi
Mid
Endo
ΔCaD
Donor
Failing
p<0.01
p<0.01
p<0.01
Δ(CaD-APD):β1-baseline
p<0.01
p=0.04
ns
Δ(CaD-APD):β1-baseline
ns
ns
ns
C
APbaseline
CaTbaseline
APβ2
CaTβ2
80%
baseline
β2
100ms
(CaD-APD)baseline
(CaD-APD)β2
D
CaD30/CaD80 ratio map
Baseline
β2
β1
β1+β2
D
F
E
Average CaD30/CaD80 ratio
p<0.01
p<0.01
p<0.01
Donor
Failing
Baseline
β2
β1
β1+β2
F
Layer distribution of CaD30/CaD80 ratio
Donor
Failing
p=0.02
p=0.02
p=0.01
p<0.01
p<0.01
p=0.05
p=0.01
p=0.02
epi
mid
endo
Baseline
β2
β1
β1+β2
G
(ms)
Baseline
β2
T50
CaT Decay Constant
ns
ns
ns
epi
mid
endo
Donor
Failing

Figure 5.8 Effects of β adrenergic stimulation on Calcium Signaling. A) Representative calcium signal and CaD_{80} maps color-coded for different β-stimulation conditions. CaD_{80} was reduced after all β-stimulations. B) ΔCaD produced from β_2-stimulation showed no difference between two groups of hearts, however β_1 produced significant difference between F vs. D hearts. No transmural spatial differences were observed under either condition. C) Δ(CaD-APD) at epi and mid in F hearts was significantly increased during β_2-stimulation leading to a relatively higher $[Ca^{2+}]_i$ level at the same membrane potential compared to that of the baseline condition as labeled with green arrow. β_1-stimulation did not produce a significant effect. D) Representative CaD_{30}/CaD_{80} ratio maps during baseline and β-stimulations are constructed. E) Averaged CaD_{30}/CaD_{80} ratio in F hearts was significantly greater than in D hearts under baseline conditions. β_1 and non-selective stimulation did not change this difference, while β_2-stimulation abolished this difference. F) Transmural ratio values were analyzed. In baseline condition, dramatic differences were observed in all three layers between two groups of hearts. Spatial differences were also observed between endo and epi in both D and F hearts. The difference of ratio between D and F hearts persisted during β_1, but disappeared during β_2-stimulation. G) T_{50} was dramatically decreased after β_2-stimulation in both groups while similar Ca decay constant was observed in F hearts.

5.4.1.5 Transmurally different ΔAPD but similar ΔCaD resulted in transmural gradient of CaD-APD thus facilitating the initiation of delayed after-depolarizations (DADs) in F hearts

As shown above, β_2-stimulation produced transmurally different ΔAPD, but had similar effects on ΔCaD in F hearts. Such significant differences resulted in a transmural gradient of the CaD-APD difference, during which time intracellular $[Ca^{2+}]_i$ was maintained at a high concentration even after complete repolarization (Figure 5.8C). Increased disparity between AP and CaT leads to increased vulnerability for DAD occurrence, resulting from Na-Ca exchanger (NCX) induced Ca^{2+}_i extrusion and membrane potential depolarization. There was no significant transmural CaD-APD difference after β_1-stimulation in either D or F hearts. In contrast, β_2-stimulation dramatically increased CaD-APD in epi- and midmyocardium in F hearts (Figure 5.8C, $p<0.01$ and $p=0.04$, respectively).

5.4.1.6 β_2 AR stimulation induced a CaT morphology change in F hearts suggesting dysregulation of the late phase of Ca extrusion

CaD_{30}/CaD_{80} ratio was quantified to evaluate the morphology of CaT. In agreement with our previous study[166], we observed greater ratio in F than D hearts. This ratio also demonstrated a heterogeneous spatial distribution, with greater CaD_{30}/CaD_{80} in the endo- compared with epicardium in both groups at baseline (Figure 5.8D). β_1-stimulation did not alter CaD_{30}/CaD_{80} between F and D hearts, but eliminated transmural heterogeneity. However, β_2-stimulation completely abolished the ratio difference between two groups of hearts, indicating a change in CaT morphology resulted from β_2-stimulation (Figure 5.8E). We analyzed CaT further to determine the mechanisms of changes in different phases of the transient. Given that the rise time shows no difference (Figure5.9), we analyzed the Ca extrusion phase that has been separated into two parts: the early phase (fast Ca decline component), represented by T_{50}, and late phase (slow Ca decline component), represented by Ca decay constant (Figure 5.8G). T_{50} dramatically decreased after β_2-stimulation in both groups, whereas a similar Ca decay constant was observed before and after β_2-stimulation in F hearts, suggesting that abrogation of β_2 regulation occurred during the slow Ca decline phase.

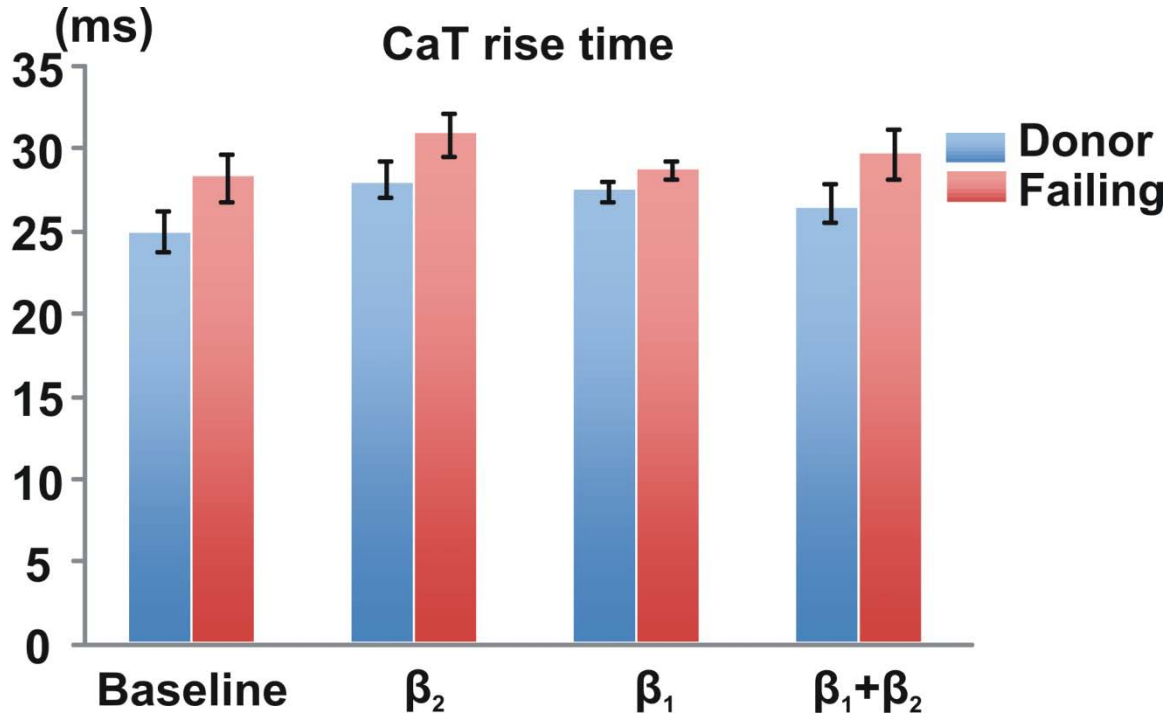

Figure 5.9 CaT rise time was calculated to evaluate the upstroke speed for CaT. No significant difference in rise time was observed between D and F hearts under all conditions.

5.4.2 Effects of β_2 versus β_1 AR stimulation on arrhythmic triggers in HF

5.4.2.1 β-AR stimulation is important for ectopic activity in human HF

Ectopic activity can trigger VT. In our study, we measured the frequency and spatial location of automaticity or premature ventricular contractions (PVC) during 8 minutes of S1S1 pacing. No spontaneous automaticity or PVCs were observed under any studied condition in D hearts. In contrast, F hearts exhibited both ectopic PVCs and automatic rhythm under all β-stimulation conditions. Automaticity and PVCs with different morphology originated in different locations as

shown in a representative example recorded after β_2-stimulation (Figure 5.10A). PVC #1 represents a series of irregularly occurring PVCs with smaller amplitude and slow upstroke that propagated through a limited area as circled before they terminated. On the other hand, PVC #2 had a greater amplitude and fast upstroke and propagated through the whole transmural surface of the preparation.

We analyzed PVCs originating from identical locations as PVC #1 and PVC #2. AP-CaT delay map confirmed that one mechanism for PVC formation is Ca-overload. Figure 5.10B shows a PVC, which was triggered by Ca release prior to the AP upstroke. Delay maps of PVC #1 were analyzed and confirmed that the PVC was Ca-driven, resulting from β_2-stimulation. These events all originated from epi- and midmyocardial layers (Figure 5B), which were the transmural regions with the prolongation of CaD-APD (Figure 5.8C), but did not occur subendocardially.

In Figure 5.10C, we confirmed that PVC #2 shared the same location with a series of regular beats of enhanced automaticity. This rhythm originated from subendocardium with a rate of 33 beats/min and was eliminated by rapid delivery of Lugol's solution to the subendocardial surface, implicating the Purkinje fiber automaticity.[172]

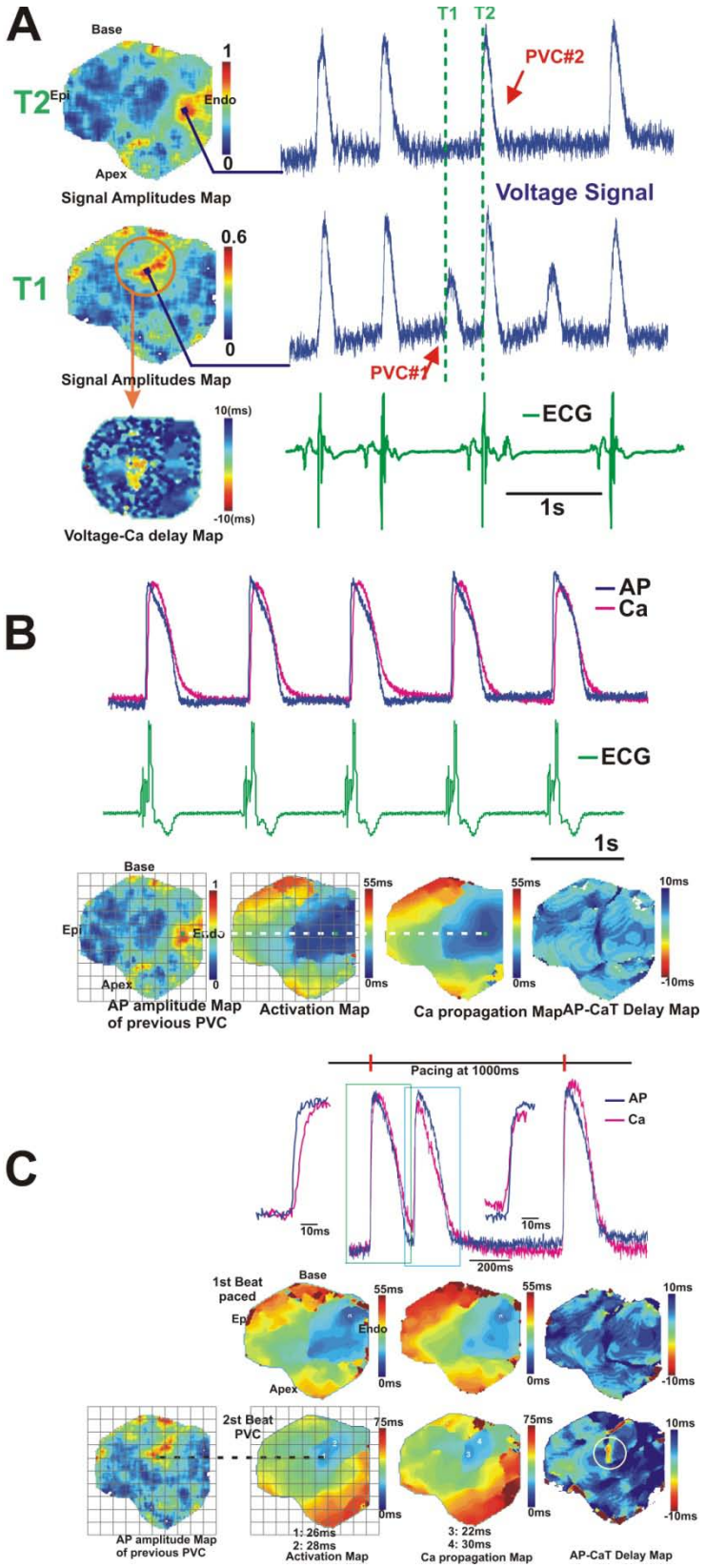
A
Base
T2
Epi
Endo
Apex
1
0
Signal Amplitudes Map
T1
T2
PVC#2
Voltage Signal
T1
0.6
0
Signal Amplitudes Map
PVC#1
10(ms)
-10(ms)
Voltage-Ca delay Map
ECG
1s
B
AP
Ca
ECG
1s
Base
Epi
Endo
Apex
1
0
55ms
0ms
55ms
0ms
10ms
-10ms
AP amplitude Map
of previous PVC
Activation Map
Ca propagation Map
AP-CaT Delay Map
C
Pacing at 1000ms
AP
Ca
10ms
10ms
200ms
1st Beat
paced
Base
Epi
Endo
Apex
55ms
0ms
55ms
0ms
10ms
-10ms
2st Beat
PVC
75ms
0ms
75ms
0ms
10ms
-10ms
AP amplitude Map
of previous PVC
1: 26ms
2: 28ms
Activation Map
3: 22ms
4: 30ms
Ca propagation Map
AP-CaT Delay Map

Figure 5.10 Multiple mechanisms of automaticity and PVC observed in F hearts. A) Multiple types of PVCs were captured in one recording after β_2-stimulation. PVC #1 represents the series of PVCs with small amplitude and slow upstroke. PVC #2 represents the series of PVCs with larger amplitude and faster upstroke. Membrane potential signal amplitudes maps were constructed at T1 and T2 time points to determine the location of the origination of both types of PVCs: PVC #1 originated from mid, while PVC #2 was from endo. Pseudo-ECG signal was also depicted. PVC #1 was not captured in ECG as it only propagated through a limited area as circled in orange before it terminated. B) A series of regular beats of enhanced automaticity were observed to share the identical location with PVC #2. C) Ca-driven PVC was confirmed by AP-CaT delay map and found to share the identical location with PVC #1. First beat showing that a paced beat (in green box) with its AP activation earlier than CaT does not exhibit the same AP-CaT delay as the second beat (in blue box) whose CaT activation preceded the AP, suggesting that the second spontaneous beat was calcium-driven. # 1, 2, 3 and 4 are labeled on the activation and Ca propagation maps of this PVC with the activation times of the 4 points shown. # 1 and 3 represent the origination on AP and CaT activation maps, respectively. # 2 and 4 represent an adjacent location close to the origination on each map, respectively. Activation time of 3 (CaT,22 ms) is earlier than 1 (AP, 26 ms), and this difference is reversed shortly after AP propagated: activation time of 2 (AP, 28 ms) is before 4 (CaT, 30 ms).

5.4.2.2 β-AR stimulation increased occurrence and frequency of spontaneous PVCs and rapid pacing induced VT in failing human hearts

The mechanisms of automaticity and ectopy illustrated in previous sections were confirmed in all studied F, but not D hearts. Using real-time pseudo-ECG and MAP during all experiments, we monitored the occurrence and calculated the frequency of PVCs as well as restitution pacing induced ventricular tachycardia (VT) (Figure 5.11A). The frequency and occurrence of PVCs and inducible VT dramatically increased after β-AR stimulation in F hearts, while neither could be induced in D hearts under any condition (Figure 5.11C). Thus, triggers were only present in F hearts. Figure 5.11B shows the spatial distribution of PVCs captured during optical imaging. Both β_1- and β_2-stimulation induced a relatively greater amount of automaticity vs. PVCs in subendocardium, which mainly originate in Purkinje fibers. Unlike β_1-stimulation, β_2 agonist treatment also induced PVCs in epi-

and midmyocardial areas in addition to endocardially, among which more than 40% of ectopy/PVCs were confirmed to be Ca-mediated. No Ca-driven PVCs were observed during β_1-stimulation.

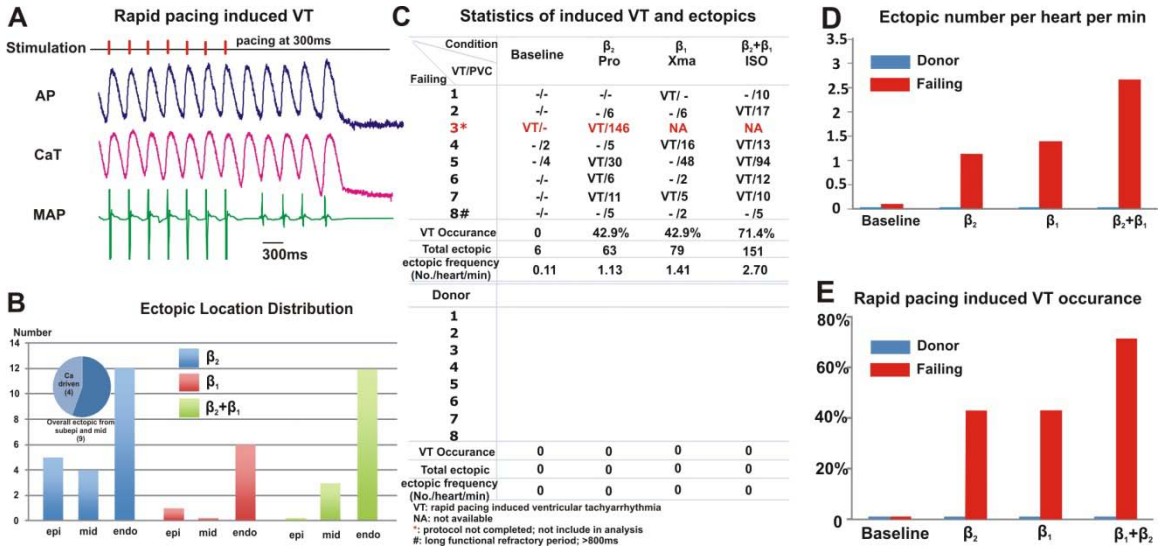

Figure 5.11 Ectopic Activity observed by location and frequency. A) Representative rapid pacing induced ectopic activity (VT) with AP, CaT, and MAP. B) Location distribution of ectopic activity with most originating from endo. All 4 Ca-driven PVCs were confirmed to only originated from epi and mid from β_2-stimulation. C) Statistic of induced VT and ectopy, all three agonist produced a large amount of ectopy and VT in F hearts as expected. Very few ectopic beats and no VT occurred at baseline. No ectopy or VT was observed D hearts. D) Expanded view of ectopy occurrence. β_1- and β_2-stimulation exhibited similar frequencies, with non-selective having more than either. E) Expanded view of VT occurrence. Again, β_1- and β_2-stimulation exhibited similar frequencies, with non-selective having more than either.

5.5 Discussion

This report demonstrates, for the first time, functional and molecular mechanisms of electrophysiological remodeling associated with differential β_1 versus β_2-AR system regulation in failing human hearts. We found that only in F hearts both β_1- and β_2-AR stimulation provoke frequent automaticity and PVCs with two different mechanisms. Both β_1 and β_2 activation increase automaticity in the Purkinje fibers. However, only β_2-AR stimulation leads to Ca-driven PVCs. We also observed that β_2-stimulation predisposes to arrhythmia more significantly as compared to β_1 by creating arrhythmogenic substrates via spatially heterogeneous augmentation of CV, repolarization, and CaD. In particular, β_2-stimulation increased the transmural difference between CaD and APD thus facilitating the formation of DAD.

5.5.1 Remodeled adrenergic control of repolarization in F hearts may be due to switching of β_2-AR coupling from G_i to G_s

Desensitization of β_1-AR and preserved effects of β_2-AR has been reported through gene/protein expression,[181] and in cardiac mechanics[165] studies in human HF patients. We confirmed gene/protein expression by q-PCR in our study (Figure 5.12). However, electrophysiological investigation had not been conducted in human until now. In this report, we present evidence for attenuated β_1 regulation of CV, APD, and CaD in F hearts. In contrast, β_2 regulation is not only maintained at a high level, but is also remodeled at the molecular and organ levels. We observed that β_2-AR stimulation resulted in significantly greater average APD reduction transmurally, particularly in epi- and midmyocardial areas, suggesting an enhanced β_2 regionally mediated ion channel regulation in F versus D hearts. This anatomically heterogeneous β_2

augmentation could be due to the switching of β_2-AR signaling from G_i to G_s. Unlike β_1-AR, β_2-AR is known to couple not only to G_s, but also G_i.[182] By coupling to G_i, it mediates an anti-apoptotic regulation through p38, MAPK activation,[183] which is considered to be protective for various cardiac diseases.[184, 185] It has been reported that β_2-AR can switch its coupling from G_s to G_i when it is phosphorylated by PKA, which in turn is also activated by G_s.[176] This forms a negative feedback control of the coupling of β_2-AR to G_s. Significantly reduced phosphorylation of β_2-AR was observed in F hearts, which could switch back the coupling of β_2-AR from G_i to G_s (Figure 5.7) switching negative feedback to positive feedback adrenergic control in HF. Therefore, β_2-AR could enhance its control of EC coupling though G_s, as evident from enhanced APD reduction in F hearts.

This theory is supported by studies from Harding's group. According to their work, the amplitude of myocyte contractions was used to evaluate the inotropic effect due to Gs signaling. Dramatically negative inotropic effect was observed in failing human ventricular cardiomyocytes after the application of a β2-AR antagonist (ICI118,551). No statistically different decrease of inotropic effect was observed in non-failing hearts. These data supported our theory that greater proportion of β2-AR coupling with Gs occurs in HF. Inhibition on this increased Gs contribution in failing hearts resulted in significantly negative inotropic effect. In non-failing hearts, as coupling of β2-AR with Gs was not comparable to that in HF, the inhibitory effect was not observed.[186] Additionally, in mouse models, when β2-AR is overexpressed, the same negative inotropic effect was also observed following treatment with ICI118,551.[186] Increased proportion of β2-AR-Gs coupling was reported in this transgenic mouse model[187], which together with the previously described work done in human hearts lends support to our theroy.[186]

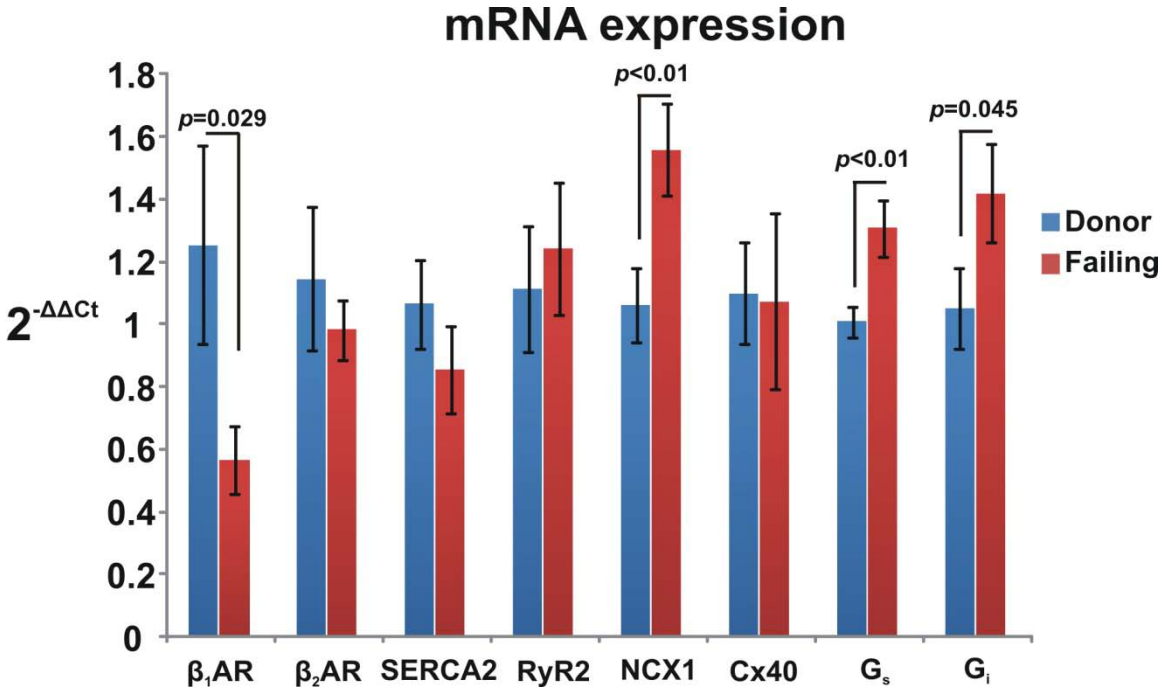

Figure 5.12 mRNA expression of selected β adrenergic signaling target proteins. mRNA expression of selected β adrenergic signaling target proteins was investigated by q-PCR. mRNA of β_1 expression is dramatically decreased in F hearts. NCX and G_i expression increased in F hearts.

The enhanced β_2-AR regulation of APD is dependent upon the transmural layer and results in pathological remodeling of spatial repolarization heterogeneity. Intrinsic APD distribution accounts for the activation delays necessary for synchronizing ventricular repolarization.[188, 189] Thus altering APD dispersion could enhance dispersion of repolarization and arrhythmia vulnerability.[190] We quantified APD and repolarization heterogeneity resulting from β_1- and β_2-stimulation in human HF. In the F hearts, APD shortening induced by β_2-stimulation was more significant in the epi- and mid-, but not in the endocardium, which is opposite from the gradient

observed in D hearts. The molecular and functional epi-endo reversal induced by activation of the β_2-system severely disrupts transmural synchronization in failing hearts.

5.5.2 Switching Coupling of β_2-AR from G_i to G_s Abrogates β_2-Stimulation Based Increase of NCX Activity

Between the two major cytoplasmic Ca extrusion influencing proteins, NCX is recognized to contribute more during CaT late phase of slow decline,[191] when membrane potential is lower than the equilibrium potential of NCX ($E_{Na/Ca}$).[192] When NCX is over-expressed, such as during HF, β_2-stimulation was reported to further up-regulate its activity through its β_2-AR coupling to G_i protein.[180] However, this increase in NCX activity from β_2-stimulation was not supported by our result showing that the CaT decay constant did not change between F vs. D hearts (Figure 5.8F). Given that NCX is over-expressed in HF (Figure 5.12), we postulate that such reduced β_2 regulation is due to a decrease of β_2 AR-G_i coupling as discussed above. This switch from G_i to G_s could explain the CaT morphology change in HF.

5.5.3 Disproportional Transmural Regulation of APD and CaD by β_2-Stimulation Provides Crucial DAD Substrate

Unlike the enhanced APD regulation, β_2-stimulation did not exhibit increased control of Ca handling in F hearts nor transmural CaD heterogeneity in either group of hearts. This resulted in an increase of CaD-APD difference, which widened a vulnerable period for DAD initiation. During

this period, when a cell has already repolarized, due to β_2 stimulation-induced shortening of the refractory period, to its excitable state [193], a net inward current is generated by NCX Ca extrusion while the $[Ca^{2+}]_i$ is still relatively high. Given upregulated mRNA expression of NCX in F hearts (Figure 5.12), we conclude that β_2-stimulation increased cardiac vulnerability to DAD in F human hearts. β-Adrenergic dependent DAD mechanism has been studied at the cellular level.[194] For the first time, we present evidence of DAD triggered PVCs in failing human LV myocardium that is associated with Ca release preceding AP upstroke. Interestingly, such PVCs were only observed during β_2-, but not β_1-stimulation. Moreover, PVCs concentrated at the subepi- and mid-myocardium, where CaD-APD is prolonged. In HF, given NCX activity is not further augmented by β_2-stimulation due to receptor uncoupling with G_i, the electrophysiological CaD-APD substrate could play a major role in DAD initiation by β-AR stimulation rather than increased NCX activity. During β_1-stimulation, on the other hand, we did not observe DADs even with upregulated NCX expression in F hearts, which could be due to unchanged CaD-APD difference during β_1-AR stimulation.

5.5.4 Purkinje fibers account for the majority of ectopy induced by β-stimulation in HF

Low frequency occurrence of PVCs in normal hearts are thought to be benign.[195] However, frequent PVCs in failing hearts have been related to LV dysfunction, and such dysfunction could be ameliorated after elimination of the PVCs by RF ablation in HF patients.[196] Given that the majority of observed PVCs originated from subendocardium, PVCs evoked by both

β_1-AR and β_2-AR selective stimulation are mainly from the Purkinje fibers in HF. This suggests that both subtypes of β_1-AR and β_2-AR preserve functional state in the Purkinje fibers, which is different in myocytes, where β_1-AR is functionally desensitized. Additionally, β_2-stimulation also evokes DAD-induced triggered activity in epi- and midmyocardium, although less frequently.

In the present study of the human failing left ventricle, β_2-stimulation was shown to increase arrhythmia vulnerability by facilitating arrhythmogenic triggers and substrates in contrast to β_1-stimulation, which suggests that non-selective or β_2-selective blockers could improve the treatment of arrhythmogenesis in HF, as compared to β_1-selective blockers. These results may also explain the limited efficiency of β_1-selective blockers in preventing arrhythmias.

Chapter 6
Summary and Future Directions

6.1 Summary

This dissertation demonstrated the design of dual optical mapping system that allows high spatial-temporal resolution imaging of action potential and Ca transient signals simultaneously. Multiple projects were applied using this system to investigate calcium remodeling through different signaling pathways in heart failure, thus revealing the complexity on how distinct impaired signaling pathways associated with arrhythmogenesis. Ca is critical in both electrical and mechanical properties of cardiac myocytes, and much is already known about its ionic basis. In HF, there are significant alterations in how cardiac Ca is regulated through different stimulatory and signaling pathways. These alterations are critical for dictating contractile dysfunction and facilitating the arrhythmias that are characteristic of heart failure. However these alterations from distinct signaling pathway impairment are not clearly revealed.

The goals of the dissertation were fulfilled by 1) investigating the role of Pyk2 in cardiac arrhythmogenesis; 2) identifying regional calcium misleading in aged *mdx* mouse during ventricular stretch conditions; and 3) confirming arrhythmogenic remodeling of β2 versus β1 adrenergic signaling in human failing heart.

Pyk2 is an important component protein along with c-Src, P38 and other proteins consisting a typical stress activated signaling pathway. Its phosphorylation was found dramatically increased in heart failure. I found huge vulnerability of arrhythmogenesis in Pyk2 knockout mice suggesting a

protective role of Pyk2 with respect to ventricular tachyarrhythmia, thus indicating the increased phosphorylation of Pyk2 in heart failure is a compensatory response.

Mechanical defect is by now the most ideal predictor of heart failure. It not only affects the contraction and results in decrease of cardiac output, but also activates cytoskeletal signaling pathways. In the study, it is suggested deficiency of dystrophin is involved in Ca regulation. Associated with mechanical stretch, it can result in significant change of Ca release from and reuptake back to SR. Such remodeling is closely related with mechanical stimulation, as it only appeared in the ventricular base, which might be due to "decent of the base". The resulting dispersion of Ca mishandling induces Ca alternans.

Over-activity of β adrenergic receptor signaling is a hall marker of heart failure. However the endpoint researches mainly focused on left ventricular functions and mechanics, leaving electrophysiological remained unclear. The electrophysiology after β adrenergic stimulation was investigated on donor and explanted human failing hearts. Different β adrenergic receptor subtype was found perform differently. The association between remodeling of action potential and Ca transient provides a crucial arrhythmic substrate in heart failure.

In summary, dysfunction of Ca handling is associated with distinct impaired signaling pathways in heart failure and directly or by associated with electrical remodeling facilities arrhythmogenesis. Revealing such mechanisms expends understands of both Ca handling and signaling in heart failure and provides potential target or directions for heart failure treatment.

6.2 Future Directions

In this dissertation we thoroughly analyzed Ca handling remodeling through three distinct signaling pathways, there are still questions to answer.

Conclusions derived from genetic manipulated mouse models need to be tested from human tissue to provide solid and accurate suggestion for clinical application. The design for mechanical stretch stimulation is by loading solution to inflate the ventricular chamber, which stretches myocytes instead of contraction while providing similar systole inner pressure. Thus, this design was not following physiological condition. Ideal stimulation should come from heart contraction but introduces motion artifact from it on the other side. The future direction requires accurate optical mapping on heart while it maintains normal contraction. The advantage of the success on beating heart optical mapping not only can facilitate the mechanical stimulation investigation, but also avoid the application of EC uncouplers, which allows a wider range of studies on signaling pathways including those EC uncoupler participated.

In the dual optical mapping system, we can accurately analyze the time scale of both action potential and Ca transient, but not the absolute amplitude of action potential or intracellular Ca concentration. These absolute values promise more comprehensive understanding of remodeling of these parameters, since intracellular Ca concentration alteration triggers different signaling pathways. However, in our system, slight change of focal distance, stability of light source and dye loading will dramatically affect fluorescent intensity and avoid appropriate interpretation on amplitude of action potential or intracellular Ca concentration they represent. Application of ratiometric dye is a future direction of optical mapping.

For β adrenergic receptor signaling investigation, further investigation work should include other subtypes of β adrenergic receptor, thus providing a thorough picture of the whole signaling system in heart failure, such as β_3 adrenergic receptor. The study by using specific Gi and Gs signaling pathway blocker will extend and promise for better understanding on β_2 adrenergic receptor switching from Gi to Gs.

After all, future work will be focusing on both experimental design and modulation.

References

1. Tomaselli, G.F. and E. Marban, *Electrophysiological remodeling in hypertrophy and heart failure.* Cardiovasc Res, 1999. **42**(2): p. 270-83.
2. Bers, D.M., *Altered cardiac myocyte Ca regulation in heart failure.* Physiology (Bethesda), 2006. **21**: p. 380-7.
3. Prestle, J., F.R. Quinn, and G.L. Smith, *Ca(2+)-handling proteins and heart failure: novel molecular targets?* Curr Med Chem, 2003. **10**(11): p. 967-81.
4. Berridge, M.J., M.D. Bootman, and H.L. Roderick, *Calcium signalling: dynamics, homeostasis and remodelling.* Nat Rev Mol Cell Biol, 2003. **4**(7): p. 517-29.
5. Lohse, M.J., S. Engelhardt, and T. Eschenhagen, *What is the role of beta-adrenergic signaling in heart failure?* Circ Res, 2003. **93**(10): p. 896-906.
6. Anilkumar, N., A. Sirker, and A.M. Shah, *Redox sensitive signaling pathways in cardiac remodeling, hypertrophy and failure.* Front Biosci (Landmark Ed), 2009. **14**: p. 3168-87.
7. de Tombe, P.P. and R.J. Solaro, *Integration of cardiac myofilament activity and regulation with pathways signaling hypertrophy and failure.* Ann Biomed Eng, 2000. **28**(8): p. 991-1001.
8. Hunter, J.J. and K.R. Chien, *Signaling pathways for cardiac hypertrophy and failure.* N Engl J Med, 1999. **341**(17): p. 1276-83.
9. Go, A.S., et al., *Heart disease and stroke statistics--2013 update: a report from the American Heart Association.* Circulation, 2013. **127**(1): p. e6-e245.
10. Sabir, I.N., et al., *Ventricular arrhythmogenesis: insights from murine models.* Prog Biophys Mol Biol, 2008. **98**(2-3): p. 208-18.
11. Marban, E., S.W. Robinson, and W.G. Wier, *Mechanisms of arrhythmogenic delayed and early afterdepolarizations in ferret ventricular muscle.* J Clin Invest, 1986. **78**(5): p. 1185-92.
12. Fink, M., P.J. Noble, and D. Noble, *Ca(2)(+)-induced delayed afterdepolarizations are triggered by dyadic subspace Ca2(2)(+) affirming that increasing SERCA reduces aftercontractions.* Am J Physiol Heart Circ Physiol, 2011. **301**(3): p. H921-35.
13. Wiener, N. and A. Rosenblueth, *The mathematical formulation of the problem of conduction of impulses in a network of connected excitable elements, specifically in cardiac muscle.* Arch Inst Cardiol Mex, 1946. **16**(3): p. 205-65.
14. Mines, G.R., *On dynamic equilibrium in the heart.* J Physiol, 1913. **46**(4-5): p. 349-83.
15. Durrer, D., et al., *The role of premature beats in the initiation and the termination of supraventricular tachycardia in the Wolff-Parkinson-White syndrome.* Circulation, 1967. **36**(5): p. 644-62.
16. Coumel, P., Cabrol, C., Fabiato, A., Gourgon, R., & Slama, R., *Tachycardie permanente par rythme reciproque.* Arch Mal Coeur, 1967. **60**: p. 34.
17. Malik, M., *Arrhythmic substrate.* Heart, 2008. **94**(4): p. 402-3.
18. de Bakker, J.M. and H.M. van Rijen, *Continuous and discontinuous propagation in heart muscle.* J Cardiovasc Electrophysiol, 2006. **17**(5): p. 567-73.

19. Song, Y.N., et al., *Connexin 43, a new therapeutic target for cardiovascular diseases.* Pharmazie, 2009. **64**(5): p. 291-5.
20. Ai, X. and S.M. Pogwizd, *Connexin 43 downregulation and dephosphorylation in nonischemic heart failure is associated with enhanced colocalized protein phosphatase type 2A.* Circ Res, 2005. **96**(1): p. 54-63.
21. Nielsen, P.M., et al., *Mathematical model of geometry and fibrous structure of the heart.* Am J Physiol, 1991. **260**(4 Pt 2): p. H1365-78.
22. Peters, N.S. and A.L. Wit, *Myocardial architecture and ventricular arrhythmogenesis.* Circulation, 1998. **97**(17): p. 1746-54.
23. Napolitano, C., et al., *Evidence for a cardiac ion channel mutation underlying drug-induced QT prolongation and life-threatening arrhythmias.* J Cardiovasc Electrophysiol, 2000. **11**(6): p. 691-6.
24. Gaita, F., et al., *Short QT Syndrome: a familial cause of sudden death.* Circulation, 2003. **108**(8): p. 965-70.
25. Choi, B.R. and G. Salama, *Simultaneous maps of optical action potentials and calcium transients in guinea-pig hearts: mechanisms underlying concordant alternans.* J Physiol, 2000. **529 Pt 1**: p. 171-88.
26. Nolasco, J.B. and R.W. Dahlen, *A graphic method for the study of alternation in cardiac action potentials.* J Appl Physiol, 1968. **25**(2): p. 191-6.
27. Qu, Z. and J.N. Weiss, *Dynamics and cardiac arrhythmias.* J Cardiovasc Electrophysiol, 2006. **17**(9): p. 1042-9.
28. Garfinkel, A., et al., *Preventing ventricular fibrillation by flattening cardiac restitution.* Proc Natl Acad Sci U S A, 2000. **97**(11): p. 6061-6.
29. Riccio, M.L., M.L. Koller, and R.F. Gilmour, Jr., *Electrical restitution and spatiotemporal organization during ventricular fibrillation.* Circ Res, 1999. **84**(8): p. 955-63.
30. Qu, Z., J.N. Weiss, and A. Garfinkel, *Cardiac electrical restitution properties and stability of reentrant spiral waves: a simulation study.* Am J Physiol, 1999. **276**(1 Pt 2): p. H269-83.
31. Koller, M.L., M.L. Riccio, and R.F. Gilmour, Jr., *Dynamic restitution of action potential duration during electrical alternans and ventricular fibrillation.* Am J Physiol, 1998. **275**(5 Pt 2): p. H1635-42.
32. Karma, A., *Spiral breakup in model equations of action potential propagation in cardiac tissue.* Phys Rev Lett, 1993. **71**(7): p. 1103-1106.
33. Verduyn, S.C., et al., *Further observations to elucidate the role of interventricular dispersion of repolarization and early afterdepolarizations in the genesis of acquired torsade de pointes arrhythmias: a comparison between almokalant and d-sotalol using the dog as its own control.* J Am Coll Cardiol, 1997. **30**(6): p. 1575-84.
34. Verduyn, S.C., et al., *Role of interventricular dispersion of repolarization in acquired torsade-de-pointes arrhythmias: reversal by magnesium.* Cardiovasc Res, 1997. **34**(3): p. 453-63.
35. Pruvot, E.J., et al., *Role of calcium cycling versus restitution in the mechanism of repolarization alternans.* Circ Res, 2004. **94**(8): p. 1083-90.
36. Berridge, M.J., P. Lipp, and M.D. Bootman, *The versatility and universality of calcium signalling.* Nat Rev Mol Cell Biol, 2000. **1**(1): p. 11-21.

37. Wehrens, X.H. and A.R. Marks, *Novel therapeutic approaches for heart failure by normalizing calcium cycling.* Nat Rev Drug Discov, 2004. **3**(7): p. 565-73.
38. Fill, M. and J.A. Copello, *Ryanodine receptor calcium release channels.* Physiol Rev, 2002. **82**(4): p. 893-922.
39. Bers, D.M., *Cardiac excitation-contraction coupling.* Nature, 2002. **415**(6868): p. 198-205.
40. Bers, D.M. and J.H. Bridge, *Relaxation of rabbit ventricular muscle by Na-Ca exchange and sarcoplasmic reticulum calcium pump. Ryanodine and voltage sensitivity.* Circ Res, 1989. **65**(2): p. 334-42.
41. Jones, L.R., et al., *Purification and characterization of phospholamban from canine cardiac sarcoplasmic reticulum.* J Biol Chem, 1985. **260**(12): p. 7721-30.
42. O'Rourke, B., et al., *Mechanisms of altered excitation-contraction coupling in canine tachycardia-induced heart failure, I: experimental studies.* Circ Res, 1999. **84**(5): p. 562-70.
43. Pogwizd, S.M., et al., *Upregulation of Na(+)/Ca(2+) exchanger expression and function in an arrhythmogenic rabbit model of heart failure.* Circ Res, 1999. **85**(11): p. 1009-19.
44. Chen, X., et al., *L-type Ca2+ channel density and regulation are altered in failing human ventricular myocytes and recover after support with mechanical assist devices.* Circ Res, 2002. **91**(6): p. 517-24.
45. Joyner, R.W., et al., *Modulating L-type calcium current affects discontinuous cardiac action potential conduction.* Biophys J, 1996. **71**(1): p. 237-45.
46. Luscher, C., et al., *Control of action potential propagation by intracellular Ca2+ in cultured rat dorsal root ganglion cells.* J Physiol, 1996. **490 (Pt 2)**: p. 319-24.
47. Rohr, S. and J.P. Kucera, *Involvement of the calcium inward current in cardiac impulse propagation: induction of unidirectional conduction block by nifedipine and reversal by Bay K 8644.* Biophys J, 1997. **72**(2 Pt 1): p. 754-66.
48. Chudin, E., et al., *Intracellular Ca(2+) dynamics and the stability of ventricular tachycardia.* Biophys J, 1999. **77**(6): p. 2930-41.
49. Blatter, L.A., et al., *Local calcium gradients during excitation-contraction coupling and alternans in atrial myocytes.* J Physiol, 2003. **546**(Pt 1): p. 19-31.
50. Diaz, M.E., D.A. Eisner, and S.C. O'Neill, *Depressed ryanodine receptor activity increases variability and duration of the systolic Ca2+ transient in rat ventricular myocytes.* Circ Res, 2002. **91**(7): p. 585-93.
51. Wehrens, X.H., et al., *FKBP12.6 deficiency and defective calcium release channel (ryanodine receptor) function linked to exercise-induced sudden cardiac death.* Cell, 2003. **113**(7): p. 829-40.
52. Salama, G. and B. London, *Mouse models of long QT syndrome.* J Physiol, 2007. **578**(Pt 1): p. 43-53.
53. Demolombe, S., et al., *Transgenic mice overexpressing human KvLQT1 dominant-negative isoform. Part I: Phenotypic characterisation.* Cardiovasc Res, 2001. **50**(2): p. 314-27.
54. Nerbonne, J.M., et al., *Genetic manipulation of cardiac K(+) channel function in mice: what have we learned, and where do we go from here?* Circ Res, 2001. **89**(11): p. 944-56.

55. Guo, W., et al., *Molecular basis of transient outward K+ current diversity in mouse ventricular myocytes.* J Physiol, 1999. **521 Pt 3**: p. 587-99.
56. Nerbonne, J.M., *Studying cardiac arrhythmias in the mouse--a reasonable model for probing mechanisms?* Trends Cardiovasc Med, 2004. **14**(3): p. 83-93.
57. Liu, G., et al., *In vivo temporal and spatial distribution of depolarization and repolarization and the illusive murine T wave.* J Physiol, 2004. **555**(Pt 1): p. 267-79.
58. Lang, D., et al., *Optical mapping of action potentials and calcium transients in the mouse heart.* J Vis Exp, 2011(55).
59. Kleber AG, J.M., Fast VG, *Normal and abnormal conduction in the heart*, in *Handbook of Physiology*. 2001, Oxford University Press. p. 455-530.
60. Efimov, I.R., Rendt, J.M. & Salama, G, *Optical maps of intracellular [Ca2+]i transients and action-potentials from the surface of perfused guinea-pig hearts.* Circulation, 1994. **90**: p. 1.
61. Efimov, I.R., V.P. Nikolski, and G. Salama, *Optical imaging of the heart.* Circ Res, 2004. **95**(1): p. 21-33.
62. Fast, V.G., *Recording action potential using voltage sensitive dyes*, in *Practical methods in cardiovascular research*, F.W.M. In S. Dhein, & M. Delmoar, Editor. 2005, Springer: New York. p. 233-255.
63. Efimov, I.R., et al., *Optical mapping of repolarization and refractoriness from intact hearts.* Circulation, 1994. **90**(3): p. 1469-80.
64. Kim, J.H., et al., *Imaging of cerebellar surface activation in vivo using voltage sensitive dyes.* Neuroscience, 1989. **31**(3): p. 613-23.
65. Holcomb, M.R., et al., *The potential of dual camera systems for multimodal imaging of cardiac electrophysiology and metabolism.* Exp Biol Med (Maywood), 2009. **234**(11): p. 1355-73.
66. Glukhov, A.V., et al., *Differential K(ATP) channel pharmacology in intact mouse heart.* J Mol Cell Cardiol, 2009.
67. Baker, L.C., et al., *Enhanced dispersion of repolarization and refractoriness in transgenic mouse hearts promotes reentrant ventricular tachycardia.* Circ Res, 2000. **86**(4): p. 396-407.
68. Sutherland, F.J. and D.J. Hearse, *The isolated blood and perfusion fluid perfused heart.* Pharmacol Res, 2000. **41**(6): p. 613-27.
69. Efimov, I.R., et al., *Virtual electrode polarization in the far field: implications for external defibrillation.* Am J Physiol Heart Circ Physiol, 2000. **279**(3): p. H1055-70.
70. Hammouda, M. and R. Kinosita, *The coronary circulation in the isolated heart.* J Physiol, 1926. **61**(4): p. 615-28.
71. Salama, G. and S.M. Hwang, *Simultaneous optical mapping of intracellular free calcium and action potentials from Langendorff perfused hearts.* Curr Protoc Cytom, 2009. **Chapter 12**: p. Unit 12 17.
72. Lou, Q., et al., *Quantitative panoramic imaging of epicardial electrical activity.* Ann Biomed Eng, 2008. **36**(10): p. 1649-58.
73. Salama, G., et al., *Properties of new, long-wavelength, voltage-sensitive dyes in the heart.* J Membr Biol, 2005. **208**(2): p. 125-40.
74. Lang, D., et al., *Role of Pyk2 in cardiac arrhythmogenesis.* Am J Physiol Heart Circ Physiol, 2011. **301**(3): p. H975-83.

75. Kyriakis, J.M., et al., *The stress-activated protein kinase subfamily of c-Jun kinases.* Nature, 1994. **369**(6476): p. 156-60.
76. Levi, A.J., et al., *Role of intracellular sodium overload in the genesis of cardiac arrhythmias.* J Cardiovasc Electrophysiol, 1997. **8**(6): p. 700-21.
77. Scoote, M. and A.J. Williams, *Myocardial calcium signalling and arrhythmia pathogenesis.* Biochem Biophys Res Commun, 2004. **322**(4): p. 1286-309.
78. Tokiwa, G., et al., *Activation of Pyk2 by stress signals and coupling with JNK signaling pathway.* Science, 1996. **273**(5276): p. 792-4.
79. Avraham, H., et al., *RAFTK/Pyk2-mediated cellular signalling.* Cell Signal, 2000. **12**(3): p. 123-33.
80. Lev, S., et al., *Protein tyrosine kinase PYK2 involved in Ca(2+)-induced regulation of ion channel and MAP kinase functions.* Nature, 1995. **376**(6543): p. 737-45.
81. Dikic, I., et al., *A role for Pyk2 and Src in linking G-protein-coupled receptors with MAP kinase activation.* Nature, 1996. **383**(6600): p. 547-50.
82. Park, S.Y., H.K. Avraham, and S. Avraham, *RAFTK/Pyk2 activation is mediated by trans-acting autophosphorylation in a Src-independent manner.* J Biol Chem, 2004. **279**(32): p. 33315-22.
83. Felsch, J.S., T.G. Cachero, and E.G. Peralta, *Activation of protein tyrosine kinase PYK2 by the m1 muscarinic acetylcholine receptor.* Proc Natl Acad Sci U S A, 1998. **95**(9): p. 5051-6.
84. Schaller, M.D., *Cellular functions of FAK kinases: insight into molecular mechanisms and novel functions.* J Cell Sci, 2010. **123**(Pt 7): p. 1007-13.
85. Bayer, A.L., et al., *Pyk2 expression and phosphorylation in neonatal and adult cardiomyocytes.* J Mol Cell Cardiol, 2001. **33**(5): p. 1017-30.
86. Murasawa, S., et al., *Role of calcium-sensitive tyrosine kinase Pyk2/CAKbeta/RAFTK in angiotensin II induced Ras/ERK signaling.* Hypertension, 1998. **32**(4): p. 668-75.
87. Sabri, A., et al., *Calcium- and protein kinase C-dependent activation of the tyrosine kinase PYK2 by angiotensin II in vascular smooth muscle.* Circ Res, 1998. **83**(8): p. 841-51.
88. Frank, G.D., et al., *PYK2/CAKbeta represents a redox-sensitive tyrosine kinase in vascular smooth muscle cells.* Biochem Biophys Res Commun, 2000. **270**(3): p. 761-5.
89. Matsui, A., et al., *Central role of calcium-dependent tyrosine kinase PYK2 in endothelial nitric oxide synthase-mediated angiogenic response and vascular function.* Circulation, 2007. **116**(9): p. 1041-51.
90. Bayer, A.L., et al., *PYK2 expression and phosphorylation increases in pressure overload-induced left ventricular hypertrophy.* Am J Physiol Heart Circ Physiol, 2002. **283**(2): p. H695-706.
91. Melendez, J., et al., *Activation of pyk2/related focal adhesion tyrosine kinase and focal adhesion kinase in cardiac remodeling.* J Biol Chem, 2002. **277**(47): p. 45203-10.
92. Heidkamp, M.C., et al., *PYK2 regulates SERCA2 gene expression in neonatal rat ventricular myocytes.* Am J Physiol Cell Physiol, 2005. **289**(2): p. C471-82.
93. Melendez, J., et al., *Cardiomyocyte apoptosis triggered by RAFTK/pyk2 via Src kinase is antagonized by paxillin.* J Biol Chem, 2004. **279**(51): p. 53516-23.

94. Hirotani, S., et al., *Ca(2+)-sensitive tyrosine kinase Pyk2/CAK beta-dependent signaling is essential for G-protein-coupled receptor agonist-induced hypertrophy.* J Mol Cell Cardiol, 2004. **36**(6): p. 799-807.
95. Guo, J., et al., *Alpha1-adrenergic receptors activate AKT via a Pyk2/PDK-1 pathway that is tonically inhibited by novel protein kinase C isoforms in cardiomyocytes.* Circ Res, 2006. **99**(12): p. 1367-75.
96. Menashi, E.B. and J.C. Loftus, *Differential effects of Pyk2 and FAK on the hypertrophic response of cardiac myocytes.* Cell Tissue Res, 2009. **337**(2): p. 243-55.
97. Hart, D.L., et al., *CRNK gene transfer improves function and reverses the myosin heavy chain isoenzyme switch during post-myocardial infarction left ventricular remodeling.* J Mol Cell Cardiol, 2008. **45**(1): p. 93-105.
98. Okigaki, M., et al., *Pyk2 regulates multiple signaling events crucial for macrophage morphology and migration.* Proc Natl Acad Sci U S A, 2003. **100**(19): p. 10740-5.
99. Schindler, E.M., et al., *The role of proline-rich protein tyrosine kinase 2 in differentiation-dependent signaling in human epidermal keratinocytes.* J Invest Dermatol, 2007. **127**(5): p. 1094-106.
100. Fabritz, C.L., et al., *Myocardial vulnerability to T wave shocks: relation to shock strength, shock coupling interval, and dispersion of ventricular repolarization.* J Cardiovasc Electrophysiol, 1996. **7**(3): p. 231-42.
101. Fedorov, V.V., et al., *Atria are more susceptible to electroporation than ventricles: implications for atrial stunning, shock-induced arrhythmia and defibrillation failure.* Heart Rhythm, 2008. **5**(4): p. 593-604.
102. Rockman, H.A., et al., *Segregation of atrial-specific and inducible expression of an atrial natriuretic factor transgene in an in vivo murine model of cardiac hypertrophy.* Proc Natl Acad Sci U S A, 1991. **88**(18): p. 8277-81.
103. Rockman, H.A., et al., *Molecular and physiological alterations in murine ventricular dysfunction.* Proc Natl Acad Sci U S A, 1994. **91**(7): p. 2694-8.
104. Huang, Y., et al., *CAKbeta/Pyk2 kinase is a signaling link for induction of long-term potentiation in CA1 hippocampus.* Neuron, 2001. **29**(2): p. 485-96.
105. Ling, S., J.Z. Sheng, and A.P. Braun, *The calcium-dependent activity of large-conductance, calcium-activated K+ channels is enhanced by Pyk2- and Hck-induced tyrosine phosphorylation.* Am J Physiol Cell Physiol, 2004. **287**(3): p. C698-706.
106. Cheng, Y.J., et al., *Focal but reversible diastolic sheet dysfunction reflects regional calcium mishandling in dystrophic mdx mouse hearts.* Am J Physiol Heart Circ Physiol, 2012. **303**(5): p. H559-68.
107. Bigger, J.T., Jr., et al., *The relationships among ventricular arrhythmias, left ventricular dysfunction, and mortality in the 2 years after myocardial infarction.* Circulation, 1984. **69**(2): p. 250-8.
108. Laurita, K.R. and D.S. Rosenbaum, *Cellular mechanisms of arrhythmogenic cardiac alternans.* Prog Biophys Mol Biol, 2008. **97**(2-3): p. 332-47.
109. McGavin, M.D.a.J.F.Z., *Congenital or Inherited Myopathies*, in *Pathologic Basis of Veterinary Disease (4th Edition)*. 2007, Mosby/Elsevier St. Louis. p. 1026-1027.
110. Gulati, S., et al., *Duchenne muscular dystrophy: prevalence and patterns of cardiac involvement.* Indian J Pediatr, 2005. **72**(5): p. 389-93.
111. Wagner, K.R., N. Lechtzin, and D.P. Judge, *Current treatment of adult Duchenne muscular dystrophy.* Biochim Biophys Acta, 2007. **1772**(2): p. 229-37.

112. Ahuja, R., et al., *Prevalence and patterns of cardiac involvement in duchenne muscular dystrophy.* Indian Pediatr, 2000. **37**(11): p. 1246-51.
113. Ishikawa, Y., J.R. Bach, and R. Minami, *Cardioprotection for Duchenne's muscular dystrophy.* Am Heart J, 1999. **137**(5): p. 895-902.
114. McNally, E.M., *Duchenne muscular dystrophy: how bad is the heart?* Heart, 2008. **94**(8): p. 976-7.
115. Romfh, A. and E.M. McNally, *Cardiac assessment in duchenne and becker muscular dystrophies.* Curr Heart Fail Rep, 2010. **7**(4): p. 212-8.
116. Nolan, M.A., et al., *Cardiac assessment in childhood carriers of Duchenne and Becker muscular dystrophies.* Neuromuscul Disord, 2003. **13**(2): p. 129-32.
117. Hermans, M.C., et al., *Hereditary muscular dystrophies and the heart.* Neuromuscul Disord, 2010. **20**(8): p. 479-92.
118. Finsterer, J. and C. Stollberger, *Cardiac involvement determines the prognosis of Duchenne muscular dystrophy.* Indian J Pediatr, 2007. **74**(2): p. 209; author reply 210-2.
119. Townsend, D., S. Yasuda, and J. Metzger, *Cardiomyopathy of Duchenne muscular dystrophy: pathogenesis and prospect of membrane sealants as a new therapeutic approach.* Expert Rev Cardiovasc Ther, 2007. **5**(1): p. 99-109.
120. Gailly, P., *New aspects of calcium signaling in skeletal muscle cells: implications in Duchenne muscular dystrophy.* Biochim Biophys Acta, 2002. **1600**(1-2): p. 38-44.
121. Li, W., et al., *Early manifestation of alteration in cardiac function in dystrophin deficient mdx mouse using 3D CMR tagging.* J Cardiovasc Magn Reson, 2009. **11**: p. 40.
122. van Deutekom, J.C., et al., *Antisense-induced exon skipping restores dystrophin expression in DMD patient derived muscle cells.* Hum Mol Genet, 2001. **10**(15): p. 1547-54.
123. Banks, G.B. and J.S. Chamberlain, *The value of mammalian models for duchenne muscular dystrophy in developing therapeutic strategies.* Curr Top Dev Biol, 2008. **84**: p. 431-53.
124. Cullen, M.J. and E. Jaros, *Ultrastructure of the skeletal muscle in the X chromosome-linked dystrophic (mdx) mouse. Comparison with Duchenne muscular dystrophy.* Acta Neuropathol, 1988. **77**(1): p. 69-81.
125. Tanabe, Y., K. Esaki, and T. Nomura, *Skeletal muscle pathology in X chromosome-linked muscular dystrophy (mdx) mouse.* Acta Neuropathol, 1986. **69**(1-2): p. 91-5.
126. Bulfield, G., et al., *X chromosome-linked muscular dystrophy (mdx) in the mouse.* Proc Natl Acad Sci U S A, 1984. **81**(4): p. 1189-92.
127. Allen, D.G., et al., *Calcium and the damage pathways in muscular dystrophy.* Can J Physiol Pharmacol, 2010. **88**(2): p. 83-91.
128. Williams, I.A. and D.G. Allen, *Intracellular calcium handling in ventricular myocytes from mdx mice.* Am J Physiol Heart Circ Physiol, 2007. **292**(2): p. H846-55.
129. Fanchaouy, M., et al., *Pathways of abnormal stress-induced Ca2+ influx into dystrophic mdx cardiomyocytes.* Cell Calcium, 2009. **46**(2): p. 114-21.
130. Balzer, P., et al., *Regional assessment of wall curvature and wall stress in left ventricle with magnetic resonance imaging.* Am J Physiol, 1999. **277**(3 Pt 2): p. H901-10.
131. DeAnda, A., Jr., et al., *Estimation of regional left ventricular wall stresses in intact canine hearts.* Am J Physiol, 1998. **275**(5 Pt 2): p. H1879-85.

132. Ashford, M.W., Jr., et al., *Occult cardiac contractile dysfunction in dystrophin-deficient children revealed by cardiac magnetic resonance strain imaging.* Circulation, 2005. **112**(16): p. 2462-7.
133. Dellorusso, C., et al., *Tibialis anterior muscles in mdx mice are highly susceptible to contraction-induced injury.* Journal of muscle research and cell motility, 2001. **22**(5): p. 467-75.
134. Chen, J., et al., *Regional ventricular wall thickening reflects changes in cardiac fiber and sheet structure during contraction: quantification with diffusion tensor MRI.* Am J Physiol Heart Circ Physiol, 2005. **289**(5): p. H1898-907.
135. Munch, D.F., H.T. Comer, and J.M. Downey, *Barium contracture: a model for systole.* Am J Physiol, 1980. **239**(3): p. H438-42.
136. Toyota, E., et al., *Dynamic changes in three-dimensional architecture and vascular volume of transmural coronary microvasculature between diastolic- and systolic-arrested rat hearts.* Circulation, 2002. **105**(5): p. 621-6.
137. Judd, R.M., et al., *Feasibility of 19F imaging of perfluorochemical emulsions to measure myocardial vascular volume.* Magn Reson Med, 1992. **28**(1): p. 129-36.
138. Dunphy, G., et al., *The effects of mannitol, albumin, and cardioplegia enhancers on 24-h rat heart preservation.* The American journal of physiology, 1999. **276**(5 Pt 2): p. H1591-8.
139. Watts, J.A. and P.C. Maiorano, *Trace amounts of albumin protect against ischemia and reperfusion injury in isolated rat hearts.* Journal of molecular and cellular cardiology, 1999. **31**(9): p. 1653-62.
140. Robinson, L.A. and D.L. Harwood, *Lowering the calcium concentration in St. Thomas' Hospital cardioplegic solution improves protection during hypothermic ischemia.* J Thorac Cardiovasc Surg, 1991. **101**(2): p. 314-25.
141. Scollan, D.F., et al., *Histological validation of myocardial microstructure obtained from diffusion tensor magnetic resonance imaging.* Am J Physiol, 1998. **275**(6 Pt 2): p. H2308-18.
142. Tseng, W.Y., et al., *Diffusion tensor MRI of myocardial fibers and sheets: correspondence with visible cut-face texture.* J Magn Reson Imaging, 2003. **17**(1): p. 31-42.
143. LeGrice, I.J., Y. Takayama, and J.W. Covell, *Transverse shear along myocardial cleavage planes provides a mechanism for normal systolic wall thickening.* Circ Res, 1995. **77**(1): p. 182-93.
144. Pope, A.J., et al., *Three-dimensional transmural organization of perimysial collagen in the heart.* Am J Physiol Heart Circ Physiol, 2008. **295**(3): p. H1243-H1252.
145. LeGrice, I.J., et al., *Laminar structure of the heart: ventricular myocyte arrangement and connective tissue architecture in the dog.* Am J Physiol, 1995. **269**(2 Pt 2): p. H571-82.
146. Gilbert, S.H., et al., *Regional localisation of left ventricular sheet structure: integration with current models of cardiac fibre, sheet and band structure.* European journal of cardio-thoracic surgery : official journal of the European Association for Cardio-thoracic Surgery, 2007. **32**(2): p. 231-49.
147. Helm, P., et al., *Measuring and mapping cardiac fiber and laminar architecture using diffusion tensor MR imaging.* Annals of the New York Academy of Sciences, 2005. **1047**: p. 296-307.

148. Costa, K.D., et al., *Laminar fiber architecture and three-dimensional systolic mechanics in canine ventricular myocardium.* Am J Physiol, 1999. **276**(2 Pt 2): p. H595-607.
149. Nielsen, J.M., et al., *Left ventricular volume measurement in mice by conductance catheter: evaluation and optimization of calibration.* Am J Physiol Heart Circ Physiol, 2007. **293**(1): p. H534-40.
150. Simonson, J.S. and N.B. Schiller, *Descent of the base of the left ventricle: an echocardiographic index of left ventricular function.* J Am Soc Echocardiogr, 1989. **2**(1): p. 25-35.
151. !!! INVALID CITATION !!!
152. Sapp, J.L., J. Bobet, and S.E. Howlett, *Contractile properties of myocardium are altered in dystrophin-deficient mdx mice.* Journal of the neurological sciences, 1996. **142**(1-2): p. 17-24.
153. Phillips, M.F. and R. Quinlivan, *Calcium antagonists for Duchenne muscular dystrophy.* Cochrane Database Syst Rev, 2008(4): p. CD004571.
154. Wachter, S.B. and E.M. Gilbert, *Beta-adrenergic receptors, from their discovery and characterization through their manipulation to beneficial clinical application.* Cardiology, 2012. **122**(2): p. 104-12.
155. Lombardi, W.L. and E.M. Gilbert, *Carvedilol in the failing heart.* Clin Cardiol, 2001. **24**(12): p. 757-66.
156. Anderson, J.L., et al., *ACC/AHA 2007 guidelines for the management of patients with unstable angina/non ST-elevation myocardial infarction: a report of the American College of Cardiology/American Heart Association Task Force on Practice Guidelines (Writing Committee to Revise the 2002 Guidelines for the Management of Patients With Unstable Angina/Non ST-Elevation Myocardial Infarction): developed in collaboration with the American College of Emergency Physicians, the Society for Cardiovascular Angiography and Interventions, and the Society of Thoracic Surgeons: endorsed by the American Association of Cardiovascular and Pulmonary Rehabilitation and the Society for Academic Emergency Medicine.* Circulation, 2007. **116**(7): p. e148-304.
157. Krum, H., *The Task Force for the diagnosis and treatment of chronic heart failure of the European Society of Cardiology. Guidelines for the diagnosis and treatment of chronic heart failure: full text (update 2005).* Eur Heart J, 2005. **26**(22): p. 2472; author reply 2473-4.
158. Connolly, S.J., et al., *Comparison of beta-blockers, amiodarone plus beta-blockers, or sotalol for prevention of shocks from implantable cardioverter defibrillators: the OPTIC Study: a randomized trial.* JAMA, 2006. **295**(2): p. 165-71.
159. Ferreira-Gonzalez, I., L. Dos-Subira, and G.H. Guyatt, *Adjunctive antiarrhythmic drug therapy in patients with implantable cardioverter defibrillators: a systematic review.* Eur Heart J, 2007. **28**(4): p. 469-77.
160. Singh, B.N. and D.E. Jewitt, *Beta-adrenergic receptor blocking drugs in cardiac arrhythmias.* Drugs, 1974. **7**(6): p. 426-61.
161. Ruwald, M.H., et al., *Effect of metoprolol versus carvedilol on outcomes in MADIT-CRT (multicenter automatic defibrillator implantation trial with cardiac resynchronization therapy).* J Am Coll Cardiol, 2013. **61**(14): p. 1518-26.
162. Poole-Wilson, P.A., et al., *Comparison of carvedilol and metoprolol on clinical outcomes in patients with chronic heart failure in the Carvedilol Or Metoprolol*

European Trial (COMET): randomised controlled trial. Lancet, 2003. **362**(9377): p. 7-13.
163. Lechat, P., et al., *Clinical effects of beta-adrenergic blockade in chronic heart failure: a meta-analysis of double-blind, placebo-controlled, randomized trials.* Circulation, 1998. **98**(12): p. 1184-91.
164. de Peuter, O.R., et al., *A systematic review of selective and non-selective beta blockers for prevention of vascular events in patients with acute coronary syndrome or heart failure.* Neth J Med, 2009. **67**(9): p. 284-94.
165. Bristow, M.R., et al., *Beta 1- and beta 2-adrenergic-receptor subpopulations in nonfailing and failing human ventricular myocardium: coupling of both receptor subtypes to muscle contraction and selective beta 1-receptor down-regulation in heart failure.* Circ Res, 1986. **59**(3): p. 297-309.
166. Lou, Q., et al., *Transmural heterogeneity and remodeling of ventricular excitation-contraction coupling in human heart failure.* Circulation. **123**(17): p. 1881-90.
167. Lang, D., et al., *Optical mapping of action potentials and calcium transients in the mouse heart.* J Vis Exp, (55).
168. Noguchi, K., et al., *Cardiac effects of beta-2 adrenoceptor stimulation with intracoronary procaterol in the absence and presence of regional myocardial ischemia in dogs.* J Pharmacol Exp Ther, 1991. **259**(2): p. 732-7.
169. Bartel, S., et al., *New insights into beta2-adrenoceptor signaling in the adult rat heart.* Cardiovasc Res, 2003. **57**(3): p. 694-703.
170. Sato, H., et al., *Hemodynamic effects of the beta 1-adrenoceptor partial agonist xamoterol in relation to plasma norepinephrine levels during exercise in patients with left ventricular dysfunction.* Circulation, 1987. **75**(1): p. 213-20.
171. Engelhardt, S., et al., *Constitutive activity of the human beta(1)-adrenergic receptor in beta(1)-receptor transgenic mice.* Mol Pharmacol, 2001. **60**(4): p. 712-7.
172. Damiano, R.J., Jr., et al., *The effect of chemical ablation of the endocardium on ventricular fibrillation threshold.* Circulation, 1986. **74**(3): p. 645-52.
173. Myles, R.C., et al., *Local beta-adrenergic stimulation overcomes source-sink mismatch to generate focal arrhythmia.* Circ Res, 2012. **110**(11): p. 1454-64.
174. Beuckelmann, D.J., M. Nabauer, and E. Erdmann, *Alterations of K+ currents in isolated human ventricular myocytes from patients with terminal heart failure.* Circ Res, 1993. **73**(2): p. 379-85.
175. Xiao, R.P., et al., *Coupling of beta2-adrenoceptor to Gi proteins and its physiological relevance in murine cardiac myocytes.* Circ Res, 1999. **84**(1): p. 43-52.
176. Daaka, Y., L.M. Luttrell, and R.J. Lefkowitz, *Switching of the coupling of the beta2-adrenergic receptor to different G proteins by protein kinase A.* Nature, 1997. **390**(6655): p. 88-91.
177. Nobles, K.N., et al., *Distinct phosphorylation sites on the beta(2)-adrenergic receptor establish a barcode that encodes differential functions of beta-arrestin.* Sci Signal. **4**(185): p. ra51.
178. Gerhardstein, B.L., et al., *Identification of the sites phosphorylated by cyclic AMP-dependent protein kinase on the beta 2 subunit of L-type voltage-dependent calcium channels.* Biochemistry, 1999. **38**(32): p. 10361-70.
179. Simmerman, H.K. and L.R. Jones, *Phospholamban: protein structure, mechanism of action, and role in cardiac function.* Physiol Rev, 1998. **78**(4): p. 921-47.

180. Sato, M., et al., *Loss of beta-adrenoceptor response in myocytes overexpressing the Na+/Ca(2+)-exchanger.* J Mol Cell Cardiol, 2004. **36**(1): p. 43-8.
181. Beau, S.L., T.K. Tolley, and J.E. Saffitz, *Heterogeneous transmural distribution of beta-adrenergic receptor subtypes in failing human hearts.* Circulation, 1993. **88**(6): p. 2501-9.
182. Asano, T., et al., *Activation of the inhibitory GTP-binding protein of adenylate cyclase, Gi, by beta-adrenergic receptors in reconstituted phospholipid vesicles.* J Biol Chem, 1984. **259**(15): p. 9351-4.
183. Communal, C., W.S. Colucci, and K. Singh, *p38 mitogen-activated protein kinase pathway protects adult rat ventricular myocytes against beta -adrenergic receptor-stimulated apoptosis. Evidence for Gi-dependent activation.* J Biol Chem, 2000. **275**(25): p. 19395-400.
184. Zhu, W.Z., et al., *Dual modulation of cell survival and cell death by beta(2)-adrenergic signaling in adult mouse cardiac myocytes.* Proc Natl Acad Sci U S A, 2001. **98**(4): p. 1607-12.
185. Zheng, M., Q.D. Han, and R.P. Xiao, *Distinct beta-adrenergic receptor subtype signaling in the heart and their pathophysiological relevance.* Sheng Li Xue Bao, 2004. **56**(1): p. 1-15.
186. Gong, H., et al., *Specific beta(2)AR blocker ICI 118,551 actively decreases contraction through a G(i)-coupled form of the beta(2)AR in myocytes from failing human heart.* Circulation, 2002. **105**(21): p. 2497-503.
187. Milano, C.A., et al., *Enhanced myocardial function in transgenic mice overexpressing the beta 2-adrenergic receptor.* Science, 1994. **264**(5158): p. 582-6.
188. Litovsky, S.H. and C. Antzelevitch, *Rate dependence of action potential duration and refractoriness in canine ventricular endocardium differs from that of epicardium: role of the transient outward current.* J Am Coll Cardiol, 1989. **14**(4): p. 1053-66.
189. Glukhov, A.V., et al., *Transmural dispersion of repolarization in failing and nonfailing human ventricle.* Circ Res. **106**(5): p. 981-91.
190. Akar, F.G. and D.S. Rosenbaum, *Transmural electrophysiological heterogeneities underlying arrhythmogenesis in heart failure.* Circ Res, 2003. **93**(7): p. 638-45.
191. Crespo, L.M., C.J. Grantham, and M.B. Cannell, *Kinetics, stoichiometry and role of the Na-Ca exchange mechanism in isolated cardiac myocytes.* Nature, 1990. **345**(6276): p. 618-21.
192. Bers, D., *Excitation-contraction coupling and cardiac contractile force*. Vol. Vol. 237. 2001: Kluwer Academic Pub.
193. Sharma, A.D., M.B. Waxman, and F.I. Huerta, *Effect of adrenergic stimulation and blockade on ventricular defibrillation in the rat.* J Pharmacol Exp Ther, 1983. **227**(3): p. 716-22.
194. Desantiago, J., et al., *Arrhythmogenic effects of beta2-adrenergic stimulation in the failing heart are attributable to enhanced sarcoplasmic reticulum Ca load.* Circ Res, 2008. **102**(11): p. 1389-97.
195. Kennedy, H.L., et al., *Long-term follow-up of asymptomatic healthy subjects with frequent and complex ventricular ectopy.* N Engl J Med, 1985. **312**(4): p. 193-7.
196. Bogun, F., et al., *Radiofrequency ablation of frequent, idiopathic premature ventricular complexes: comparison with a control group without intervention.* Heart Rhythm, 2007. **4**(7): p. 863-7.